Dissertation

submitted to the
Combined Faculties of the Natural Sciences and Mathematics
of the Ruperto-Carola-University of Heidelberg, Germany
for the degree of
Doctor of Natural Sciences

Put forward by
Johannes Maria René Welter
born in Starnberg, Germany

Oral examination: December 20th, 2017

Phenomenology of neutrino magnetic moments

Referees: Prof. Dr. Manfred Lindner

Prof. Dr. Joerg Jaeckel

Abstract

The neutrino magnetic moment (NMM) in the Standard Model, minimally extended allowing for massive neutrinos, is many orders of magnitude below current and expected experimental sensitivities. A potential measurement would therefore strongly hint to new physics beyond the Standard Model. It raises the question how a positive NMM signal in future experiments could be explained in a theoretically consistent way. After a brief theoretical introduction, we summarize existing experimental bounds and systematically analyze the possibilities of model building for accommodating large NMMs in beyond the Standard Model frameworks. As a by-product, we derive new limits on millicharged particles from the non-observation of NMMs. The tight connection of NMMs and neutrino masses generically leads to a fine-tuning problem in typical models that predict sizable NMMs. We explicitly demonstrate this problem using a model in which NMMs are proportional to neutrino masses. Finally, we investigate mechanisms that provide large NMMs and at the same time avoid the fine-tuning problem. As a result, we find only two such mechanisms that are not yet excluded and in which large transition magnetic moments can be realized for Majorana neutrinos only.

Zusammenfassung

Das magnetische Moment eines Neutrinos (MMN) im um Neutrino-Massen minimal erweiterten Standardmodell der Teilchenphysik liegt um einige Größenordnungen unter den aktuellen und zu erwartenden experimentellen Sensitivitäten. Eine potentielle Messung wäre daher ein deutlicher Hinweis auf die Existenz neuer Physik jenseits des Standardmodells. Das wirft die Frage auf, wie ein mögliches positives MMN-Signal zukünftiger Experimente theoretisch konsistent erklärt werden könnte. Nach einer knappen Einführung in die theoretischen Grundlagen fassen wir die bisherigen experimentellen Ergebnisse zusammen und suchen systematisch nach möglichen Modellen jenseits des Standardmodells, die große MMN vorhersagen können. Als Nebenprodukt leiten wir aus der Nichtbeobachtung von MMN neue obere Schranken für Masse und Ladung milligeladener Teilchen her. Der enge Zusammenhang zwischen MMN und Neutrinomassen führt dazu, dass es in typischen Modellen mit großen MMN ein sogenanntes Feintuning-Problem gibt. Wir demonstrieren dieses Problem anhand eines Modells, in dem die MMN proportional zu den Neutrino-Massen sind. Schließlich untersuchen wir Mechanismen, die ein messbares MMN liefern und gleichzeitig das Feintuning-Problem umgehen. Als Resultat finden wir nur zwei mögliche Mechanismen, die noch nicht ausgeschlossen sind und in denen sich große Übergangs-Momente, allerdings nur für Majorana Neutrinos, realisieren lassen.

Contents

Disclaimer

This work contains parts of the supervised research performed during the course of this Ph.D. Among several projects, two of them have been published in a peer-reviewed journal. The first of them was published in "The Not-So-Sterile 4th Neutrino: Constraints on New Gauge Interactions from Neutrino Oscillation Experiments" [1] (in collaboration with J. Kopp) and is not included in this work. Chaps. 4 and 5 contain yet unpublished projects. The content of the second publication, "Revisiting large neutrino magnetic moments" [2] (in collaboration with M. Lindner and B. Radovčić), is presented in Chap. 6.

Acknowledgements

First of all, I would like to thank my supervisor Manfred Lindner for the opportunity to work in an excellent and stimulating working environment as well as for his continuous encouragement and support. I am also very grateful for the initial support and collaboration of my former supervisor Joachim Kopp during the first phase of my doctoral studies.

I thank Joerg Jaeckel for agreeing to take over the tasks of the second referee as well as to Stephanie Hansmann-Menzemer and Björn Malte Schäfer for accepting being part of the examination committee.

I am indebted to Branimir Radovčić and Hiren Patel for many interesting discussions, helpful explanations and suggestions. I thank all the group members for contributing to a nice atmosphere, especially Juri Smirnov and Shao-Feng who I shared an office with. For carefully proof-reading parts of this work I owe my gratitude to Stefan Brünner, Miguel Campos, Alexander Helmboldt and Moritz Platscher.

Finally, I would like to thank my wife Esther without whom I would not have had the necessary emotional and practical support as well as my parents Heidi and René for their ongoing encouragement.

Chapter 1

Introduction

With the discovery of the Higgs boson at the LHC in 2012 [3, 4], the particle content of the Standard Model (SM) is experimentally verified. Among the shortcomings of this remarkably successful theory, the experimentally most striking one is provided by the phenomenon of neutrino oscillations. It inevitably implies the existence of small, but non-zero neutrino masses and thus requires the SM to be extended such that neutrinos become massive. Up to now, the absolute value of neutrino masses is still unknown. Current upper limits show that neutrino masses considerably larger than 0.2 eV are in conflict with cosmological observations [5].

The idea that neutrinos oscillate was first proposed by Pontecorvo in 1957 [6] and is considered as well-established since together with the results for atmospheric neutrinos by the Super-Kamiokande experiment in 1998 [7] and for solar neutrinos in 2002 by SNO [8] the discrepancy between the expected and measured solar neutrino fluxes could be explained. In the context of this discrepancy, also known as the solar neutrino problem, the possibility of a solution by a large neutrino magnetic moment (NMM) led to an increasing interest in theoretical models that can generate NMMs of sufficient size [9–17]. It eventually turned out that the solar neutrino problem is solved by resonant neutrino flavor transitions inside the sun, thereby ruling out the NMM-solution of the solar neutrino problem. In the subsequent years experiments measuring reactor, atmospheric, accelerator as well as solar neutrinos continuously improved the precision of the neutrino mixing parameters.

The current sensitivity to NMMs, on the other hand, is still far away from the SM prediction[1]. The best direct upper limit is obtained in the reactor neutrino experiment GEMMA which measures the electron recoil of antineutrino-electron scattering

[1] In the original Standard Model neutrinos are massless. As a consequence the NMM is exactly zero. In the context of NMM predictions, we thus refer by 'SM' to minimally extensions of the Standard Model that allow for massive neutrinos as introduced in Sec. 2.1.

near the reactor core. It constrains the effective magnetic moment to be less than $2.9 \cdot 10^{-11}\mu_B$ [18]. In the SM, the NMM is of the order $10^{-19}\mu_B(m_\nu/\text{eV})$ [19–23] (in units of the Bohr magneton $\mu_B = \frac{e}{2m_e}$ and the neutrino mass m_ν) which is eight orders of magnitude below the GEMMA limit. The smallness of the SM prediction implies that a measurement of a finite NMM would be a clear indication for new physics beyond the SM. Upcoming experiments are expected to reach NMMs of the order $\mu_\nu \gtrsim 10^{-12}\mu_B$ [24–27]. Consequently, it suggests itself to ask what kind of new physics could explain such large NMMs. In this work, we hence want to analyze the possibilities of generating large NMMs in a theoretically consistent way. Typically, one is looking for suitable models at high energy scales, but we also study the interesting connection of large NMMs with light millicharged particles.

The outline of this thesis is as follows. The theoretical background of neutrino mass and mixing, neutrino oscillations as well as neutrino electromagnetic properties and the neutrino magnetic moment is introduced in Chap. 2, followed by a brief summary of current direct laboratory experiments as well as astrophysical observations that constrain the size of NMMs in Chap. 3. In a systematic study of theoretical NMM predictions in Chap. 4, we explicitly rederive the SM prediction for Dirac as well as Majorana neutrinos and thereby explain the computation procedure. We then classify the potential generic NMM couplings and calculate the corresponding results in the case of Dirac and Majorana neutrinos as well as for the zeroth and first order in neutrino mass. We apply and cross-check our results in the two simplest scenarios, a model with a charged scalar singlet and the left-right-symmetric model, in which the proportionality to the neutrino mass can be avoided. It turns out that in both cases large NMMs can only be introduced by paying the price of fine-tuned neutrino masses due to large radiative corrections. In Chap. 5 we use the result of our generic calculation and apply it to models where millicharged particles couple to right-handed neutrinos. The non-observation of NMMs leads to new constraints for such scenarios which however turn out to be less stringent than limits from astrophysical observations. The problem of generating large NMMs, while simultaneously avoiding the fine-tuning of neutrino masses is explained and tackled in Chap. 6. We investigate the possibility of NMMs in a model with millicharged particles and find that there seems to be no room for large NMMs. We then explain the generic difficulty of generating large NMMs due to the tight connection with the neutrino mass by means of a particularly insightful model and conclude that it is necessary to introduce new symmetries in order to obtain naturally large NMMs. We review, update and discuss three promising models that provide such a symmetry. It turns out that

currently there is no idea for consistently incorporating large NMMs for Dirac neutrinos. For Majorana neutrinos, a $SU(2)_H$ horizontal symmetry can realize a large ν_e-ν_μ transition moment. In the Barr-Freire-Zee model, which relies on a spin-suppression mechanism, it is also possible to generate sizable ν_e-ν_μ as well as ν_e-ν_τ and ν_μ-ν_τ Majorana transition moments.

Chapter 2

Theoretical preliminaries

In this chapter, we give a brief introduction to the basic concepts of neutrino masses, neutrino oscillations and the neutrino magnetic moment (NMM). In favor of conciseness, the scope of this chapter is restricted to what we consider necessary for the understanding of this thesis. For more details about neutrino physics and basic quantum field theory, we refer to the extensive literature, see e.g. Refs. [28–35].

2.1. Neutrino masses and mixing

Except for the neutrinos all fermions in the original Standard Model (SM) consist of right- and left-chiral fields. For introducing neutrino masses it is therefore straightforward to simply add three new right-handed neutrinos to the SM particle content. In analogy to the other right-handed fermions of the SM it is assumed that they are $SU(2)_L$ singlets. Since neutrinos are electrically neutral this implies a zero hypercharge, which makes them total SM singlets.

When introducing such right-handed neutrino fields ν_R, it immediately leads to the additional Lagrangian terms

$$\mathcal{L}^D = -\sum_{\alpha,\beta=e,\mu,\tau} Y_{\alpha\beta}\overline{L_\alpha}\tilde{\phi}\nu_{\beta R} + h.c., \tag{2.1}$$

$$\mathcal{L}^M = \frac{1}{2}\sum_{\alpha,\beta=e,\mu,\tau} M^R_{\alpha\beta}\overline{\nu^c_{\alpha R}}\nu_{\beta R} + h.c., \tag{2.2}$$

where L_α are the SM lepton doublets, $Y_{\alpha\beta}$ is the Yukawa coupling matrix, $M^R_{\alpha\beta}$ is a Majorana mass matrix for right-handed neutrinos and $\tilde{\phi} = i\sigma_2\phi^*$ using the Higgs doublet ϕ and the second Pauli matrix σ_2. The superscript c denotes the charge conjugated field defined by $\nu^c = C\bar{\nu}^T$ with the charge conjugation matrix C.

After electroweak symmetry breaking Eq. (2.1) induces Dirac neutrino masses, while Eq. (2.2) is a Majorana mass term for the right-handed neutrinos. Note that the latter violates total lepton number conservation, which is an accidental symmetry of the pure SM. In principle one could force the Majorana mass term to be absent, by imposing total lepton number conservation. In this case the neutrinos are of Dirac type as will be discussed in Sec. 2.1.1. However there do not exist compelling arguments for demanding a priori the conservation of lepton number. The presence of a right-handed Majorana neutrino mass rather provides an interesting and popular mechanism for explaining the smallness of the neutrino mass. We elaborate on this scenario in more detail in Sec. 2.1.2.

2.1.1. Dirac neutrinos

When assuming total lepton number conservation the Yukawa interaction, Eq. (2.1), is the only source of neutrino mass. After spontaneous electroweak symmetry breaking the neutral component of the Higgs acquires a non-zero vacuum expectation value $\langle\phi^0\rangle = v/\sqrt{2}$. Eq. (2.1) then contains the neutrino mass term

$$-\mathcal{L}^D \supset \sum_{\alpha,\beta=e,\mu,\tau} \overline{\nu_{\alpha L}} M^D_{\alpha\beta} \nu_{\beta R} + h.c., \tag{2.3}$$

where the mass matrix given by $M^D_{\alpha\beta} = v/\sqrt{2}Y_{\alpha\beta}$. The diagonalization of the mass matrix is achieved by unitary transformation matrices U^L, U^R in such a way that M^D becomes diagonal, i.e. $(U^{L\dagger} M^D U^R)_{ij} = \delta_{ij} m_{\nu_i}$. The transformation of the neutrino fields into the basis of mass eigenstates ν_1, ν_2, ν_3 is then given by

$$\nu_{\alpha L/R} = \sum_{k=1}^{3} U^{L/R}_{\alpha k} \nu_{kL/R} \tag{2.4}$$

and leads to

$$-\mathcal{L}^D_m = \sum_{i=1}^{3} m_{\nu_i} \overline{\nu_{iL}} \nu_{iR} + h.c. = \sum_{i=1}^{3} m_{\nu_i} \overline{\nu_i} \nu_i \tag{2.5}$$

with the Dirac field $\nu_i = \nu_{iL} + \nu_{iR}$.

Similarly, the diagonalization of the mass matrix for the charged lepton fields

$\ell' = e', \mu', \tau'$ gives the transformation

$$\ell'_{L/R} = \sum_{\ell=e,\mu,\tau} V^{L/R}_{\ell'\ell} \ell_{L/R}, \tag{2.6}$$

such that in the mass eigenstate basis e, μ, τ the charged lepton mass is diagonal. In the electroweak neutral current interaction the transformation matrices cancel each other due to their unitarity. The only term in the diagonalized Lagrangian, where those transformation matrices appear is the charged current coupling, which reads

$$\mathcal{L}_{CC} = \sum_{\ell=e,\mu,\tau} \frac{g}{\sqrt{2}} W^+_\mu \overline{\ell'_L} \gamma^\mu \nu_{\ell L} + h.c. \tag{2.7}$$

$$= \sum_{\ell=e,\mu,\tau} \sum_{k=1}^{3} \frac{g}{\sqrt{2}} W^+_\mu \overline{\ell_L} \gamma^\mu U_{\ell k} \nu_{kL} + h.c. \tag{2.8}$$

Here, we have defined the matrix in flavor space $U = V^{L\dagger} U^L$, which is called the Pontecorvo-Maki-Nakagawa-Sakata (PMNS) matrix after the works of Refs. [6, 36]. Since the only physical effect of mixing is in the charged current coupling, it is convenient to work in a basis, where the charged lepton mass is diagonal. The mixing is then considered to be present only in the neutrino fields. One therefore defines the neutrino flavor states ν_e, ν_μ, ν_τ such that the charged current interaction takes it simple form of Eq. (2.7) with the direct coupling to the charged lepton fields e, μ, τ. The neutrino mass matrix written in this basis is not diagonal. Performing the transformation into the mass eigenstates via the PMNS matrix according to $\nu_\alpha = U_{\alpha i} \nu_i$ results in a diagonal mass, but then the in the PMNS matrix appear in the charged current coupling.

Since the PMNS matrix is a 3×3 unitary matrix, it can be parametrized by three rotation angles and six complex phases. Except for the charged current term, where the PMNS matrix is present, the rest of the Lagrangian is invariant under a global phase shift of the charged lepton fields. One can thus absorb three complex phases by exploiting the freedom of choosing such a phase shift accordingly. In addition, one can redefine the Dirac neutrino fields and absorb two further complex phases. This is not possible with Majorana neutrinos. However, since those two phases are irrelevant for neutrino oscillations, we will ignore them even in the Majorana case. For more

details see for example Refs. [31, 33, 37]. We arrive at the parametrization

$$U = \begin{pmatrix} c_{12}c_{13} & s_{12}c_{13} & s_{13}e^{-i\delta} \\ -s_{12}c_{23} - c_{12}s_{13}s_{23}e^{i\delta} & c_{12}c_{23} - s_{12}s_{13}s_{23}e^{i\delta} & c_{13}s_{23} \\ s_{12}s_{23} - c_{12}s_{13}c_{23}e^{i\delta} & -c_{12}s_{23} - s_{12}s_{13}c_{23}e^{i\delta} & c_{13}c_{23} \end{pmatrix}, \tag{2.9}$$

where $s_{ij} = \sin\theta_{ij}$ and $c_{ij} = \cos\theta_{ij}$ with the mixing angles θ_i and the CP-violating phase δ. Neutrino oscillations will be discussed in Sec. 2.2 in more detail. We first turn to the case of Majorana neutrinos.

2.1.2. Majorna neutrinos

Without the assumption of total lepton number conservation the extension of the SM by right-handed neutrinos introduces the Majorana mass term in Eq. (2.2). Note that the quantum numbers of the left-handed neutrino field do not allow for an analogous Majorana mass term of the left-handed neutrinos. Such a term would require more model building effort, like for example introducing extra scalar triplets. See Refs. [28,34] for more details. In this brief discussion of Majorana neutrino masses we stick to the minimal SM extension of just adding right-handed neutrinos. Then, the two Lagrangian terms, Eqs. (2.2) and (2.3), can be rewritten into [28]

$$\mathcal{L}^D + \mathcal{L}^M \supset -\frac{1}{2}\overline{N_L^c} \begin{pmatrix} 0 & M^{D^T} \\ M^D & M^R \end{pmatrix} N_L + h.c. \tag{2.10}$$

by defining a vector consisting out of the six neutrino fields

$$N_L^T = \begin{pmatrix} \nu_{eL} & \nu_{\mu L} & \nu_{\tau L} & \nu_{eR}^c & \nu_{\mu R}^c & \nu_{\tau R}^c \end{pmatrix}. \tag{2.11}$$

One can block-diagonalize the 6×6 mass matrix of Eq. (2.10) by assuming the right-handed Majorana mass matrix to be much heavier than the Dirac mass term. This assumption is reasonable, since M^D is generated after electroweak symmetry breaking at low scale, while M^R could be related to a high-energy completion of the SM and therefore be at a high energy scale. The diagonalization yields a light and a heavy 3×3 Majorana mass matrix M_l, M_h. In the limit $M^R \gg M^D$ they are given by (see Ref. [28] and references therein)

$$M_l = -M^{D^T}(M_R)^{-1}M^D, \qquad M_h = M^R. \tag{2.12}$$

In this way one obtains three light Majorana neutrinos with their masses being the eigenvalues of M_l and three heavy Majorana neutrinos with the mass matrix M_R. It is important to point out that the mechanism presented here provides a reasonable explanation for the smallness of the three left-handed neutrino masses simply by assuming the masses of the right-handed neutrinos M^R to be much larger than the electroweak scale (which is the maximum vale of M^D as argued above). M_l can therefore be naturally pushed to the sub-eV scale. This interesting and well-studied mechanism known as seesaw mechanism [38–42].

Accordingly, the low-energy effective mass term of the left-handed neutrinos is given by

$$\mathcal{L}_{\text{eff}}^{M} = -\frac{1}{2} \sum_{\alpha,\beta=e,\mu,\tau} (M_l)_{\alpha\beta} \overline{\nu_{\alpha L}^{c}} \nu_{\beta L} + h.c. \tag{2.13}$$

The diagonalization is achieved by means of a unitary transformation matrix $\tilde{U}$ such that $(\tilde{U}^T M_l \tilde{U})_{ij} = \delta_{ij} m_{\nu_i}$ resulting in

$$\mathcal{L}_{\text{eff}}^{M} = -\frac{1}{2} \sum_{i=1}^{3} m_{\nu_i} \overline{\nu_{iL}^{c}} \nu_{iL} + h.c. = -\frac{1}{2} \sum_{i=1}^{3} m_{\nu_i} \overline{\nu_{i}^{c}} \nu_{i}, \tag{2.14}$$

where we have defined the Majorana neutrino field $\nu_i = \nu_{iL} + \nu_{iL}^c$ with the property $\nu_i^c = \nu_i$ implying that it is its own antiparticle.

Analogous to the Dirac case the mixing matrix for Majorana neutrinos is given by $U = V^{L\dagger} \tilde{U}$ and appears in the charged current interaction.

2.2. Neutrino oscillations

We have seen in the previous sections that the presence of a non-zero neutrino mass directly results in the mixing of neutrino mass and flavor eigenstates. This in turn manifests itself in the observable effect of neutrino oscillations. Conversely, the observation of neutrino oscillations provides a proof that neutrinos carry mass. In 2015, Takaaki Kajita from the Super-Kamiokande Collaboration [37] and Arthur B. McDonald from the Sudbury Neutrino Observatory (SNO) [43] Collaboration received jointly the Nobel prize [44] for the discovery of neutrino oscillations. In the following, we briefly discuss the concept of neutrino oscillations, since oscillation effects play a role in understanding the physical observables of the NMM.

We want to consider a neutrino source producing neutrinos of flavor α in some

distance L of a detector, which is sensitive to incoming neutrinos of flavor β. The probability of the flavor transition $\nu_\alpha \to \nu_\beta$ in vacuum can be calculated by the quantum mechanical amplitude according to

$$P_{\nu_\alpha \to \nu_\beta} = \left| \langle \nu_\beta | \nu_\alpha(t) \rangle \right|^2 = \left| \sum_{i=1}^{3} \sum_{\gamma=e,\mu,\tau} \langle \nu_\beta | \, U^*_{\alpha i} e^{-itE_i} U_{\gamma i} \, | \nu_\gamma \rangle \right|^2. \tag{2.15}$$

Note that the neutrino flavor states are no eigenstates of the Hamiltonian. The neutrino field has therefore to be transformed into the mass basis and back again, yielding two insertions of the PMNS matrix. This property causes the probability of detecting the neutrino in a certain flavor state to oscillate over time. The probability can now be further simplified by using $\langle \nu_\beta | \nu_\gamma \rangle = \delta_{\beta\gamma}$ and assuming a relativistic neutrino $t \approx L$ as well as a definite three-momentum which is the same for all contributing mass eigenstates. Using this assumption, one can write the neutrino energy approximately as $E_i \approx |\mathbf{p}| + \frac{m_i^2}{2|\mathbf{p}|} \approx |\mathbf{p}| + \frac{m_i^2}{2E}$ and obtain

$$\begin{aligned} P_{\nu_\alpha \to \nu_\beta} &= \left| \sum_{i=1}^{3} U^*_{\alpha i} e^{-iLE_i} U_{\beta i} \right|^2 = \left| \sum_{i=1}^{3} U^*_{\alpha i} e^{-iL|\mathbf{p}|} e^{-iL\frac{m_i^2}{2E}} e^{-iL\frac{\Delta m_{i1}^2}{2E}} U_{\beta i} \right|^2 \\ &= \left| \sum_{i=1}^{3} U^*_{\alpha i} e^{-iL\frac{\Delta m_{i1}^2}{2E}} U_{\beta i} \right|^2, \end{aligned} \tag{2.16}$$

where $\Delta m_{ij}^2 = m_i^2 - m_j^2$. The result of this simplified derivation of the oscillation probability agrees with the correct treatment accounting for the momentum spread of the neutrino and using the full quantum field theoretical formalism [31, 34].

Experiments are usually not sensitive to all oscillation phases $\Delta m_{ij}^2 L/(2E)$ simultaneously. The best sensitivity is achieved for $\Delta m_{ij}^2 L/(2E) \sim \mathcal{O}(1)$. If instead $\Delta m_{ij}^2 L/(2E) \gg 1$, the oscillation is averaged out so that the oscillation pattern can not be detected due to the finite detector resolution. An experiment with $\Delta m_{ij}^2 L/(2E) \ll 1$, on the other hand, could not measure flavor transitions at all. Let us assume, for example, that $\Delta m_{21}^2 L/(2E) \ll 1$ while $\Delta m_{31}^2 L/(2E) \approx \Delta m_{32}^2 L/(2E) \sim \mathcal{O}(1)$. This is reasonable, since the mass square differences indeed satisfy $|\Delta m_{21}^2| \ll |\Delta m_{31}^2| \approx |\Delta m_{32}^2|$. The oscillation probability then takes the simple form [33]

$$P_{\nu_\alpha \to \nu_\beta} \approx 4|U_{\alpha 3}|^2 |U_{\beta 3}|^2 \sin^2\left(\frac{\Delta m_{31}^2}{4E} L\right). \tag{2.17}$$

This case is applicable for atmospheric, accelerator and reactor experiments. The

quantity $\Delta m^2_{31} \sim 10^{-3}\,\mathrm{eV}^2$ is therefore also called the atmospheric mass square difference. For solar and very long baseline experiments, $\Delta m^2_{21} \sim 10^{-5}\,\mathrm{eV}^2$ is the relevant quantity, also called the solar mass square difference. From Eq. (2.17), one can see that the amplitude is determined by the matrix elements while the oscillation length is given by $L_{\mathrm{osc}} = 4\pi E/\Delta m^2_{31}$.

So far, we implicitly assumed that the neutrino stays in a coherent superposition of neutrino mass eigenstates. It is only justified as long as the path length L is much smaller than the coherence length $L_{\mathrm{coh}} = 4\sqrt{2}E^2\Delta L/|\Delta m^2|$ [31]. The coherency depends on the spatial uncertainties of the neutrino detection and production, referred to as ΔL. Once the path length becomes much larger, i.e. $L \gg L_{\mathrm{coh}}$, as it is the case for example in solar neutrino experiments, the oscillation probability is calculated via the incoherent sum

$$\begin{aligned} P^{\mathrm{incoh}}_{\nu_\alpha\to\nu_\beta} &= \sum_i P_{\nu_\alpha\to\nu_i}\cdot P_{\nu_i\to\nu_\beta} = \sum_i \left|\,\langle\nu_i|\nu_\alpha(t)\rangle\,\right|^2 \cdot \left|\,\langle\nu_\beta|\nu_i\rangle\,\right|^2 \\ &= \sum_i \left|U^*_{\alpha i} e^{-iL\frac{\Delta m^2_{i1}}{2E}}\right|^2 \cdot |U_{\beta i}|^2 = \sum_i |U_{\alpha i}|^2\cdot|U_{\beta i}|^2. \end{aligned} \tag{2.18}$$

Up to this point, we considered only neutrino oscillations in vacuum. When neutrinos travel through matter, they experience the effect of a matter potential induced by coherent forward scattering off electrons, protons and neutrons. While the neutral current interaction is the same for all flavors, only the electron neutrinos take part in the charged current scattering off electrons. The difference in the scalar potential among the flavors causes the eigenstates of the Hamiltonian and the mass eigenstates to be not identical anymore (which is the case in vacuum). This in turn effects the oscillation pattern and leads to a dependence on the matter density. Neutrinos that travel through a varying matter profile, like for example neutrinos produced inside the sun, can underlie resonant flavor transitions, which is called Mikheyev-Smirnov-Wolfenstein (MSW) effect [45, 46]. For more details see for example Ref. [33].

In order to conclude this brief discussion of neutrino oscillations, we want to point out that in the last decades many neutrino experiments have been developed. They determined the oscillation parameters to good precision. On-going experiments will even further improve the precision. For the analyses in this work, we use the global fit values of Ref. [47]. Since the value of the CP-violating phase δ in the PMNS matrix, Eq. (2.9), is not determined yet, we assume it to be zero for the purposes in this thesis.

2.3. Electromagnetic form factors

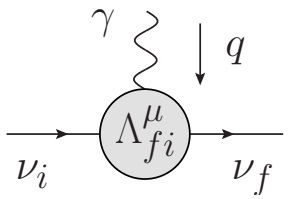

Figure 2.1.: The effective neutrino-photon vertex.

Since the neutrino is neutral, its electromagnetic properties appear only at loop level. A convenient way of studying these properties on a model-independent level is to consider the effective neutrino photon interaction. In the one-photon approximation, the effective electromagnetic interaction Hamiltonian is given by [28]

$$\mathcal{H}(x) = J_\mu(x)A^\mu(x) = \sum_{f,i=1}^{3} \overline{\nu_f}(x)\Lambda_\mu^{fi}\nu_i(x)A^\mu(x). \tag{2.19}$$

The indices $f, i \in \{1, 2, 3\}$ refer to the neutrino mass eigenstates, J_μ is the effective neutrino photon current and Λ_μ^{fi} is the corresponding vertex function. Within a certain model, it is obtained by applying the Feynman rules to diagrams of the type Fig. 2.1 and removing the neutrino spinors and the polarization vector of the photon. To be more precise, the neutrino part of the amplitude is given by

$$\langle \nu_f(p')|\, J_\mu(x)\, |\nu_i(p)\rangle = e^{i(p'-p)x}\bar{u}(p')\Lambda_\mu^{fi}(q)u(p), \tag{2.20}$$

where q is the four-momentum of the photon as indicated in the Feynman diagram in Fig. 2.1. The effective neutrino electromagnetic vertex function can be decomposed into Lorentz invariant bilinears. The most general form is [28]

$$\begin{aligned}\Lambda_\mu^{fi}(q) =& \mathcal{F}_1^{fi}(q^2)\left(\gamma_\mu - \frac{q_\mu \not{q}}{q^2}\right) + \mathcal{F}_2^{fi}(q^2)\frac{i\sigma_{\mu\nu}q^\nu}{(m_{\nu_f}+m_{\nu_i})} \\ &+ \mathcal{F}_3^{fi}(q^2)\frac{2q_\mu}{m_{\nu_f}+m_{\nu_i}} + \mathcal{G}_1^{fi}(q^2)\left(\gamma_\mu - \frac{q_\mu \not{q}}{q^2}\right)\gamma_5 \\ &+ \mathcal{G}_2^{fi}(q^2)\frac{i\sigma_{\mu\nu}q^\nu}{(m_{\nu_f}+m_{\nu_i})}\gamma_5 + \mathcal{G}_3^{fi}(q^2)\frac{2q_\mu}{m_{\nu_f}+m_{\nu_i}}\gamma_5,\end{aligned} \tag{2.21}$$

where $\mathcal{F}_k^{fi}$, $\mathcal{G}_k^{fi}$ are the neutrino electromagnetic form factors, i refers to the initial, f

to the final neutrino mass eigenstate and $\sigma^{\mu\nu} = i/4[\gamma^\mu, \gamma^\nu]$ as well as $\gamma_5 = i\gamma^0\gamma^1\gamma^2\gamma^3$ are matrices in Dirac space given by the Dirac matrices γ^μ.

For an appropriate definition of the magnetic moment μ and electric moment ϵ in terms of the form factors, one has to make sure that in the non-relativistic limit the classical definition is reproduced. The classical electric/magnetic moment describes the interaction of the spin with the electric/magnetic field $\mathbf{E}/\mathbf{B}$ according to the Hamiltonian [48]

$$\mathcal{H}^{\mu}_{\text{non-rel.}} = -\mu_B(0+a)\boldsymbol{\sigma}\cdot\mathbf{B}, \qquad \mathcal{H}^{\epsilon}_{\text{non-rel.}} = -\epsilon\boldsymbol{\sigma}\cdot\mathbf{E}, \tag{2.22}$$

where $\boldsymbol{\sigma}$ is the vector of Pauli matrices, $\mu_B = 2/(2m_e)$ is the Bohr magneton, m_e the electron mass and a is the anomalous magnetic moment. Since neutrinos are neutral, there is no tree-level electromagnetic interaction and the magnetic moment is thus given by its anomalous magnetic moment only. For electrons, for example, one has to replace $(0+a)$ with $(1+a)$. For the neutrino it is convenient to define $\mu := a\mu_B$ and call it the neutrino magnetic moment. One can show (see for example [48]) that the non-relativistic limit, Eq. (2.22), is reproduced by defining

$$\mu = i\frac{\mathcal{F}_2(q\simeq 0)}{m_{\nu_f}+m_{\nu_i}}, \qquad \epsilon = \frac{\mathcal{G}_2(q\simeq 0)}{m_{\nu_f}+m_{\nu_i}}. \tag{2.23}$$

In doing so, μ and ϵ are considered as matrices in flavor space, accounting for the possibility to have off-diagonal entries, also called transition moments. The corresponding high-energy effective Lagrangian terms are then given by (using Eqs. (2.19), (2.21) and (2.23))

$$\mathcal{L}^{\mu}_{\text{eff}} = -\mathcal{H}^{\mu}_{\text{eff}} = -\frac{1}{2}\frac{i\mathcal{F}_2(q^2)}{m_{\nu_f}+m_{\nu_i}}\bar{\nu}(x)\sigma^{\mu\nu}\nu(x)F_{\mu\nu}(x), \tag{2.24}$$

$$\mathcal{L}^{\epsilon}_{\text{eff}} = -\mathcal{H}^{\epsilon}_{\text{eff}} = -\frac{i}{2}\frac{\mathcal{G}_2(q^2)}{m_{\nu_f}+m_{\nu_i}}\bar{\nu}(x)\sigma^{\mu\nu}\gamma_5\nu(x)F_{\mu\nu}(x), \tag{2.25}$$

where $F_{\mu\nu}$ is the electromagnetic field tensor.

The Hamiltonian and the neutrino photon current are Hermitian, which implies for the vertex function $\Lambda_\mu(q) = \gamma^0\Lambda^\dagger_\mu(-q)\gamma^0$ and thus for the Dirac electric and magnetic moment matrices to be Hermitian as well. In the case of Majorana neutrinos there exists one additional contraction of the neutrino fields, because Majorana particles

are its own anti-particles. The amplitude is then given by

$$\langle \nu_f(p')|\, J_\mu(x)\, |\nu_i(p)\rangle = e^{i(p'-p)x}\left(\bar{u}(p')\Lambda_\mu^{fi}(q)u(p) - \bar{v}(p)\Lambda_\mu^{if}(q)v(p')\right). \tag{2.26}$$

Using the Majorana spinor relation $v = u^c = C\overline{u}^T$, one arrives at the Majorana vertex function

$$\Lambda_\mu^{Mfi} = \Lambda_\mu^{fi} + \mathcal{C}(\Lambda_\mu^{if})^T\mathcal{C}^{-1}. \tag{2.27}$$

In contrast to the Dirac electric and magnetic moment matrices, this results in μ and ϵ to be Hermitian and anti-symmetric, i.e. to be purely imaginary. In addition, if CP is conserved, one can show that either μ or ϵ is zero [28]. At this point, it is interesting to notice the possibility of discriminating between the Dirac and Majorana nature of the neutrino field by measuring the NMM, since for Majorana neutrinos only the off-diagonal components exist.

Early systematic studies of neutrino electromagnetic properties can be found in Refs. [19, 20, 49–54]. For a recent and detailed review see [28].

2.4. Effective neutrino magnetic moment

In general, neutrino experiments can not directly measure the electric and magnetic moment matrices in the basis of neutrino mass eigenstates as introduced in Eq. (2.23). Instead, the physical observable is a combination of the electric and magnetic moment. Furthermore, neutrino oscillation effects have to be taken into account, since the neutrino source typically emits neutrinos which are in a superposition of mass eigenstates [55, 56].

In App. B we explicitly derive the cross-section for the neutrino electromagnetic scattering process, which is the detection channel in laboratory experiments achieving the currently best sensitivity on NMMs. From the derivation in Eq. (B.25) one can infer that the cross-section is proportional to the combination $|\mu_{fi} - i\epsilon_{fi}|^2$. By simply inserting the spinor $u_-(p)$ for the initial neutrino in the scattering matrix element in Eq. (B.1), we implicitly assume the initial neutrino field to be in the pure neutrino mass eigenstate $|\nu_i\rangle$. Let us change this assumption by considering neutrinos that are produced in a specific flavor state $|\nu_\alpha\rangle$ instead. When the neutrinos are detected after traveling a distance $t \approx L$ between source and detector, at the time of detection the neutrino fields are in the quantum state $|\nu_\alpha(t)\rangle = \sum_k U_{\alpha k}^* e^{-iE_k L}\,|\nu_k\rangle$. The field contraction then yields $\overbrace{\nu\,|\nu_\alpha}(t)\rangle \propto \sum_k U_{\alpha k}^* e^{-iE_k L}$. Again using the approximation as

used in the derivation of Eq. (2.16) this implies for the cross-section

$$\sum_{f=1}^{3} \frac{d\sigma(\nu_\alpha \to \nu_f)}{dT} \propto \sum_{f=1}^{3} \left| \sum_{k=1}^{3} U_{\alpha k}^{*} e^{-iL\frac{\Delta m_{kf}^2}{2E}} \left(\mu_{fk} - i\epsilon_{fk}\right) \right|^2 =: \left(\mu_{\nu_\alpha}^{\text{eff}}\right)^2 , \tag{2.28}$$

where $\mu_{\nu_\alpha}^{\text{eff}}$ is the effective neutrino magnetic moment. Although ϵ and μ contribute to equal amount, it is sometimes also called 'magnetic moment'. For antineutrinos one has to substitute μ_{fk} with $-\mu_{fk}^{*}$, ϵ_{fk} with $-\epsilon_{fk}^{*}$ as well as U with U^{*} effectively leading to [28]

$$\left(\mu_{\bar{\nu}_\alpha}^{\text{eff}}\right)^2 = \sum_{f=1}^{3} \left| \sum_{k=1}^{3} U_{\alpha k}^{*} e^{iL\frac{\Delta m_{kf}^2}{2E}} \left(\mu_{fk} - i\epsilon_{fk}\right) \right|^2 , \tag{2.29}$$

i.e., the only difference is the different sign in front of the oscillation phase.

For reactor and accelerator experiments with short baselines, such that for the largest mass square difference $L \ll 2E/\Delta m^2$ holds, the effective magnetic moment can be simplified by the approximation

$$\left(\mu_{\nu_\alpha}^{\text{eff}}\right)^2 \approx \left(\mu_{\bar{\nu}_\alpha}^{\text{eff}}\right)^2 \approx \sum_{f=1}^{3} \left| \sum_{k=1}^{3} U_{\alpha k}^{*} \left(\mu_{fk} - i\epsilon_{fk}\right) \right|^2 , \tag{2.30}$$

which is the same for neutrinos and antineutrinos. In experiments with long baselines, $L \gg 2E/\Delta m^2$, on the other hand, neutrino oscillation is washed out as discussed in Sec. 2.2. This leads to

$$\left(\mu_{\nu_\alpha}^{\text{eff}}\right)^2 \approx \left(\mu_{\bar{\nu}_\alpha}^{\text{eff}}\right)^2 \approx \sum_{k=1}^{3} |U_{\alpha k}|^2 \sum_{f=1}^{3} \left|\left(\mu_{fk} - i\epsilon_{fk}\right)\right|^2 . \tag{2.31}$$

Finally, for solar neutrino experiments, matter effects have to be taken into account. Since in this case the neutrino path length corresponds to the Sun Earth distance, the long-baseline approximation, Eq. (2.31), can be applied, where one has to replace the PMNS matrix by the effective mixing matrix in matter at the point of neutrino production inside the sun.

Chapter 3

Experimental status

The presence of neutrino magnetic moments (NMMs) would lead to a rich phenomenology. In this chapter we give an overview over the most important observables and the resulting constraints on the NMM. Due to the numerous amount of observations effecting the NMM, we restrict ourself to those yielding the most stringent constraints. For more details we refer to Ref. [28, 57–59].

3.1. Terrestrial experiments

The most sensitive and widely used method for constraining NMMs is to measure the electron recoil due to elastic neutrino-electron scattering with reactor, solar or accelerator neutrinos. We calculate the corresponding electromagnetic scattering cross-section $(d\sigma/dT)_{\mathrm{NMM}}$ explicitly in App. B. In addition to the NMM induced scattering, the electroweak neutrino-electron scattering has to be taken into account. In the ultrarelativistic limit the Standard Model (SM) weak interaction conserves the helicity while in the NMM interaction the helicity is changed. Thus, the experimentally observed cross-section is a incoherent sum of both processes. The small interference term due to finite neutrino masses can be neglected [55, 60, 61]. The cross-section is therefore given by

$$\frac{d\sigma}{dT} = \left(\frac{d\sigma}{dT}\right)_{\mathrm{SM}} + \left(\frac{d\sigma}{dT}\right)_{\mathrm{NMM}}, \tag{3.1}$$

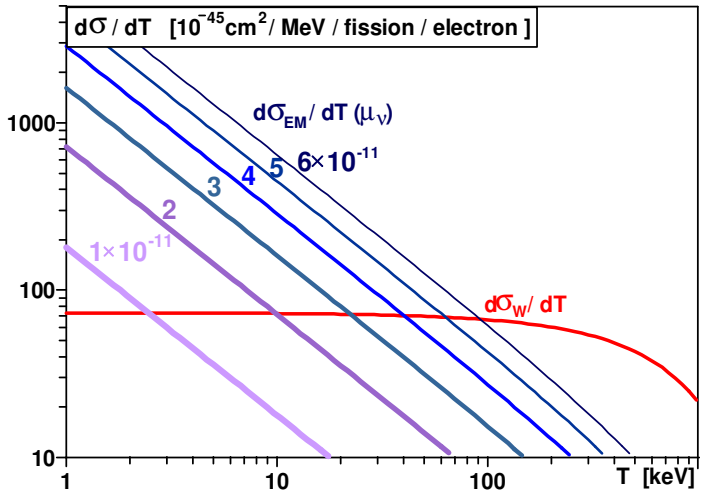

Figure 3.1.: Neutrino electron scattering cross-sections averaged over the typical antineutrino reactor spectrum. The colored lines correspond to the electromagnetic contribution for different NMM values near the current best upper limit of $2.9 \cdot 10^{-11}\mu_B$. The electroweak contribution is shown in red. Figure taken from [18].

where the SM electroweak cross-section, here for $\bar{\nu}_e$-e scattering, can be written as [62]

$$\left(\frac{d\sigma}{dT}\right)_{\mathrm{SM}} = \frac{G_F^2 m_e}{2\pi}\left[\left(1-\frac{T}{E_\nu}\right)^2 (1+2\sin^2\theta_W)^2 + 4\sin^2\theta_W - 2(1+2\sin^2\theta_W)\sin^2\theta_W \frac{m_e T}{E_\nu^2}\right]. \tag{3.2}$$

Here, G_F is the Fermi constant, θ_W the Weinberg angle, E_ν the neutrino energy and T the electron recoil energy. Fig. 3.1, taken from [18], shows the two cross-sections for different NMM values near the current experimental sensitivity. One can see, that it is necessary to build neutrino detectors that are able to measure electron recoils as low as $T < 100$ keV in order to further increase the sensitivity on NMMs. From Eqs. (3.2) and (B.25), one can estimate that the NMM signal exceeds the SM background if

$$T \lesssim \frac{\pi^2\alpha^2}{G_F^2 m_e^3}\left(\frac{\mu_\nu^{\mathrm{eff}}}{\mu_B}\right)^2 \tag{3.3}$$

is fulfilled [59]. Here, μ_ν^{eff} is the effective NMM (compare to Sec. 2.4) and μ_B the Bohr magneton. In principal, it is also possible to investigate the NMM via neutrino-nucleus scattering. It would, however, require a sensitivity to tiny atomic recoil

energies, e.g. for germanium ($Z = 32$) it would be around $T \sim 0.04$ eV, see Ref. [63] and references therein for more details.

The strategy of direct laboratory experiments is to decrease the electron recoil energy threshold while simultaneously suppressing background radiation by appropriate shielding methods. Constraints on the effective NMM can then be derived from the lack of any observable distortion in the electron recoil energy spectrum. The first experiment measuring the $\bar{\nu}_e$-e elastic scattering was performed in the 50's at the Savannah River Laboratory [64–66] (see also Ref. [59] for a short review of the detector details) using a detector consisting out of 15.9 kg plastic scintillator. For shielding against cosmic rays they used a 300 kg NaI crystal shielded by led and cadmium and enclosed in 2200 liters of liquid scintillator. They measured the recoil energy of electrons from the scattering with reactor antielectron neutrinos in the range 1.5 MeV to 4.5 MeV. An improved analysis in Ref. [62] hinted at a NMM signal of the order of $\mu^{\text{eff}}_{\bar{\nu}_e} \sim (2-4) \cdot 10^{-10} \mu_B$. However, in the 90's the two follow-up reactor experiments Krasnoyarsk [67] and Rovno [68] also measured the antielectron neutrino scattering and found upper limits for the effective NMM of $\mu^{\text{eff}}_{\bar{\nu}_e} < 2.4 \cdot 10^{-10} \mu_B$ and $\mu^{\text{eff}}_{\bar{\nu}_e} < 1.9 \cdot 10^{-10} \mu_B$ respectively, thereby ruling out the previous signal. The currently best laboratory limit was obtained by the GEMMA experiment [18] located close to the reactor core of the Kalinin Nuclear Power Plant. The higher sensitivity could be achieved by the use of a 1.5 kg high purity Germanium detector with an energy threshold as low as 2.8 keV. They obtained the upper limit

$$\mu^{\text{eff}}_{\bar{\nu}_e} < 2.9 \cdot 10^{-11} \mu_B \ (90\%\, CL). \tag{3.4}$$

The competing reactor experiment TEXONO [69] located at the Kuo-Sheng nuclear power plant also used a germanium detector with a threshold of 12 keV. They obtained an upper limit of $\mu^{\text{eff}}_{\bar{\nu}_e} < 7.4 \cdot 10^{-11} \mu_B$.

There have been several accelerator experiments that also searched for NMMs. For a review, see e.g. [28]. Among them the experiments BNL-E734 [70] and LSND [71] measured the elastic electron scattering of muon neutrinos, DONUT [72] measured ν_τ-e as well as $\bar{\nu}_\tau$-e scattering and LAMPF [73] was able to detect both, ν_e-e as well as ν_μ-e scattering. Due to the lower neutrino rate, those experiments are less sensitive

compared to the reactor experiments. They obtained the upper limits of

$$\mu^{\text{eff}}_{\nu_e} < 1.1 \cdot 10^{-9} \mu_B \quad \text{(LAMPF [73])}, \tag{3.5}$$

$$\mu^{\text{eff}}_{\nu_\mu} < 6.8 \cdot 10^{-10} \mu_B \quad \text{(LSND [71])}, \tag{3.6}$$

$$\mu^{\text{eff}}_{\nu_\tau} < 3.9 \cdot 10^{-7} \mu_B \quad \text{(DONUT [72])}. \tag{3.7}$$

Finally, it is also possible to constrain NMMs by data from solar neutrino experiments, for which the expected weak scattering rates are a priori unknown. As we have seen in Fig. 3.1, in the case of reactor antineutrinos, the dependence on the electron recoil energy is quite different between the weak and NMM induced scattering cross-sections. The NMM limits are therefore extracted by a shape analysis and are thus independent of the underlying standard solar model [56]. Data from the Super-Kamiokande neutrino experiment lead in this way to the limit on the solar effective NMM $\mu^{\text{eff}}_{\text{solar}} < 1.1 \cdot 10^{-10} \mu_B$ [74]. Very recently the solar neutrino experiment Borexino presented as a result of their physe-II data an even more stringent limit of $\mu^{\text{eff}}_{\text{solar}} < 2.8 \cdot 10^{-11} \mu_B$ [75], which is of comparable size to the GEMMA limit.

Several planned future experiments will potentially increase the sensitivity on NMMs down to values of the order of $\mu^{\text{eff}}_{\nu} \gtrsim 10^{-12} \mu_B$ [24–27].

3.2. Astrophysical observations

Neutrino-electron electromagnetic elastic scattering also play a role in core-collapse supernovae. As discussed in the previous section, the neutrino helicity is flipped in the NMM induced scattering process. If the neutrino is of Dirac nature, left-handed neutrinos are thereby transformed into right-handed neutrinos. Those in turn are sterile, i.e. do not participate in SM interactions, and can thus freely escape the interior of a supernova. The so induced energy-loss should not be larger than the total neutrino luminosity and hence leads to an upper bound of the order of $\mu^{\text{eff}}_{\nu} \lesssim (0.1 - 0.4) \cdot 10^{-11} \mu_B$ [76, 77], which is a slight improvement of the previous result in Ref. [78].

Another NMM-induced process is the radiative decay of a heavy neutrino into a lighter one by the the emission of a photon $\nu_i \to \nu_f + \gamma$. The Feynman diagram for this decay is depicted in Fig. 3.2 (a), where the blob denotes the effective electromagnetic neutrino interaction. From the magnetic and electric moment contribution to the

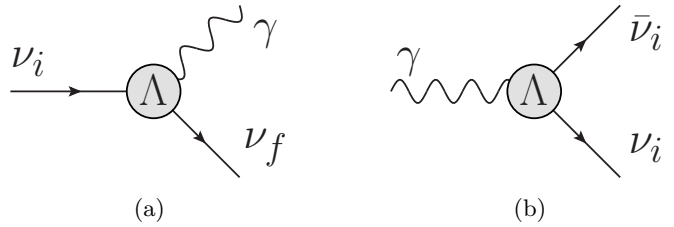

Figure 3.2.: Feynman diagrams for radiative decay (a) and plasmon decay (b) generated by the presence of a non-zero NMM.

vertex function Λ_μ^{fi}, see Eq. (2.21), one can derive the decay rate [79–81]

$$\Gamma_{\nu_i \to \nu_f + \gamma} = \frac{1}{8\pi}(|\mu_{fi}|^2 + |\epsilon_{fi}|^2)\left(\frac{m_{\nu_i}^2 - m_{\nu_f}^2}{m_{\nu_i}}\right)^3 . \tag{3.8}$$

The phase space is suppressed due to the small neutrino mass. The resulting limits are thus weaker than those obtained in other processes. From the absence of the decay photons one can derive limits from reactor, solar, supernova as well as cosmic background neutrinos. The latter give the dominant limit of $(|\mu_{fi}|^2 + |\epsilon_{fi}|^2)^{1/2} < 10^{-11}(eV/m_\nu)^{9/4}\mu_B$, see also Refs. [28, 81] and references therein. Note that this combination of the electric and magnetic moments is different than the effective NMM discussed in the context of neutrino-electron scattering. For comparing the upper limits one has to account for the PMNS matrix, the neutrino energy, the neutrino path length and the mass square differences according to Eq. (2.28).

The more interesting process for constraining NMMs is the plasmon decay $\gamma^* \to \bar{\nu}_i + \nu_i$, shown in Fig. 3.2 (b). It is kinematically allowed in very dense media, where a dispersion relation of $\omega^2 - \mathbf{k}^2 > 0$ makes the photon to behave like a particle with an effective mass. This process was first studied in Ref. [82] in the context of solar energy-loss channels. Demanding the energy-loss via plasmon decay not to exceed the standard solar model luminosity gives the upper limit $(\sum_{ij} |\mu_{ij}|^2 + |\epsilon_{ij}|^2)^{1/2} < 4 \cdot 10^{-10}\mu_B$. A stronger constraint is obtained from red giant stars in globular clusters. The helium burning inside the core depends sensitively on the temperature. The energy-loss for a high plasmon decay rate would lead to a cooling and a delay of the helium ignition. This in turn would imply a larger core mass which is in conflict with observations. The resulting NMM limit is even stronger than those from direct laboratory experiments. However, as the other constraints presented in

this section, it is inly an indirect limit, i.e. astrophysical model-dependent. First derived in Refs. [83, 84], the updated limit is [85]

$$\sqrt{\sum_{ij}\left(|\mu_{ij}|^2+|\epsilon_{ij}|^2\right)} < 2.6\cdot 10^{-12}\mu_B \ (68\%\, CL). \tag{3.9}$$

The authors of Ref. [86] showed that large plasmon decay rates not only effect the time scale of helium burning, but also qualitatively change the structure and evolution of stars. They estimated the sensitivity of those effects on the NMM to be of the order $(2-4)\cdot 10^{-11}\mu_B$.

When charged particles move with a velocity greater than the speed of light inside the environmental medium, they emit Cherenkov radiation. The same is true for neutrinos with a non-zero NMM. The Cherenkov radiation process is helicity flipping, analogous to the radiative decay $\nu_L \to \nu_R + \gamma$. It was first studied in Ref. [87] in the context of solar neutrinos. It was found that the resulting energy-loss of solar neutrinos is not efficient enough for reducing the solar neutrino flux significantly. Later in Ref. [88] it was shown that although it is a small effect, it can have an impact on core-collapse supernova. Cherenkov radiation for Dirac neutrinos implies that more energy is carried away due to the helicity flip which transforms the left-handed active neutrinos into right-handed sterile neutrinos. By requiring that the energy-loss of this mechanism is less than the total neutrino luminosity of a typical core-collapse supernovae, the authors of Ref. [88] found an upper limit for the Dirac diagonal magnetic dipole moment of $2\cdot 10^{-14}\mu_B$.

Let us finally mention the studies on neutrino spin-flavor precession [19, 89–91]. Neutrinos propagating in an electromagnetic field are effected by an effective potential similar to matter effects in the context of neutrino oscillations, see Sec. 2.2. The potential is induced by the coherent forward elastic (NMM-induced) scattering and depends on the electric and magnetic moments. It is especially interesting to consider Majorana neutrinos, since the NMM interaction generates ν-$\bar{\nu}$ transitions (due to the chirality flip). In this way, one can derive bounds on the Majorana transition moments from the measured solar neutrino flux. For more details and a theoretical description of this process see Ref. [28] and references therein.

Chapter 4

Neutrino magnetic moment predictions

In view of the experimental sensitivity on neutrino magnetic moment (NMM) signals, we want to investigate theoretical frameworks predicting NMM values of observable size. Note that in the pure Standard Model (SM) neutrinos are massless and the NMM is thus zero. Since it is by now considered as an experimental fact that neutrinos are massive, in the following, we refer by 'SM' to those minimally extended SM frameworks allowing either for massive Majorana neutrinos or massive Dirac neutrinos, respectively, as introduced in Sec. 2.1. In this chapter, we start by studying the NMM in those SM extensions in Sec. 4.1. We then analyze and classify generic NMM couplings in Sec. 4.2. The two simplest scenarios which, at first sight, seem to be suitable for generating large NMMs are discussed in Secs. 4.3 and 4.4, thereby applying and cross-checking our results of Sec. 4.2.

4.1. Neutrino magnetic moments in the Standard Model

The computation of the NMM in the SM at one loop order was already done in the literature, see for example Refs. [19–22]. In order to understand the calculation in full detail, cross-check our computation procedure as well as compare the outcome to other models we explicitly derive and reproduce the former results in this section. To begin with, we present the calculation, assuming three right-handed neutrinos leading to Dirac neutrino masses. Afterwards, we explain the difference for the case of Majorana neutrinos. We stick to minimal extensions of the SM in the sense that we just assume the Dirac/Majorana nature of the neutrino without accounting for possible additional contributions that could for example emerge from an extended (model-dependent) scalar sector.

4.1.1. Dirac neutrinos

The six Feynman diagrams contributing to the NMM, when evaluating diagrams at one loop order in Feynman gauge are depicted in Fig. 4.1. First of all, we start by calculating the neutrino-photon vertex function Λ_μ^{fi}, where i refers to the initial and f to the final neutrino flavor. This vertex function was already introduced in Eq. (2.21). It is given by the coherent sum of all contributing Feynman diagrams. Applying the SM Feynman rules as summarized in App. A we arrive at the contributions D_x with x referring to the corresponding Feynman diagram in Fig. 4.1. For the explicit loop-integrals, see Eqs. (D.1) - (D.6) in App. D.

Here, we are only interested in the electric and magnetic dipole moments. For this purpose, one can extract from the full vertex function,

$$\Lambda_\mu^{fi} = \sum_{x=1}^{6} D_x, \tag{4.1}$$

the contribution of a single form factor by using appropriate projection operators. The relevant form factors F_2^{fi} and G_2^{fi} are then obtained from the Dirac trace

$$F_2^{fi} = \mathrm{tr}\left[P_{F_2}\Lambda_\mu^{fi}\right], \qquad G_2^{fi} = \mathrm{tr}\left[P_{G_2}\Lambda_\mu^{fi}\right]. \tag{4.2}$$

The explicit derivation of the projection operators P_{F_2} , P_{G_2} can be found in App. C.

From the form factors one can directly calculate the magnetic and electric dipole moment matrices by taking the limit $q^2 \to 0$ according to Eq. (2.23). As in the rest of this work we use `Mathematica Package-X` [92] for the analytical computation of one loop integrals. The result for Dirac neutrinos at first order in the neutrino mass is

$$\mu_{fi}^D = \frac{3eG_F(m_{\nu_f} + m_{\nu_i})}{16\sqrt{2}\pi^2} \sum_{l=e,\mu,\tau} f(a_l) U_{lf}^* U_{li}, \tag{4.3}$$

$$\epsilon_{fi}^D = \frac{3ieG_F(m_{\nu_f} - m_{\nu_i})}{16\sqrt{2}\pi^2} \sum_{l=e,\mu,\tau} f(a_l) U_{lf}^* U_{li}, \tag{4.4}$$

with the loop function

$$f(a_l) = \frac{1}{2}\left(1 + \frac{1}{1-a_l} - \frac{2a_l}{(1-a_l)^2} - \frac{2a_l^2 \ln a_l}{(1-a_l)^3}\right), \tag{4.5}$$

where $G_F = \sqrt{2}g_2^2/(8M_W^2)$ is the Fermi constant, U_{li} the PMNS matrix and $a_l = (m_l/M_W)^2$

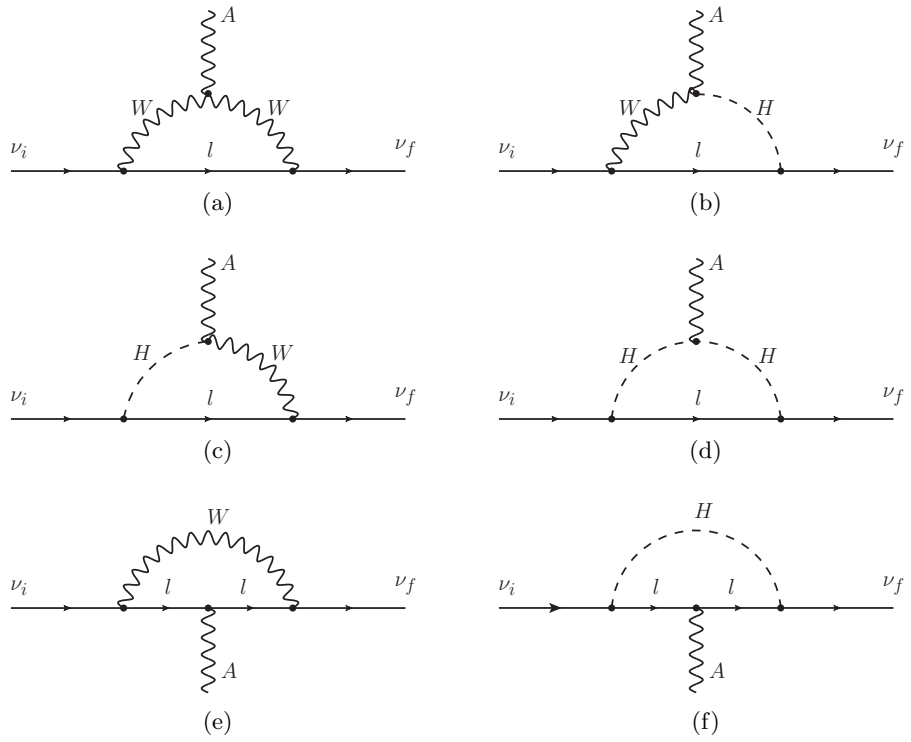

Figure 4.1.: Feynman diagrams contributing to the vertex function Λ_μ^{fi}.

is the ratio between the charged lepton and the W boson mass.

The diagonal entries of the Dirac electric dipole moments are zero in the SM, while for the magnetic dipole moment we can use $\sum_l U_{li}^* U_{li} = \sum_l |U_{li}|^2 = 1$ due to the unitarity of the neutrino mixing matrix. With $f(a_l) \approx 1$ one obtains the well-known result (e.g. compare to [19–22])

$$\mu_{ii}^D \approx \frac{3eG_F m_{\nu_i}}{8\sqrt{2}\pi^2} \approx 3.2 \times 10^{-20} \mu_B \left(\frac{m_{\nu_i}}{0.1 \text{ eV}}\right), \tag{4.6}$$

which is highly suppressed due to the smallness of the neutrino mass. This prediction is about nine orders of magnitude below the currently best direct laboratory upper bound, see Eq. (3.4), even for neutrino masses of $m_\nu \sim 0.2$ eV which is just below current experimental bounds [5].

For the transition dipole moments one can use the unitarity relation $\sum_l U_{lf}^* U_{li} = 0$. Taking into account the expansion $f(a_l) \approx 1 - \frac{a_l}{2}$, the leading order is now proportional

to a_l

$$\mu^D_{fi} \approx -\frac{3eG_F(m_{\nu_f}+m_{\nu_i})}{32\sqrt{2}\pi^2}\sum_l a_l U^*_{lf}U_{li} \sim \mathcal{O}\left(10^{-24}\right)\mu_B, \tag{4.7}$$

$$\epsilon^D_{fi} \approx -i\frac{3eG_F(m_{\nu_f}-m_{\nu_i})}{32\sqrt{2}\pi^2}\sum_l a_l U^*_{lf}U_{li} \sim \mathcal{O}(10^{-24})\mu_B. \tag{4.8}$$

Here we have used that the ratio of charged lepton mass to W boson mass is at most $a_l \leq a_\tau = (m_\tau/M_W)^2 \approx 5\times 10^{-4}$ as well as a neutrino mass of $m_\nu \sim 0.1\,\text{eV}$. This additional suppression is analogous to the GIM-mechanism, suppressing flavor-changing neutral currents in hadronic interactions.

As a cross-check we also performed the calculation in unitarity gauge, where only the diagrams (a) and (e) of Fig. 4.1 contribute. The loop-integrals are the same as in Eqs. (D.1) and (D.5) with the W boson propagator in Feynman gauge replaced by the unitarity gauge propagator given in App. A.1. The result agrees with the Feynman gauge computation.

4.1.2. Majorana neutrinos

Because each Majorana fermion is its own anti-particle, we have to take into account additional field contractions for the case of Majorana neutrinos. Hence we need to calculate the extra contributions and add it to those for the Dirac case. A general treatment, how to compute all relevant Majorana Feynman diagrams is explained in App. A.3. However, in this case, there is a simple alternative. Given the Dirac dipole moments of the previous section, we can already read off the NMM matrices for Majorana neutrinos from the relation of the vertex function in Eq. (2.27). This equation implies for the electric and magnetic form factors

$$\begin{aligned}\mathcal{F}_2^{Mfi}\frac{i\sigma_{\mu\nu}q^\nu}{(m_{\nu_f}+m_{\nu_i})} &= \mathcal{F}_2^{fi}\frac{i\sigma_{\mu\nu}q^\nu}{(m_{\nu_f}+m_{\nu_i})} + \mathcal{C}\left(\mathcal{F}_2^{if}\frac{i\sigma_{\mu\nu}q^\nu}{(m_{\nu_f}+m_{\nu_i})}\right)^T\mathcal{C}^{-1}\\ &= \left(\mathcal{F}_2^{fi}-\mathcal{F}_2^{if}\right)\frac{i\sigma_{\mu\nu}q^\nu}{(m_{\nu_f}+m_{\nu_i})},\end{aligned} \tag{4.9}$$

$$\begin{aligned}\mathcal{G}_2^{Mfi}\frac{i\sigma_{\mu\nu}q^\nu}{(m_{\nu_f}+m_{\nu_i})} &= \mathcal{G}_2^{fi}\frac{i\sigma_{\mu\nu}q^\nu}{(m_{\nu_f}+m_{\nu_i})}\gamma_5 + \mathcal{C}\left(\mathcal{F}_2^{if}\frac{i\sigma_{\mu\nu}q^\nu}{(m_{\nu_f}+m_{\nu_i})}\gamma_5\right)^T\mathcal{C}^{-1}\\ &= \left(\mathcal{G}_2^{fi}-\mathcal{G}_2^{if}\right)\frac{i\sigma_{\mu\nu}q^\nu}{(m_{\nu_f}+m_{\nu_i})}\gamma_5,\end{aligned} \tag{4.10}$$

where we have used the defining relation of the charge conjugation matrix $\mathcal{C}^{-1}\gamma_\mu\mathcal{C} = -\gamma_\mu^T$ as well as

$$\mathcal{C}\sigma_{\mu\nu}^T\mathcal{C}^{-1} = -\sigma_{\mu\nu}, \qquad \mathcal{C}(\sigma_{\mu\nu}\gamma_5)^T\mathcal{C}^{-1} = -\sigma_{\mu\nu}\gamma_5. \tag{4.11}$$

We therefore obtain the Majorana NMM matrices from the simple relation

$$\mu_{fi}^M = \mu_{fi}^D - \mu_{if}^D, \qquad \epsilon_{fi}^M = \epsilon_{fi}^D - \epsilon_{if}^D. \tag{4.12}$$

Using the result of the previous section one immediately arrives at

$$\mu_{fi}^M = i\frac{3eG_F(m_{\nu_f} + m_{\nu_i})}{8\sqrt{2}\pi^2}\sum_l f(a_l)\mathrm{Im}\left(U_{lf}^* U_{li}\right), \tag{4.13}$$

$$\epsilon_{fi}^M = i\frac{3eG_F(m_{\nu_f} - m_{\nu_i})}{8\sqrt{2}\pi^2}\sum_l f(a_l)\mathrm{Re}\left(U_{lf}^* U_{li}\right). \tag{4.14}$$

As expected for Majorana neutrinos the electric and magnetic moment matrices are antisymmetric and purely imaginary (see Sec. 2.3). Hence, there exist no diagonal dipole moments. For the transition moments, $i \neq f$, one can use the unitarity of the PMNS matrix as in the Dirac case. At leading order in $a_l = (m_l/M_W)^2$ the Majorana NMM matrices are

$$\mu_{fi}^M = -i\frac{3eG_F(m_{\nu_f} + m_{\nu_i})}{16\sqrt{2}\pi^2}\sum_l a_l\mathrm{Im}\left(U_{lf}^* U_{li}\right), \tag{4.15}$$

$$\epsilon_{fi}^M = -i\frac{3eG_F(m_{\nu_f} - m_{\nu_i})}{16\sqrt{2}\pi^2}\sum_l a_l\mathrm{Re}\left(U_{lf}^* U_{li}\right). \tag{4.16}$$

The Majorana moments are of similar size than the transition magnetic and electric moments in the Dirac case. However, one can not directly compare them due to the difference of the PMNS matrix.

As a cross-check we also compute the Majorana contribution by applying the Feynman rules of App. A.3. In doing so, we use the unitarity gauge and find the expressions for the two additional Majorana loop-integrals, emerging from the Feynman diagrams depicted in Fig. 4.2. They can be found in Eqs. (D.7) and (D.8) in App. D. The other two contributing diagrams are those of Fig. 4.1 (a) and (e). The corresponding loop-integrals are Eqs. (D.1) and (D.5) with the W boson propagator replaced by the one for unitarity gauge. Summing over those four diagrams and projecting out the form factors, taking the limit $q^2 \to 0$ and expanding in neutrino mass as for the Dirac case,

we get the same result as via using Eq. (4.12).

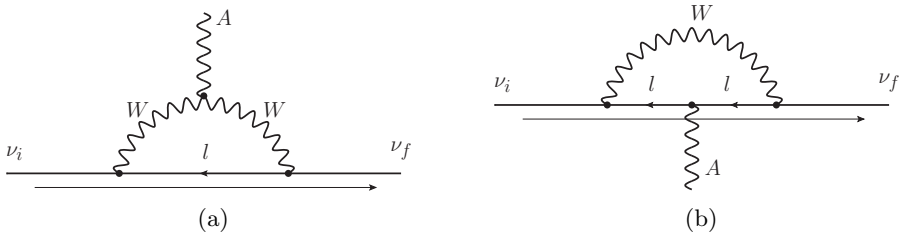

Figure 4.2.: Additional Majorana Feynman diagrams contributing to the vertex function for Majorana neutrinos Λ_μ^{Mfi}. The extra line below the fermion line indicates the fermion number flow.

4.2. Classification of neutrino magnetic moment couplings

Let us now turn to neutrino magnetic and electric dipole moments beyond the SM. In order to understand what kind of NMM contributions could exist, a systematic analysis is presented in this section. We classify the possible generic couplings, that can lead to NMMs with special interest in avoiding the proportionality to the neutrino mass, that is responsible for the small SM prediction.

4.2.1. Chirality flip

In this sense it is an important observation that the NMM interaction is chirality changing, which can be seen by considering the effective electric and magnetic dipole moment operators as introduced in Eqs. (2.24) and (2.25). The relevant Dirac matrices are $\sigma_{\mu\nu}$ and $\sigma_{\mu\nu}\gamma_5$. Sandwiching those between neutrino spinors of same chirality gives

$$\overline{\nu}_{L/R}\sigma_{\mu\nu}\nu_{L/R} = \overline{\nu}P_{R/L}\sigma_{\mu\nu}P_{L/R}\nu = \overline{\nu}\sigma_{\mu\nu}P_{R/L}P_{L/R}\nu = 0, \tag{4.17}$$

$$\overline{\nu}_{L/R}\sigma_{\mu\nu}\gamma_5\nu_{L/R} = \overline{\nu}P_{R/L}\sigma_{\mu\nu}\gamma_5P_{L/R}\nu = \overline{\nu}\sigma_{\mu\nu}\gamma_5P_{R/L}P_{L/R}\nu = 0. \tag{4.18}$$

Therefore, neutrinos taking part in the NMM interaction need to be of different chirality. Note that this also holds for Majorana neutrinos, with the definition $\nu = \nu_L + \nu_R = \nu_L + \nu_L^C$. A pictorial way to understand this property is to look at the Feynman diagram in the basis of chiral fermions, i.e. treating the fermions as massless with the mass terms of the Lagrangian as two-point interactions. For the generation

of a NMM at one-loop level, one necessarily needs a charged fermion F inside the loop. Additionally there has to be at least one charged boson field B (scalar or vector) for closing the loop appropriately. In this picture, the necessary chirality flip implies the need of a mass insertion either at the internal fermion line or at one of the external neutrino legs as depicted in Fig. 4.3.

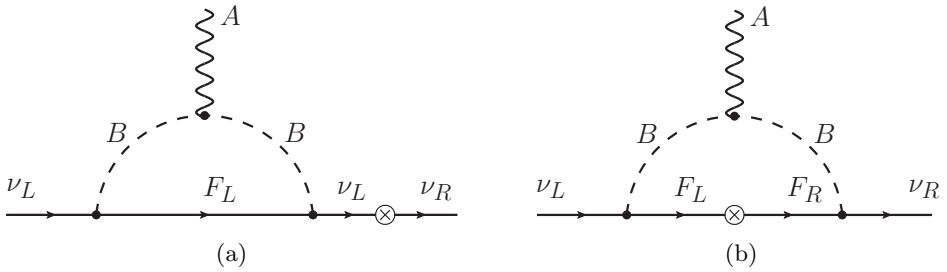

Figure 4.3.: Generic NMM Feynman diagrams in the chiral basis, treating fermion mass contributions as two-point vertices indicated with a cross. Since the effective NMM operator is chirality flipping, one needs a mass insertion either at one of the external legs as in (a) or at the internal fermion line, figure (b). Note that there are additional diagrams with the photon line attached to the internal fermion.

Following this line of thought, one understands why the SM prediction is proportional to the neutrino mass. Due to the absence of right-handed electroweak charged current interactions Feynman diagrams of the type in Fig. 4.3 (b) are not present in the SM. All contributing NMM diagrams include the neutrino mass insertion at one of the external legs as depicted in Fig. 4.3 (a). Accordingly, the NMM is proportional to the neutrino mass. Avoiding this proportionality is only possible, when introducing couplings to both, the left-handed and the right-handed neutrino field simultaneously.

4.2.2. Generic couplings for Dirac neutrinos

As discussed in the previous section, generating a neutrino magnetic moment at one loop requires at least one charged fermion F plus either a charged scalar S or a charged vector particle V_μ in the loop. Note that F, due to its charge, has to be a Dirac fermion with $F = F_L + F_R$. For the same reason, S and V_μ have to be complex fields. We only want to account for renormalizable and Lorentz invariant interactions. Ignoring the $SU(2)$ structure for the moment, these requirements lead directly to four different Lorentz invariant generic couplings (and their hermitian conjugates), namely $\bar{\nu}_L F_R S$, $\bar{\nu}_R F_L S$, $\bar{\nu}_L \gamma_\mu F_L V^\mu$, $\bar{\nu}_R \gamma_\mu F_R V^\mu$.

We assume a right-handed as well as a left-handed coupling simultaneously[1]. In this way, one also obtains contributions that avoid the proportionality to the neutrino mass (see Sec. 4.2.1). We thus start with the following interaction Lagrangian for the scalar case

$$\mathcal{L}_{\text{int, scalar}} = g_{ij}\bar{\nu}_i P_L F_j S + h_{ij}\bar{\nu}_i P_R F_j S + \text{h.c.}, \tag{4.19}$$

and for the vector case

$$\mathcal{L}_{\text{int, vector}} = g_{ij}\bar{\nu}_i \not{V} P_L F_j + h_{ij}\bar{\nu}_i \not{V} P_R F_j + \text{h.c.} \tag{4.20}$$

Here, we are working in the basis of neutrino mass eigenstates, i.e. the indices i, j refer to the three neutrino mass states. By assigning such an index also to the fermion, we assume that it comes with three generations and that there is an implicit sum over i and j. This is model-dependent and does not necessarily have to be the case. If one wants to introduce a vector-like fermion with the same coupling to all flavors, one should drop the index j from the fermion field as well as from the coupling matrices g_{ij}, h_{ij}.

The computation of the electric and magnetic moment matrices is performed as for the SM calculation of Sec. 4.1.1. The photon couplings are assumed to be the same as in the SM. Note that this could in principle be a restriction to the model-independent generic case, especially for the vector-photon coupling. For the application to models with an enlarged gauge-sector, one therefore has to make sure to use the correct gauge-invariant Feynman rules. In the following we use the unitarity gauge. For the calculation with scalar couplings, the Feynman diagrams are essentially the same as in Fig. 4.1 (d), (f), when exchanging the Goldstone boson and the charged lepton by the generic scalar and fermion. They lead to the loop integrals in Eqs. (D.9), (D.10) in App. D. For the vector couplings, the Feynman diagrams are analogous to to those in Fig. 4.1 (a), (e) and lead to the loop integrals in Eqs. (D.11), (D.12). Note that the charges of the scalar/vector and fermion have to fulfill $Q_F = -Q_{V/S}$ due to charge conservation. The electric and magnetic dipole moment matrices are obtained via summing over the loop integrals $D_a + D_b$, performing the integration, projecting out the corresponding form factors, taking the limit $q^2 \to 0$ and finally expanding up to first order in neutrino mass, analogous to Sec. 4.1.1. The resulting NMM matrices are summarized in Sec. 4.2.4.

[1] This assumption can later simply be dropped by sending the left- or right-handed coupling to zero in the final result.

4.2.3. Generic couplings for Majorana neutrinos

For completeness we also derive the NMM matrices in the case of Majorana neutrinos. The discussion for Dirac neutrinos in the previous section also apply to this case where the right-handed neutrino given by the charge conjugated field $\nu_R = P_R\nu = \nu_L^c$. The difference for Majorana neutrinos is that we now need to include additional contributions. As for the SM calculation, those can be obtained using the Majorana Feynman rules of App. A.3. For the calculation of the NMM with vector particles the contributing diagrams are the same as in Fig. 4.2 with the internal particles exchanged by the generic vector and fermion. For the scalar case, one also has to exchange the vector boson line with the one for a scalar particle.

Applying the Feynman rules for the generic scalar and vector couplings then lead to the loop integrals depicted in Eqs. (D.13)-(D.16) in App. D.

The NMM matrices for Majorana neutrinos are obtained in the same way as for Dirac neutrinos, but now summing over the two Majorana and Dirac loop integrals $D_a + D_b + D_a^M + D_b^M$. Applying the computation procedure described in the previous section we arrive at the electric and magnetic moment matrices as summarized in Sec. 4.2.4. As a cross-check we derive the Majorana NMM matrices also from the relation derived in Eq. (4.12). We arrive at the same results.

4.2.4. Results and discussion

Tab. 4.1 contains the list of electric and magnetic dipole moment matrices obtained from the generic model-independent couplings, as introduced in the previous sections. The results contain the NMM contributions generated by scalar as well as vector couplings, for Dirac as well as Majorana neutrinos and categorize the contributions according to their power in neutrino mass. For better readability, the full mass dependence is hidden in the loop functions $f_{0/1}^{S/V}$ that we define for the scalar and vector case and for the zeroth and first order in neutrino mass, respectively. The normalization is chosen such that they equal to one, if the masses of the particles running in the loop are of same size. The loop functions depend only on the mass

ratio $a_l = m_{F_l}/m_S$ or $a_l = m_{F_l}/m_V$, respectively, and are given by

$$f_0^S(a) = 2a\left(\frac{1}{a^2-1} - \frac{\log a^2}{(a^2-1)^2}\right), \tag{4.21}$$

$$f_1^S(a) = 3\left(\frac{1}{a^2-1} + \frac{2}{(a^2-1)^2} - \frac{2a^2\log a^2}{(a^2-1)^3}\right), \tag{4.22}$$

$$f_0^V(a) = \frac{2a}{5}\left(1 - \frac{3}{a^2-1} + \frac{3a^2\log a^2}{(a^2-1)^2}\right), \tag{4.23}$$

$$f_1^V(a) = \frac{3}{5}\left(1 - \frac{1}{a^2-1} - \frac{2a^2}{(a^2-1)^2} + \frac{2a^4\log a^2}{(a^2-1)^3}\right). \tag{4.24}$$

		$\mathcal{O}(m_\nu^0)$	$\mathcal{O}(m_\nu^1)$
scalar	$\mu_{fi}^D =$	$-\frac{eQ_S}{64\pi^2 m_S}(g_{fl}h_{il}^* + g_{il}^*h_{fl})f_0^S(a_l)$	$-\frac{eQ_S(m_{\nu_f}+m_{\nu_i})}{384\pi^2 m_S^2}(g_{fl}g_{il}^* + h_{fl}h_{il}^*)f_1^S(a_l)$
	$\epsilon_{fi}^D =$	$-i\frac{eQ_S}{64\pi^2 m_S}(g_{fl}h_{il}^* - g_{il}^*h_{fl})f_0^S(a_l)$	$+i\frac{eQ_S(m_{\nu_f}-m_{\nu_i})}{384\pi^2 m_S^2}(g_{fl}g_{il}^* - h_{fl}h_{il}^*)f_1^S(a_l)$
	$\mu_{fi}^M =$	$-i\frac{eQ_S}{32\pi^2 m_S}\mathrm{Im}[g_{fl}h_{il}^* + g_{il}^*h_{fl}]f_0^S(a_l)$	$-i\frac{eQ_S(m_{\nu_f}+m_{\nu_i})}{192\pi^2 m_S^2}\mathrm{Im}[g_{fl}g_{il}^* + h_{fl}h_{il}^*]f_1^S(a_l)$
	$\epsilon_{fi}^M =$	$-i\frac{eQ_S}{32\pi^2 m_S}\mathrm{Re}[g_{fl}h_{il}^* - g_{il}^*h_{fl}]f_0^S(a_l)$	$+i\frac{eQ_S(m_{\nu_f}-m_{\nu_i})}{192\pi^2 m_S^2}\mathrm{Re}[g_{fl}g_{il}^* - h_{fl}h_{il}^*]f_1^S(a_l)$
vector	$\mu_{fi}^D =$	$-\frac{5eQ_V}{64\pi^2 m_V}(g_{fl}h_{il}^* + g_{il}^*h_{fl})f_0^V(a_l)$	$+\frac{5eQ_V(m_{\nu_f}+m_{\nu_i})}{128\pi^2 m_V^2}(g_{fl}g_{il}^* + h_{fl}h_{il}^*)f_1^V(a_l)$
	$\epsilon_{fi}^D =$	$+i\frac{5eQ_V}{64\pi^2 m_V}(g_{fl}h_{il}^* - g_{il}^*h_{fl})f_0^V(a_l)$	$+i\frac{5eQ_V(m_{\nu_f}-m_{\nu_i})}{128\pi^2 m_V^2}(g_{fl}g_{il}^* - h_{fl}h_{il}^*)f_1^V(a_l)$
	$\mu_{fi}^M =$	$-i\frac{5eQ_V}{32\pi^2 m_V}\mathrm{Im}[g_{fl}h_{il}^* + g_{il}^*h_{fl}]f_0^V(a_l)$	$+i\frac{5eQ_V(m_{\nu_f}+m_{\nu_i})}{64\pi^2 m_V^2}\mathrm{Im}[g_{fl}g_{il}^* + h_{fl}h_{il}^*]f_1^V(a_l)$
	$\epsilon_{fi}^M =$	$+i\frac{5eQ_V}{32\pi^2 m_V}\mathrm{Re}[g_{fl}h_{il}^* - g_{il}^*h_{fl}]f_0^V(a_l)$	$+i\frac{5eQ_V(m_{\nu_f}-m_{\nu_i})}{64\pi^2 m_V^2}\mathrm{Re}[g_{fl}g_{il}^* - h_{fl}h_{il}^*]f_1^V(a_l)$

Table 4.1.: Neutrino electric and magnetic dipole moment matrices for generic scalar and vector couplings up to first order in neutrino mass.

From Tab. 4.1, one can see that the NMM matrices at zeroth order in neutrino mass are only non-zero if both, the left- and right-handed couplings are present. For either $g = 0$ or $h = 0$, the NMM is suppressed because of the proportionality to the neutrino mass as in the SM. This is due to the fact, that the NMM operator is chirality changing as discussed in Sec. 4.2.1. Accordingly, for $h = 0$, the $\mathcal{O}(m_\nu^1)$ calculation reproduces the SM result, compare to Eqs. (4.3), (4.4) and (4.13), (4.14). The second observation is that all of the matrices are hermitian and those for Majorana neutrinos are antisymmetric and purely imaginary as expected, see Sec. 2.3.

Let us now turn to the mass dependence. Fig. 4.4 shows the loop functions from Eqs. (4.21)-(4.24) plotted against the fermion to scalar and fermion to vector mass

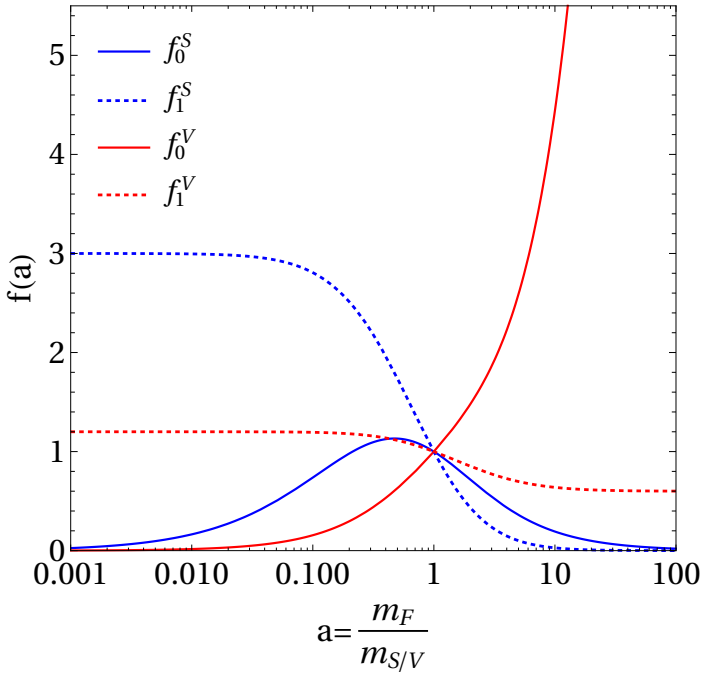

Figure 4.4.: Loop functions of the NMMs for generic scalar (blue) and vector (red) couplings. The solid lines correspond to the contribution proportional to the neutrino mass, while dotted lines are obtained from zeroth order in m_ν, present only if a right- and left-handed coupling to the neutrino exists.

ratio respectively. We have seen that all diagrams contributing to the the zeroth order in neutrino mass (solid lines in Fig. 4.4) contain a mass insertion of the internal fermion. Therefore in the limit $m_F \to 0$, the NMMs goes to zero as well, while for the first order in m_ν (dotted lines in Fig. 4.4) it stays finite.

At the first look, the asymptotic behavior for large fermion mass is surprising, because the loop function for the vector coupling is divergent for large mass ratios a (red solid line in Fig. 4.4). Usually one would expect a decoupling, when sending the mass of an particle inside the loop to infinity. However, in a gauge-invariant theory, a coupling of ν and F to the same gauge boson implies that they have to be in the same multiplet. Hence, the non-decoupling of the $\mathcal{O}(m_\nu^0)$ NMM contribution indicates that in a gauge-invariant theory, one can not simply send $m_F \to \infty$ independently of the neutrino mass. Note that in our computation procedure, when evaluating the loop integrals we expand in neutrino mass to lowest order. Therefore, the appearent non-decoupling in the $m_F \to \infty$ limit is unphysical.

Expanding the loop functions from Eqs. (4.21)-(4.24) in the limit of large scalar or

vector mass for finite m_F, the scalar and vector particles decouple and the NMMs goes to zero as expected.

So far we only investigated generic scalar and vector couplings that are renormalizable, i.e. of dimension four, and Lorentz invariant. We did not consider the $SU(2)_L$ structure yet. Starting with the SM doublet $L = (\nu_L, e_L)^T$ with isospin $I = 1/2$, we are interested in possible couplings to two additional $SU(2)$ multiplets M_1 and M_2. Without loss of generality let M_1 be the higher n-plet. The possible gauge invariant combinations are then given by Tab. 4.2. Note that a $SU(2)_L$ n-plet has isospin $(n-1)/2$.

M_1	M_2
$I = 1/2$	$I = 0$
$I = 1$	$I = 1/2$
$I = 3/2$	$I = 1$
$I = 2$	$I = 3/2$
...	...
$I = (n-1)/2$	$I = (n-2)/2$

Table 4.2.: Possible SU(2) multiplet combinations coupling to a doublet.

One of the multiplets M_1, M_2 has to be the fermion and the other one a scalar or vector. We thus can use the previous results and account for gauge invariance by using Tab. 4.2 as well as the requirement of conserved hypercharge, i.e. summing over the hypercharges of the combinations of L, M_1, M_2 have to give zero. According to the Gell-Mann-Nishijima formula (first given in Ref. [93]), the electric charge is then given by the sum of the hypercharge and the third component of the isospin $Q = I_3 + Y$. In this way the formulas of Tab. 4.1 together with the requirement of gauge invariance categorize all possible NMM contributions at one loop level.

The most important observation in this analysis is that the smallness of the NMM is a generic feature, in the sense that the NMM (generated at one loop level) will always be proportional to the neutrino mass, unless there exists a diagram like in Fig. 4.3 with a mass insertion of the internal fermion. In order to generate such a NMM contribution one is forced to introduce a charged Dirac fermion with couplings to both, the left- and right-handed neutrino field. In addition, for being able to close the NMM diagram at one loop level, the third particle (scalar or vector) needs to be part of both couplings.

In the following, we want to study the simplest scenarios beyond the SM that incorporate this idea. Simple in this context means that we introduce a number of

new particles as low as possible and preferable lower $SU(2)_L$ multiplets. Restricting ourself to singlet and doublet particles we are left with the following four possibilities[2] for the coupling to the SM doublet L with isospin $I = 1/2$ and hypercharge $Y = -1/2$ (in our notation convention $L(1/2, -1/2)$):

1) scalar $S(0, Y_S)$, fermion $F_L(1/2, 1/2 - Y_S)$: $\mathcal{L} \supset g\overline{L^c} i\sigma_2 F_L S + h.c.$

2) scalar $S(1/2, Y_S)$, fermion $F_R(0, -Y_S - 1/2)$: $\mathcal{L} \supset g\overline{L} S F_R + h.c.$

3) vector $V(0, Y_V)$, fermion $F_L(1/2, -Y_V - 1/2)$: $\mathcal{L} \supset g\overline{L} \not{V} F_L + h.c.$

4) vector $V(1/2, Y_V)$, fermion $F_R(0, 1/2 - Y_V)$: $\mathcal{L} \supset g\overline{L^c} i\sigma_2 \not{V} F_R + h.c.$

Here, σ_2 is the second Pauli matrix, acting in the $SU(2)$-space. In all of these cases, a second coupling with the right-handed neutrino and the right- or left-handed counterpart of the charged Dirac fermion is required. Otherwise the generated NMM matrices would still be suppressed by the proportionality to m_ν as in the SM. This leads us directly to the following additional couplings to the right-handed neutrino (a total singlet in the SM $\nu_R(0, 0)$) and requires the introduction of one extra fermion field for each of the four possibilites.

1) fermion $F_R(0, -Y_S)$: $\mathcal{L} \supset h\overline{\nu_R} F_R S + h.c.$

2) fermion $F_L(1/2, Y_S)$: $\mathcal{L} \supset h\overline{\nu_R} S^\dagger F_L + h.c.$

3) fermion $F_R(0, -Y_V)$: $\mathcal{L} \supset h\overline{\nu_R} \not{V} F_R + h.c.$

4) fermion $F_L(1/2, -Y_V)$: $\mathcal{L} \supset h\overline{\nu_R} \not{V} F_L + h.c.$

One other essential ingredient is the mass term of the Dirac fermion which can be introduced by a Higgs mechanism as in the SM. For example in the first case, the mass is generated with the help of the SM Higgs H via the Yukawa term $\overline{F_L} H F_R$.

At this point we are able to see that the simplest model generating a sizable NMM (not suppressed by m_ν) is obtained by adding a scalar singlet (couplings 1)) with hypercharge 1, because we then already have all required coupling terms without adding additional particles. The role of the fermion doublet is played by the SM doublet $F_L = L$ and the singlet by the SM right-handed charged leptons $F_R = l_R$. We consider this model in Sec. 4.3 in more detail.

The other interesting – and in a model building perspective appealing – possibility

[2]Note that we use the convention to write all fermion singlet fields as right-handed.

is to use the SM W boson with couplings of the type 4) in the well-known left-right-symmetric model, which is discussed in more detail in Sec. 4.4.

4.3. Neutrino magnetic moment with a charged scalar

The probably simplest model generating large NMM is the one proposed by Fukugita and Yanagida in Refs. [32,94]. It was originally introduced in order to have magnetic moments of the size $(10^{-10} - 10^{-11})\mu_B$ in the context of the solar neutrino problem. As indicated in the previous section, introducing a singly charged scalar singlet S^+ with hypercharge +1 leads to the interaction Lagrangian

$$\begin{aligned}\mathcal{L}_{\text{int}} &= g_{ij}\overline{\nu_{Ri}}l^c_{Rj}S^- + \frac{1}{2}h'_{ij}\overline{L_i}i\sigma_2 L^c_j S^- + h.c. \\ &= g_{ij}\overline{\nu}_i P_L l^c_j S^- + h_{ij}\overline{\nu}_i P_R l^c_j S^- + h.c.,\end{aligned} \tag{4.25}$$

where h_{ij} is the antisymmetric part of h'_{ij} and we have used the relation

$$\begin{aligned}\frac{1}{2}h'_{ij}\overline{L_i}i\sigma_2 L^c_j &= \frac{1}{2}h'_{ij}(\overline{\nu_{Li}}l^c_{Lj} - \overline{l_{Li}}\nu^c_{Lj}) = \frac{1}{2}h'_{ij}(\overline{\nu_{Li}}l^c_{Lj} - \overline{\nu_{Lj}}l^c_{Li}) \\ &= \frac{1}{2}(h'_{ij} - h'_{ji})\overline{\nu_{Li}}l^c_{Lj} = h_{ij}\overline{\nu_{Li}}l^c_{Lj} = h_{ij}\overline{\nu}_i P_R l^c_j.\end{aligned} \tag{4.26}$$

In order to apply the result of our computation of the NMM for the generic Lagrangian, Eq. (4.19), we identify $F = l^c$ and $Q_S = -1$. For the contraction of two charge conjugated fermion fields one finds

$$\begin{aligned}\overbrace{\psi^c(x)\overline{\psi^c}}(y) &= \langle 0|\,\mathcal{T}\psi^c(x)\overline{\psi^c}(y)\,|0\rangle = -C\,\langle 0|\,\mathcal{T}\overline{\psi}^T(x)\psi^T(y)\,|0\rangle\,C^{-1} \\ &= -C\,\langle 0|\,\mathcal{T}\overline{\psi}^T(x)\psi^T(y)\,|0\rangle\,C^{-1} = C\left[\langle 0|\,\mathcal{T}\psi(y)\overline{\psi}(x)\,|0\rangle\right]^T C^{-1} \\ &= C\left[\overbrace{\psi(y)\overline{\psi}}(x)\right]^T C^{-1} = \int\frac{d^3p}{(2\pi)^3 2E_p}C(\not{p}^T + m)C^{-1}e^{-ip(y-x)} \\ &= \int\frac{d^3p}{(2\pi)^3 2E_p}(-\not{p} + m)e^{-ip(y-x)} \\ &= \int\frac{d^3p}{(2\pi)^3 2E_p}(\not{p} + m)e^{-ip(x-y)} = \overbrace{\psi(x)\overline{\psi}}(y),\end{aligned} \tag{4.27}$$

which implies that it leads to the usual fermion propagator. Thus, we are now able to read off of Tab. 4.1 the NMM for this model for Dirac neutrinos

$$\mu_{fi} = \frac{e}{64\pi^2 m_S}(g_{fl}h^*_{il} + g^*_{il}h_{fl})f_0^s(a_l), \tag{4.28}$$

$$\epsilon_{fi} = i\frac{e}{64\pi^2 m_S}(g_{fl}h^*_{il} - g^*_{il}h_{fl})f_0^s(a_l). \tag{4.29}$$

Given the interaction Lagrangian, we can read off of Tab. 4.1 the NMM generated by diagrams of the type (d) and (f) of Fig. 4.1. Expanding the loop function $f_0^s(a_l)$ to leading order in $a_l = m_l/m_S$ we reproduce the result of Refs. [32, 94]

$$\mu_{fi} = -e\frac{m_l}{32\pi^2 m_S^2}(g_{fl}h^*_{il} + g^*_{il}h_{fl})\left(1 + \log\frac{m_l^2}{m_S^2}\right), \tag{4.30}$$

$$\epsilon_{fi} = -ie\frac{m_l}{32\pi^2 m_S^2}(g_{fl}h^*_{il} - g^*_{il}h_{fl})\left(1 + \log\frac{m_l^2}{m_S^2}\right). \tag{4.31}$$

At this point it is important to mention that for such a charged scalar singlet, there are a variety of phenomenological constraints coming from processes like $\mu \to e\gamma$, contribution to $g-2$ of leptons, anomalous tauon and muon decay and constraints from primordial nucleosythesis. A detailed discussion about those can be found in Ref. [32].

Instead of introducing a scalar singlet, one could think of generating the NMM with a scalar doublet, which would correspond to the second possibility in the catalog at the end of Sec. 4.2.4. However, the phenomenology of a doublet would imply even stronger experimental constraints. For example, the neutral component of the doublet would also couple to quarks in a way that is in conflict with experimental results on the K_s^0-K_L^0 mass difference. Model variants using a scalar doublet instead of the singlet are thus stronger constrained and for the purpose of generating large NMMs it is therefore necessary to further extend such models [94].

To conclude, we want to point out that the key problem in this simple model is the radiative neutrino mass correction, introduced by the NMM Feynman diagram with the photon line removed. In order to obtain a small and finite neutrino mass one has to introduce a fine-tuned counter term in the Lagrangian that cancels the logarithmically divergent mass term as well as reproduce the right order of magnitude for the neutrino mass. We turn to the discussion about this fine-tuning problem in detail in Chap. 6, where we present variants of this model that successfully avoid the fine-tuning, while still being consistent with experimental constraints and simultaneously leading to observable (i.e. large enough) NMMs. In the simple and minimal

framework as presented in this section, however, one could generate sizable NMMs only when allowing for fine-tuning in the neutrino masses.

4.4. Neutrino magnetic moment in the left-right symmetric model

In the following, we compute the NMMs in the framework of the left-right symmetric model, where we cross-check some of the intermediate expressions with Refs. [95, 96]. Although there are already NMM predictions for left-right symmetric models in literature, see e.g. Ref [97], we redo the whole NMM calculation, because we could not find an exact analytic expression for the loop function (at zeroth order in m_ν) in the literature. Deriving this expression is in our interest in order to verify the results for the generic vector couplings in an explicit model[3]. The calculation of this section verifies our results of Sec. 4.2.4 and thus proofs the applicability of our generic ansatz of Sec. 4.2.2 even in a complete and gauge-invariant theory.

4.4.1. Framework of the left-right symmetric model

The left-right symmetric model was originally proposed in the mid 1970s [99–102]. The basic idea is that at high energies the electroweak interaction Lagrangian is invariant under parity transformations, according to the symmetry group $SU(2)_L \otimes SU(2)_R \otimes U(1)'$. Then after spontaneous symmetry breaking by a non-zero vacuum expectation value above the electroweak scale, the SM symmetry group $SU(2)_L \otimes U(1)_Y$ is recovered.

There are several physical arguments in favor of the left-right symmetric model besides the restoration of parity at high scales. First of all, it naturally generates neutrino masses and can explain its smallness via the seesaw mechanism (compare to Sec. 2.1). Second, it provides a solution to the strong CP problem, which is a fine-tuning problem in quantum chromodynamics. There the Lagrangian contains the CP-violating term

$$\mathcal{L} = \theta \frac{1}{16\pi^2} F^a_{\mu\nu} \tilde{F}^{\mu\nu a} \tag{4.32}$$

[3] There we found, that in the limit of large internal fermion mass, the loop function goes to infinity. Naively one might think that it is a violation of the decoupling theorem [98], which is not the case as indicated in Sec. 4.2.4. We explain this asymptotic behavior by the observation that the neutrino and the second fermion in the NMM interaction have to be in the same multiplet, i.e. one can not take the limit $m_F \to \infty$ while expanding to lowest order in m_ν simultaneously.

which is experimentally strongly constrained by the measurement of the neutron electric dipole moment, leading to $\theta \ll 10^{-9}$. The smallness of this θ-parameter is referred to as the strong CP-problem. Since in the left-right symmetric model, the Lagrangian can be constructed such that it respects parity, the operator in Eq. (4.32) is forbidden and the strong CP problem is solved. See also for example Ref. [103] for more details about the strong CP problem. Finally, the left-right symmetric model offers an easy opportunity for grand unification into $SO(10)$ [104].

We start by extending the SM with an additional $SU(2)_R$ symmetry such that $\mathcal{L}$ becomes symmetric under the exchange of $SU(2)_R$ and $SU(2)_L$. We work in the framework of manifest left-right symmetry, i.e. the associated coupling constants satisfy $g = g_L = g_R$. In the scalar sector, the SM Higgs is replaced by one scalar bidoublet ϕ and two scalar triplets $\Delta_{L,R}$. Starting with the gauge group $SU(2)_L \otimes SU(2)_R \otimes U(1)'$, there are now two stages of symmetry breaking. While the vacuum expectation value of Δ_L can be chosen to be zero, the one of Δ_R is non-zero and thus responsible for the spontaneous breaking to the SM gauge group. This could also be done by scalar doublets instead. However, this possibility is less popular since it does not allow explaining small neutrino masses via the seesaw mechanism. In the second stage, the bidoublet ϕ acquires a vacuum expectation value, so that at low energies the SM phenomenology is restored. It is also responsible for connecting left- and right-handed fields, allowing for Dirac type fermion masses. The components of the scalar particles are given by

$$\phi = \begin{pmatrix} \phi_1^0 & \phi_1^+ \\ \phi_2^- & \phi_2^0 \end{pmatrix}, \qquad \Delta_{L,R} = \begin{pmatrix} \delta_{L,R}^+/\sqrt{2} & \delta_{L,R}^{++} \\ \delta_{L,R}^0 & -\delta_{L,R}^+/\sqrt{2} \end{pmatrix}, \tag{4.33}$$

with the vacuum expectation values

$$\langle\phi\rangle = \frac{1}{\sqrt{2}} \begin{pmatrix} \kappa_1 & 0 \\ 0 & \kappa_2 \end{pmatrix}, \qquad \langle\Delta_{L,R}\rangle = \frac{1}{\sqrt{2}} \begin{pmatrix} 0 & 0 \\ v_{L,R} & 0 \end{pmatrix}. \tag{4.34}$$

4.4.2. Lepton masses

The left-right symmetry requires the right-handed leptons to form a $SU(2)_R$ doublet. For that reason, one needs the bidoublet ϕ (doublet under both $SU(2)_L$ and $SU(2)_R$) to take over the role of the SM Higgs. The scalar triplets also contribute and are responsible for the Majorana neutrino masses so that the leptonic Yukawa couplings

are given by

$$\mathcal{L}_Y = f\bar{\psi}_L\phi\psi_R + h\bar{\psi}_L\tilde{\phi}\psi_R + h_M\left(\bar{\psi}_L^c(i\tau_2)\Delta_L\psi_L + \bar{\psi}_R^c(i\tau_2)\Delta_R\psi_R\right) + h.c., \tag{4.35}$$

where ψ_L and ψ_R refer to the left- and right-handed lepton doublets, f, h, and h_M are the coupling constants and $\tilde{\phi} = \sigma_2\phi^*\sigma_2$ with the second Pauli matrix σ_2. After spontaneous symmetry breaking via Eq. (4.34) we obtain

$$\mathcal{L}_Y \supset \frac{f\kappa_1 + h\kappa_2^*}{\sqrt{2}}\bar{\nu}_L\nu_R + \frac{h_M v_L}{\sqrt{2}}\bar{\nu}_L^c\nu_L + \frac{h_M v_R}{\sqrt{2}}\bar{\nu}_R^c\nu_R + \frac{f\kappa_2 + h\kappa_1^*}{\sqrt{2}}\bar{e}_L e_R. \tag{4.36}$$

The computation of the NMMs for Majorana neutrinos is very similar and can easily be derived from the Dirac case as we have seen in Sec. 4.1.2. Therefore, we assume for now that we have only Dirac-type masses, i.e. put $h_M = 0$ for simplicity. Then, for one lepton generation, the neutrino and electron masses are given by

$$m_\nu = -\frac{f\kappa_1 + h\kappa_2^*}{\sqrt{2}}, \qquad m_e = -\frac{f\kappa_2 + h\kappa_1^*}{\sqrt{2}}. \tag{4.37}$$

4.4.3. Gauge boson mass

The gauge boson masses are derived from the scalar gauge kinetic term, when inserting the vacuum expectation values that ϕ, Δ_R and Δ_L acquire after spontaneous symmetry breaking. It is given by

$$\mathcal{L}_{\text{scalar, kin.}} = \text{tr}\left[(D_\mu\phi)^\dagger D^\mu\phi\right] + \text{tr}\left[(D_\mu\Delta_L)^\dagger D^\mu\Delta_L\right] + \text{tr}\left[(D_\mu\Delta_R)^\dagger D^\mu\Delta_R\right], \tag{4.38}$$

with the covariant derivatives

$$D_\mu\phi = \partial_\mu\phi + igW_{L\mu}\phi - ig\phi W_{R\mu}, \tag{4.39}$$

$$D_\mu\Delta_L = \partial_\mu\Delta_L + ig\left[W_{L\mu}, \Delta_L\right] + ig'B'_\mu\Delta_L, \tag{4.40}$$

$$D_\mu\Delta_R = \partial_\mu\Delta_R + ig\left[W_{R\mu}, \Delta_R\right] + ig'B'_\mu\Delta_R. \tag{4.41}$$

Using Eq. (4.34) we obtain the gauge boson mass terms

$$\begin{aligned}\mathcal{L}_{\text{scalar, kin.}} \supset\ & \frac{g^2}{2}\begin{pmatrix} W_{L\mu}^- & W_{R\mu}^- \end{pmatrix}\mathcal{M}_{\text{charged}}\begin{pmatrix} W_L^{+\mu} & W_R^{+\mu} \end{pmatrix} \\ & + \frac{1}{2}\begin{pmatrix} B'_\mu & W_{L3\mu} & W_{R3\mu} \end{pmatrix}\mathcal{M}_{\text{neutral}}\begin{pmatrix} B'^\mu \\ W_{L3}^\mu \\ W_{R3}^\mu \end{pmatrix},\end{aligned} \tag{4.42}$$

with the matrices

$$\mathcal{M}_{\text{neutral}} = \begin{pmatrix} g'^2\left(|v_L|^2+|v_R|^2\right) & -gg'|v_L|^2 & -gg'|v_R|^2 \\ -gg'|v_L|^2 & g^2\left(|v_L|^2+\frac{|\kappa|_1^2+|\kappa_2|^2}{4}\right) & -g^2\frac{|\kappa|_1^2+|\kappa_2|^2}{4} \\ -gg'|v_R|^2 & -g^2\frac{|\kappa|_1^2+|\kappa_2|^2}{4} & g^2\left(|v_R|^2+\frac{|\kappa|_1^2+|\kappa_2|^2}{4}\right) \end{pmatrix},$$
$$\mathcal{M}_{\text{charged}} = \begin{pmatrix} |v_L|^2+\frac{|\kappa|_1^2+|\kappa_2|^2}{2} & -\kappa_1\kappa_2^* \\ -\kappa_2\kappa_1^* & |v_R|^2+\frac{|\kappa|_1^2+|\kappa_2|^2}{2} \end{pmatrix}. \tag{4.43}$$

Diagonalization of $\mathcal{M}_{\text{charged}}$ results in a heavy and light eigenstate. The latter has to reproduce the phenomenology of the SM W_L gauge boson, while the former has to be heavy due to experimental constraints. Their masses are

$$M^2_{W_{h,l}} = \frac{g^2}{4}\left(|v_L|^2+|v_R|^2+|\kappa|_1^2+|\kappa_2|^2 \pm \sqrt{\left(|v_L|^2-|v_R|^2\right)^2+4|\kappa_1\kappa_2|^2}\right), \tag{4.44}$$

and in the limit $|v_R| \gg |v_L|, |\kappa|_1, |\kappa_2|$

$$M^2_{W_h} = g^2/2|v_R|^2, \tag{4.45}$$
$$M^2_{W_l} = g^2/4\left(|v_L|^2+|\kappa|_1^2+|\kappa_2|^2\right). \tag{4.46}$$

The corresponding mass eigenstates, expanded in $|v_R|^{-1}$ are given by

$$W_h^\mu = W_R^\mu - \frac{\kappa_1^*\kappa_2}{|v_R|^2}W_L^\mu + \mathcal{O}(|v_R|^{-4}), \tag{4.47}$$
$$W_l^\mu = \frac{\kappa_1^*\kappa_2}{|\kappa_1\kappa_2|}W_L^\mu + \frac{|\kappa_1\kappa_2|}{|v_R|^2}W_R^\mu + \mathcal{O}(|v_R|^{-4}). \tag{4.48}$$

Similar for the neutral masses one finds by diagonalizing the mass matrix in Eq. (4.42)

$$M_A^2 = 0 \tag{4.49}$$
$$M_Z^2 = \frac{g^2(g^2+2g'^2)}{4(g^2+g'^2)}\left(4|v_L|^2+|\kappa|_1^2+|\kappa_2|^2\right)+\mathcal{O}(|v_R|^{-2}) \tag{4.50}$$
$$M_{Z'}^2 = (g^2+g'^2)|v_R|^2+\mathcal{O}(|v_R|^0). \tag{4.51}$$

So far, we worked with, in general, complex vacuum expectation values. However, one has the freedom to use $SU(2)_R$ and $SU(2)_L$ rotations in order to remove two phases as will be explained in the next section. The computation of the corresponding

eigenstates in the limit of real-valued vacuum expectation values and $v_L \to 0$ gives

$$B = \frac{g_l A}{g'\sqrt{2+\frac{g^2}{g'^2}}} - \frac{g g' Z}{\sqrt{(g^2+g'^2)\,(g^2+2g'^2)}} - \frac{Z'}{\sqrt{1+\frac{g^2}{g'^2}}} + \mathcal{O}(\frac{1}{v_R^2}), \tag{4.52}$$

$$W_{L3} = \frac{A}{\sqrt{2+\frac{g^2}{g'^2}}} - \frac{g^2+g'^2 Z}{\sqrt{g^4+3g^2g'^2+2g'^4}} + \mathcal{O}(\frac{1}{v_R^2}), \tag{4.53}$$

$$W_{R3} = \frac{A}{\sqrt{2+\frac{g^2}{g'^2}}} + \frac{Z}{\sqrt{\frac{g^4}{g'^4}+\frac{3g^2}{g'^2}+2}} + \frac{Z'}{\sqrt{1+\frac{g'^2}{g^2}}} + \mathcal{O}(\frac{1}{v_R^2}). \tag{4.54}$$

In order to derive the Feynman rules which are relevant to compute the NMM contribution, one has to find the full basis transformation matrices between the mass and flavor eigenstates. We did this in an exact (i.e. without expanding in v_R^{-1}) analytic way with the help of `Mathematica`. For the derivation of Eqs. (4.73), we used these exact transformation where in the final step, we again made the expansion in v_R^{-1}.

4.4.4. Scalar potential

The scalar potential contains all possible combinations of the scalar fields up to dimension four that are allowed by the requirement of left-right symmetry, i.e.

$$\psi_L \longleftrightarrow e^{\theta_1}\psi_R, \qquad \Delta_L \longleftrightarrow e^{\theta_2}\Delta_R, \qquad \phi \longleftrightarrow e^{\theta_3}\phi^\dagger. \tag{4.55}$$

In order to simplify the discussion, the phases θ_i could be rotated away by global phase transformations of the scalar fields. The most general scalar potential is then given by [96]

$$\begin{aligned}
V = {} & \alpha_1 \mathrm{tr}\left[\phi\phi^\dagger\right]\left(\mathrm{tr}\left[\Delta_L\Delta_L^\dagger\right] + \mathrm{tr}\left[\Delta_R\Delta_R^\dagger\right]\right) + \alpha_2\left(\mathrm{tr}\left[\Delta_L\Delta_L^\dagger\right]\mathrm{tr}\left[\phi^\dagger\phi'\right] + \mathrm{tr}\left[\Delta_R\Delta_R^\dagger\right]\mathrm{tr}\left[\phi\phi'^\dagger\right]\right) \\
& + \alpha_2^*\left(\mathrm{tr}\left[\Delta_L\Delta_L^\dagger\right]\mathrm{tr}\left[\phi'^\dagger\phi\right] + \mathrm{tr}\left[\Delta_R\Delta_R^\dagger\right]\mathrm{tr}\left[\phi^\dagger\phi'\right]\right) + \alpha_3\left(\mathrm{tr}\left[\phi\phi^\dagger\Delta_L\Delta_L^\dagger\right] + \mathrm{tr}\left[\phi^\dagger\phi\Delta_R\Delta_R^\dagger\right]\right) \\
& + \beta_1\left(\mathrm{tr}\left[\phi\Delta_R\phi^\dagger\Delta_L^\dagger\right] + \mathrm{tr}\left[\phi^\dagger\Delta_L\phi\Delta_R^\dagger\right]\right) + \beta_2\left(\mathrm{tr}\left[\phi'\Delta_R\phi^\dagger\Delta_L^\dagger\right] + \mathrm{tr}\left[\phi'^\dagger\Delta_L\phi\Delta_R^\dagger\right]\right) \\
& + \beta_3\left(\mathrm{tr}\left[\phi\Delta_R\phi'^\dagger\Delta_L^\dagger\right] + \mathrm{tr}\left[\phi^\dagger\Delta_L\phi'\Delta_R^\dagger\right]\right) - {\mu_1}^2\mathrm{tr}\left[\phi^\dagger\phi\right] - {\mu_2}^2\left(\mathrm{tr}\left[\phi'\phi^\dagger\right] + \mathrm{tr}\left[\phi'^\dagger\phi\right]\right) \\
& - {\mu_3}^2\left(\mathrm{tr}\left[\Delta_L\Delta_L^\dagger\right] + \mathrm{tr}\left[\Delta_R\Delta_R^\dagger\right]\right) + \lambda_1\mathrm{tr}\left[\phi\phi^\dagger\right]^2 + \lambda_2\left(\mathrm{tr}\left[\phi'\phi^\dagger\right]^2 + \mathrm{tr}\left[\phi'^\dagger\phi\right]^2\right) \\
& + \lambda_3\mathrm{tr}\left[\phi'\phi^\dagger\right]\mathrm{tr}\left[\phi'^\dagger\phi\right] + \lambda_4\mathrm{tr}\left[\phi\phi^\dagger\right]\left(\mathrm{tr}\left[\phi'\phi^\dagger\right] + \mathrm{tr}\left[\phi'^\dagger\phi\right]\right) + \rho_1\left(\mathrm{tr}\left[\Delta_L\Delta_L^\dagger\right]^2 + \mathrm{tr}\left[\Delta_R\Delta_R^\dagger\right]^2\right) \\
& + \rho_2\left(\mathrm{tr}[\Delta_L\Delta_L]\mathrm{tr}\left[\Delta_L^\dagger\Delta_L^\dagger\right] + \mathrm{tr}[\Delta_R\Delta_R]\mathrm{tr}\left[\Delta_R^\dagger{\Delta_R}^\dagger\right]\right) + \rho_3\mathrm{tr}\left[\Delta_L\Delta_L^\dagger\right]\mathrm{tr}\left[\Delta_R\Delta_R^\dagger\right] \\
& + \rho_4\left(\mathrm{tr}[\Delta_R\Delta_R]\mathrm{tr}\left[\Delta_L^\dagger\Delta_L^\dagger\right] + \mathrm{tr}[\Delta_L\Delta_L]\mathrm{tr}\left[{\Delta_R}^\dagger\Delta_R^\dagger\right]\right),
\end{aligned} \tag{4.56}$$

where now all of the parameters except for α_2 are real-valued. Let us furthermore assume for simplicity that there is no explicit CP-violation in the scalar potential ($\alpha_2 > 0$). In this case there exist arguments that also all the vacuum expectation values $v_L, v_R, \kappa_1, \kappa_2$ will be real as well [96]. The next step is to enforce the correct minimum of the scalar potential. In doing so, we set $\frac{\partial V}{\partial v_R} = \frac{\partial V}{\partial v_L} = \frac{\partial V}{\partial \kappa_1} = \frac{\partial V}{\partial \kappa_2} = 0$ and find

$$\begin{aligned}
\mu_1^2 = &\left[2\lambda_1\kappa_1^4 + 4\kappa_1^3\kappa_2\lambda_4 + \alpha_1\kappa_1^2\left(v_L^2+v_R^2\right) - 2\kappa_1\left(2\kappa_2^3\lambda_4 + \beta_1\kappa_2 v_L v_R\right)\right.\\
&- 2\lambda_1\kappa_2^4 - \kappa_2^2\left((\alpha_1+\alpha_3)\left(v_L^2+v_R^2\right) + 4\beta_3 v_L v_R\right)\\
&\left.+ 2v_L^2 v_R^2(2\rho_1 - \rho_3)\right] / \left[2(\kappa_1-\kappa_2)(\kappa_1+\kappa_2)\right], \qquad (4.57)\\
\mu_2^2 = &\left[2\kappa_1^5\lambda_4 + 4\kappa_1^4\kappa_2(2\lambda_2+\lambda_3) + \kappa_1^3\left(2\alpha_2\left(v_L^2+v_R^2\right) + \beta_1 v_L v_R\right)\right.\\
&+ \kappa_1^2\kappa_2\left(-4\kappa_2^2(2\lambda_2+\lambda_3) + \alpha_3\left(v_L^2+v_R^2\right) + 2\beta_3 v_L v_R\right)\\
&+ \kappa_1\kappa_2^2\left(-2\kappa_2^2\lambda_4 - 2\alpha_2\left(v_L^2+v_R^2\right) + \beta_1 v_L v_R\right)\\
&\left.+ 2\kappa_2 v_L v_R\left(\beta_3\kappa_2^2 + v_L v_R(\rho_3 - 2\rho_1)\right)\right] / \left[4\kappa_1(\kappa_1-\kappa_2)(\kappa_1+\kappa_2)\right], \qquad (4.58)\\
\mu_3^2 = &\left(\alpha_1\kappa_1^2 + 4\alpha_2\kappa_1\kappa_2 + \kappa_2^2(\alpha_1+\alpha_3) + 2\rho_1\left(v_L^2+v_R^2\right)\right)/2, \qquad (4.59)\\
\beta_2 = &-\left(\beta_1\kappa_1\kappa_2 + \beta_3\kappa_2^2 + v_L v_R(\rho_3 - 2\rho_1)\right)/\kappa_1^2. \qquad (4.60)
\end{aligned}$$

4.4.5. Gauge fixing

With the work of the previous section, we can now further investigate the scalar sector. For a correct gauge-invariant calculation, we have to introduce a gauge fixing term and in a second step compute the resulting Goldstone boson mass. The scalar kinetic term, Eq. (4.38), contains the pure kinetic part, the gauge boson mass, the three- and four-point interaction terms of the form '$W\phi\phi$', '$WW\phi\phi$', '$WW\phi$', '$W\Delta\Delta$', '$WW\Delta\Delta$', '$WW\Delta$' as well as the following mass/kinetic mixing term which has to be cancel by the gauge-fixing term

$$\begin{aligned}
\mathcal{L}_{\text{scalar, kin.}} \supset \mathcal{L}_{m/k} = &\operatorname{tr}\left[(\partial_\mu\phi)^\dagger W^\mu \langle\phi\rangle + (W_\mu\langle\phi\rangle)^\dagger\partial^\mu\phi\right]\\
&+ \sum_{A=L,R}\operatorname{tr}\left[(\partial_\mu\Delta_A)^\dagger W^\mu\Delta_A + (W_\mu\Delta_A)^\dagger\partial^\mu\Delta_A\right]. \qquad (4.61)
\end{aligned}$$

For notational simplicity we have used the abbreviations

$$W^\mu\langle\phi\rangle \equiv ig\left(W_L^\mu\langle\phi\rangle - \langle\phi\rangle W_R^\mu\right), \qquad (4.62)$$

$$W^\mu\langle\Delta_A\rangle \equiv ig\left[W_{A\mu}, \langle\Delta_A\rangle\right] + ig' B'_\mu\langle\Delta_A\rangle. \qquad (4.63)$$

With the $SU(2)$ generators $T^a = \sigma^a/2$ and the Pauli matrices σ^a, we obtain

$$\mathcal{L}_{m/k} = i\mathrm{tr}\left[gW^a_{L\mu}\partial^\mu G^{(1)a} + gW^a_{R\mu}\partial^\mu G^{(2)a} + g'B'_\mu\partial^\mu G^{(3)}\right] \tag{4.64}$$

with

$$\begin{aligned}
\partial^\mu G^{(1)a} &= (\partial^\mu\phi)^\dagger T^a\langle\phi\rangle - \langle\phi\rangle^\dagger T^a\partial^\mu\phi + (\partial^\mu\Delta_L)^\dagger[T^a,\langle\Delta_L\rangle] - [T^a,\langle\Delta_L\rangle]^\dagger\partial^\mu\Delta_L,\\
\partial^\mu G^{(2)a} &= T^a\langle\phi\rangle^\dagger\partial^\mu\phi - (\partial^\mu\phi)^\dagger\langle\phi\rangle T^a + (\partial^\mu\Delta_R)^\dagger[T^a,\langle\Delta_R\rangle] - [T^a,\langle\Delta_R\rangle]^\dagger\partial^\mu\Delta_R,\\
\partial^\mu G^{(3)} &= (\partial^\mu\Delta_L)^\dagger\langle\Delta_L\rangle - \langle\Delta_L\rangle^\dagger\partial^\mu\Delta_L + (\partial^\mu\Delta_R)^\dagger\langle\Delta_R\rangle - \langle\Delta_R\rangle^\dagger\partial^\mu\Delta_R.
\end{aligned}$$

A convenient way is to use the class of R_ξ-gauges as described for example in Ref. [35]. In order to cancel $\mathcal{L}_{m/k}$ we thus add to our Lagrangian the gauge fixing term

$$\begin{aligned}
\mathcal{L}_{g.f.} = -\frac{1}{2\xi}\Big\{&\left(\partial_\mu W_L^{a\mu} - ig\xi\mathrm{tr}[G^{(1)a}]\right)^2 + \left(\partial_\mu W_R^{a\mu} - ig\xi\mathrm{tr}[G^{(2)a}]\right)^2\\
&+ \left(\partial_\mu B'^\mu - ig'\xi\mathrm{tr}[G^{(3)}]\right)^2\Big\}.
\end{aligned} \tag{4.65}$$

Multiplying out the square brackets results in three different terms, being proportional to ξ^{-1}, ξ^0 and ξ^1 respectively. The term independent of ξ cancels exactly with $\mathcal{L}_{m/k}$, while the term proportional to ξ^{-1} contributes to the kinetic terms and modifies the propagator accordingly. The remaining one results in

$$\mathcal{L} \supset \frac{\xi}{2}\left(g^2\mathrm{tr}[G^{(1)a}]^2 + g^2\mathrm{tr}[G^{(2)a}]^2 + g'^2\mathrm{tr}[G^{(3)}]^2\right) \tag{4.66}$$

and is responsible for the Goldstone boson mass. Choosing $\xi = 1$ corresponds to Feynman gauge. With this choice the boson propagator takes the simple form of the well-known Feynman propagator $\frac{-ig^{\mu\nu}}{p^2-m^2+i\epsilon}$ and the Goldstone bosons have exactly the same mass as their associated gauge boson. Choosing instead $\xi \to \infty$ corresponds to unitarity gauge. In this limit the Goldstone bosons decouple and the propagator becomes $\frac{-i}{p^2-m^2+i\epsilon}(g^{\mu\nu} - \frac{p^\mu p^\nu}{m^2})$.

4.4.6. Goldstone boson mass

For the purpose of calculating the neutrino magnetic moment in R_ξ-gauge, we need to know the decomposition of the Goldstone fields. Once we have diagonalized the Goldstone mass matrix and identified its eigenvectors, we can find all resulting interactions and are finally able to derive the required Feynman rules. The mass matrix

of the Goldstone bosons $G^{\pm}_{l\mu}$ and $G^{\pm}_{h\mu}$ associated with the light and heavy charged gauge boson fields $W^{\pm}_{l\mu}$ and $W^{\pm}_{h\mu}$ is fully contained in the gauge fixing Lagrangian $\mathcal{L}_{g.f.}$. Since the masses of the Goldstones depend on the gauge choice, there can not be any mass contribution arising from the scalar potential. Still, we compute the singly charged scalar mass contributions from the scalar potential. When evaluated in the basis of mass eigenstates ($G^{\pm}_{l\mu}$, $G^{\pm}_{h\mu}$), there should be no additional mass contribution which can be used as a consistency check for the correct diagonalization procedure.

Starting from $\mathcal{L}_{g.f.}$ and throwing away any term containing a neutral or doubly charged scalar field, we find

$$\mathcal{L}_{g.f.} \supset -\frac{1}{4}g^2 \begin{pmatrix} \phi_1^+ \\ \phi_2^+ \\ \delta_L^+ \\ \delta_R^+ \end{pmatrix}^T \begin{pmatrix} \kappa_1^2+\kappa_2^2 & -2\kappa_1\kappa_2 & \sqrt{2}\kappa_2 v_L & -\sqrt{2}\kappa_1 v_R \\ -2\kappa_1\kappa_2 & \kappa_1^2+\kappa_2^2 & -\sqrt{2}\kappa_1 v_L & \sqrt{2}\kappa_2 v_R \\ \sqrt{2}\kappa_2 v_L & -\sqrt{2}\kappa_1 v_L & 2v_L^2 & 0 \\ -\sqrt{2}\kappa_1 v_R & \sqrt{2}\kappa_2 v_R & 0 & 2v_R^2 \end{pmatrix} \begin{pmatrix} \phi_1^- \\ \phi_2^- \\ \delta_L^- \\ \delta_R^- \end{pmatrix}. \tag{4.67}$$

Diagonalization of the matrix in the limit of vanishing v_L gives the mass eigenstates

$$G_h^{\pm} = \left(1 - \frac{1}{4}\frac{\kappa_1^2+\kappa_2^2}{v_R^2}\right)\delta_R^{\pm} - \frac{\kappa_1}{\sqrt{2}v_R}\phi_1^{\pm} + \frac{\kappa_2}{\sqrt{2}v_R}\phi_2^{\pm} + \mathcal{O}(v_R^{-3}) \tag{4.68}$$

$$G_l^{\pm} = \frac{|\kappa_1^2-\kappa_2^2|}{\sqrt{\kappa_1^2+\kappa_2^2}}\frac{1}{\sqrt{2}v_R}\delta_R^{\pm} + \mathrm{sign}(\kappa_1^2-\kappa_2^2)\frac{\kappa_1\phi_1^{\pm}+\kappa_2\phi_2^{\pm}}{\sqrt{\kappa_1^2+\kappa_2^2}}\times \\ \times\left(1 - \frac{1}{4}\frac{(\kappa_1^2-\kappa_2^2)^2}{\kappa_1^2+\kappa_2^2}\frac{1}{v_R^2}\right) + \mathcal{O}(v_R^{-3}) \tag{4.69}$$

with the correct masses, i.e. the same as the corresponding charged gauge bosons. As a consistency check, we also perform the diagonalization of the singly charged scalar mass matrix which arises as a consequence of the scalar potential,

$$\mathcal{L} \supset -\frac{1}{2}\sum_{\text{scalars } s_i,s_j}\left(\frac{\partial}{\partial s_j}\frac{\partial}{\partial s_i}V\right)\Big|_{s=\langle s\rangle}, \tag{4.70}$$

and find that it contains no contribution to the unphysical Goldstone boson masses $G^{\pm}_{h\mu}$, $G^{\pm}_{l\mu}$ as expected.

4.4.7. Neutrino magnetic moment couplings

With the effort of the previous sections, we are able to extract the NMM-relevant couplings. Investigating the scalar gauge kinetic term, Eq. (4.38), one finds the coupling term of the form '$\phi\phi W$'. Evaluating in the basis of mass eigenstates, after spontaneous symmetry breaking and with the identification

$$e = \frac{g}{\sqrt{2 + g^2/g'^2}}, \tag{4.71}$$

we recover the interaction term of a photon with two charged Goldstone bosons which corresponds to the usual quantum electrodynamic interaction as summarized in App. A.2. In the same way, also for the light and heavy W bosons the SM-like 'WWA' coupling is reproduced from terms of the form '∂WWA' that appear in the kinetic terms of the gauge bosons

$$\mathcal{L}_W = -\frac{1}{2}\mathrm{tr}[W_L^{\mu\nu} W_{L\mu\nu}] - \frac{1}{2}\mathrm{tr}[W_R^{\mu\nu} W_{R\mu\nu}]. \tag{4.72}$$

For the triple gauge boson couplings involving a photon, a Goldston boson and a W boson we find the coupling from the '$WW\phi$' terms in $\mathcal{L}_{\text{scalar, kin.}}$, Eq. (4.38). Here, we perform the expansion in v_R^{-1} in the final step which results in

$$\begin{aligned}\mathcal{L}_{GAW} = &\frac{eg}{\sqrt{2}}\left(v_R + \frac{1}{4}\frac{\kappa_1^2+\kappa_2^2}{v_R} + \mathcal{O}(v_R^{-2})\right) A_\mu W_h^{+\mu} G_h^- \\ &+ \frac{eg}{2}\sqrt{\kappa_1^2+\kappa_2^2}\left(1 - \frac{\kappa_1^2\kappa_2^2}{\kappa_1^2+\kappa_2^2}\frac{1}{v_R^2} + \mathcal{O}(v_R^{-3})\right) A_\mu W_l^{+\mu} G_l^- + h.c.\end{aligned} \tag{4.73}$$

From the Yukawa interaction, Eq. (4.35), the Goldstone boson decomposition, Eqs. (4.68), (4.69) as well as using the expressions for the lepton masses, Eq. (4.37), we derive the 'νGe' coupling

$$\begin{aligned}\mathcal{L}_{\nu Ge} = &-\frac{\sqrt{2}}{\sqrt{\kappa_1^2+\kappa_2^2}}\overline{e}\,(m_e P_L - m_\nu P_R)\,\nu G_l^- - \frac{1}{v_R}\overline{e}\,(m_e P_R - m_\nu P_L)\,\nu G_h^- \\ &+ \frac{\sqrt{2}\kappa_1\kappa_2}{(\kappa_1^2+\kappa_2^2)^{3/2} v_R^2}\overline{e}\big[(\kappa_1^2+\kappa_2^2)(m_\nu P_L - m_e P_R) \\ &+ \kappa_1\kappa_2(m_\nu P_R - m_e P_L)\big]\nu G_l^- + \mathcal{O}(v_R^{-3}) + h.c.\end{aligned} \tag{4.74}$$

Finally, the charged current interactions are derived from the leptonic gauge kinetic term similar as in the SM case, see App. A.2, but here with the difference that the

leptons are also charged under $SU(2)_R$. This leads to a left- and right-handed current. Using the diagonalized gauge boson fields we arrive at

$$\begin{aligned}\mathcal{L}_{CC} = &-\frac{g}{\sqrt{2}}\bar{e}\left(\gamma_\mu P_L + \frac{\kappa_1\kappa_2}{v_R^2}\gamma_\mu P_R + \mathcal{O}(v_R^{-4})\right)\nu W_l^{+\mu} \\ &-\frac{g}{\sqrt{2}}\bar{e}\left(\gamma_\mu P_R - \frac{\kappa_1\kappa_2}{v_R^2}\gamma_\mu P_L + \mathcal{O}(v_R^{-4})\right)\nu W_h^{+\mu} + h.c. \end{aligned} \tag{4.75}$$

4.4.8. Result

The Feynman diagrams contributing to the NMM are similar to the SM case, see Fig. 4.1. For the left-right symmetric model, however, there are twice as many diagrams, because one now has two different Goldstone bosons and W bosons that contribute. We calculate all 12 diagrams in Feynman gauge. Those that contain the heavy boson mass eigenstates lead to contributions of the order v_R^{-3} or higher and are thus highly suppressed compared to the other contributions. Since we compute the final result only up to the leading order in v_R^{-1}, we do not give the loop integrals for diagrams containing the heavy bosons. Those are of higher order in v_R^{-1}. The Feynman diagrams, containing the light bosons, lead to the loop-integrals in Eqs. (D.17) - (D.22) in App. D.

Following the procedure as explained in detail in Sec. 4.1.1, we compute the magnetic dipole moment for Dirac neutrinos in the left-right symmetric model

$$\mu_\nu = -\frac{5eg^2}{64\pi^2 M_{W_l}}\frac{\kappa_1\kappa_2}{v_R^2} f_0^v(m_e/m_{W_l}) + \mathcal{O}(m_\nu) + \mathcal{O}(v_R^{-3}), \tag{4.76}$$

with the loop function f_0^v given by Eq. (4.23). Note that in the previous sections, we have worked with only one lepton generation, for simplicity. However, a generalization for the case of three generations can easily be achieved by introducing a leptonic mixing matrix. The structure of the final result would then look exactly like our formula for generic vector couplings of Tab. 4.1. Comparing the generic vector coupling, as introduced in Eq. (4.20), with the charged currents in the left-right symmetric model we identify

$$g_{ij} \to -\frac{g}{\sqrt{2}}, \qquad\qquad h_{ij} \to -\frac{g}{\sqrt{2}}\frac{\kappa_1^2\kappa_2^2}{v_R^2}, \tag{4.77}$$

with real-valued couplings and for one lepton generation. In this way, we reproduce Eq. (4.76) using the result of our generic computation. The result for the electric dipole moment is very similar. We explicitly checked that applying Eq. (4.77) to the

generic result in Tab. 4.1 reproduces exactly what we obtain from the full computation.

We perform two further consistency checks. First, we calculate the NMM also in unitarity gauge, i.e. using only two Feynman diagrams, similar to Figs. 4.1 (a) and (e) with the appropriate gauge boson propagators in unitarity gauge (see App. A.1). We reproduce the result of the Feynman gauge calculation and thereby proving explicitly the gauge-independence of the final result. Second, we compare the leading order term to the literature result. For that purpose, we define the mixing angle θ of the gauge bosons according to

$$\begin{pmatrix} W_l^\pm \\ W_h^\pm \end{pmatrix} = \begin{pmatrix} \cos\theta & -\sin\theta \\ \sin\theta & \cos\theta \end{pmatrix} \begin{pmatrix} W_L^\pm \\ W_R^\pm \end{pmatrix}. \tag{4.78}$$

Together with Eqs. (4.47), (4.48) one finds for real-valued vacuum expectation values

$$\cos\theta = 1 + \mathcal{O}(v_R^{-4}), \tag{4.79}$$

$$\sin\theta = -\frac{\kappa_1\kappa_2}{v_R^2} + \mathcal{O}(v_R^{-4}). \tag{4.80}$$

In the limit $M_{W_l} \gg m_e$ we reproduce the result of Ref. [97], here for one lepton generation

$$\mu_\nu = \frac{eg^2 m_e}{8\pi^2 M_{W_l}^2} \sin\theta\cos\theta + \mathcal{O}(m_\nu) + \mathcal{O}(v_R^{-3}). \tag{4.81}$$

The rich phenomenological consequences of the left-right symmetric model are discussed extensively in the literature, see for example in Ref. [104]. Depending on the Majorana or Dirac nature of the neutrino as well as the mass of the right-handed neutrino, one can derive bounds from leptonic and non-leptonic decays on the W_L-W_R mixing angle of the order $\theta \leq 10^{-3}$. In this way the authors of Ref. [97] showed that for the Dirac case one can get the diagonal magnetic dipole moments

$$\mu_{\nu_e\nu_e} = 10^{-21}\mu_B, \tag{4.82}$$

$$\mu_{\nu_\mu\nu_\mu} = 10^{-17}\mu_B, \tag{4.83}$$

$$\mu_{\nu_\tau\nu_\tau} = 10^{-16}\mu_B, \tag{4.84}$$

and for the Majorana case the transition magnetic moments can at maximum be of

the order

$$\mu_\nu \sim 6.4 \cdot 10^{-11} \mu_B. \tag{4.85}$$

However, as for example also discussed in Ref. [105], such large values for the NMMs are impossible, if one wants to avoid fine-tuning the neutrino masses. In the framework of the minimal left-right symmetric model as discussed in this section, but with the Majorana Yukawa couplings switched on (i.e. $h_M \neq 0$ in Eq. (4.35)), the authors of Ref. [105] find that the NMM can not exceed $10^{-19}\mu_B$. Models that avoid this fine-tuning issue and allow for large NMMs are addressed in Chap. 6.

Chapter 5

New limits on millicharged particles

In the previous chapter, we have systematically analyzed what kind of scalar and vector interactions lead to neutrino magnetic moments (NMMs) and computed the corresponding electric and magnetic moment matrices at one-loop order. From the results in Tab. 4.1, one can see that the $\mathcal{O}(m_\nu^1)$-term is approximately proportional to the ratio of charge $Q \cdot e$ and squared mass m^2 of the particles running inside the loop[1]

$$\mu, \epsilon \ \sim \ Qe/m^2. \tag{5.1}$$

Experimental bounds imply strong constraints for the masses of new particles below the TeV scale. When thinking about theoretical frameworks beyond the Standard Model (SM) that can realize large NMMs, the typical paradigm is therefore to search for new physics at high energy scales. However, Eq. (5.1) is quadratic in $1/m$ and just linear in Q. It thus motivates to study NMMs of observable size in the context of light millicharged particles.

In the following, we present new limits on millicharged particles obtained from the non-observation of NMMs. First, we briefly explain the idea of millicharged particles in Sec. 5.1. We then give an overview over current phenomenological limits in Sec. 5.2 and continue in Sec. 5.3 with the derivation of the new limits. Finally, we present and discuss the results in Sec. 5.4.

[1] This proportionality is exact, when assuming that the two particles inside the NMM-loop have equal masses.

5.1. Millicharged particles

The question of the quantization of the electric charge is a long standing and well studied topic in elementary particle physics, see for example the reviews in Refs. [106, 107]. Although the experimental observation is that the electric charge of all particles are integer multiples of one third of the electron charge, it would be theoretically consistent to introduce particles with arbitrary real-valued charge. As this would lead to a better understanding of the fundamental properties of quantum electrodynamics, it is still of high physical interest to further study the possibility of millicharged particles experimentally as well as theoretically.

There are several options how millicharged particles can arise in a theoretically consistent way [108]. The simplest way would be to add a Dirac fermion which is a SM singlet except for a finite fractional hypercharge $Y = Qe$ with a small real-valued Q. However, this seems to be in tension with the possibility of embedding the low-energy theory into a grand unified model [109]. A second possibility is that neutrinos carry a small electric charge. There exist theoretically consistent frameworks in which this can be achieved, while preserving the SM anomaly cancellation [106, 107]. However, current constraints on the millicharge for neutrinos are very strong [28]. For example, from the neutrality of matter, one can derive an upper bound on the electron neutrino millicharge of $Q \lesssim 3 \cdot 10^{-21}$ [80]. In the work of Ref. [110] the authors derive an astrophysical limit on the neutrinos millicharge from mechanisms in the context of a supernova explosion of $Q \lesssim 1.3 \cdot 10^{-19}$. This limit applies to all neutrino flavors.

The third and more promising possibility is the existence of a paraphoton with an extra hidden gauged $U(1)'$ [111]. Such models are also studied in the context of dark matter candidates and arise naturally in string theory constructions, see for example Refs. [112, 113] and references therein. The basic idea is that there exists a dark sector of new particles, charged under the new $U(1)'$ gauge group, but not under the SM gauge group. If the associated gauge boson, the paraphoton (sometimes also called dark photon or hidden photon), is massless, it can kinetically mix with the SM photon. In this way, the particles being charged under the new gauge group, obtain an effective fractional electric charge.

A possible way through which such a dark sector can interact with observable particles is via the right-handed neutrino. Since it is the only particle being a total SM singlet, this is one of only a few well-motivated portals between the SM and the dark sector [112]. The existence of millicharged particles in such a dark sector, would immediately lead to NMM loop processes via the neutrino portal. Since NMMs are

not observed, this imposes new limits on millicharged particles.

5.2. Current constraints

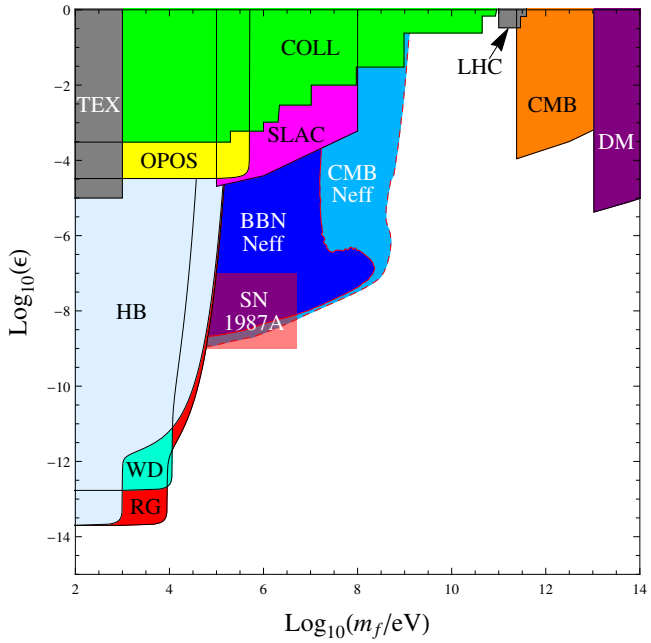

Figure 5.1.: Constraints on millicharged particles in the plane of mass (here m_f) and fractional charge (here ϵ) from various observations as explained in the text. The figure is taken from [114].

It is convenient to summarize the experimental constraints on millicharged particles in a charge vs. mass diagram like in Fig. 5.1 taken from Ref. [114]. The limits are obtained by many different observations over the last decades which are briefly summarized in the following.

Direct searches at collider and beam dump experiments (green shaded region in Fig. 5.1) do not rely on additional theoretical assumptions and are therefore to be considered rather robust [112]. The bounds include the LEP (Large Electron-Positron collider) results of the Z width requiring that the millicharged particles should not contribute to the invisible width more than the experimental 2 σ error [108], as well as the limits from the ASP (Anomalous Single Photon) search carried out at SLAC (Stanford Linear Accelerator Center) during the PEP (Positron-Electron Project). There, the constraint is derived from the absence of processes $e^+e^- \to \gamma X$ in electron-positron collisions, where X could be any weakly interacting particle [108, 115]. The

proton beam dump experiment E613 at Fermilab can be used as another direct probe of millicharged particles. Here, the sensitivity on charge and mass is given by decays of vector mesons V, $pp \to V + \cdots \to \bar{X}X$, and the direct production $pp \to \gamma^* \to \bar{X}X$ [116,117]. Moreover the electron beam dump experiment at SLAC leads to limits obtained from the absence of trident produced[2] pairs of millicharged particles [115]. The purple area in Fig. 5.1 corresponds to the constraint obtained in an experiment at SLAC that was uniquely designed for that purpose [119]. This limit therefore dominates the other direct bounds. At even lower masses, the authors of Ref. [120] derived limits from the TEXONO experiment. They showed that the TEXONO detector is sensitive to millicharged particles produced by Compton scattering $e^- + \gamma \to e^- + \gamma^* \to e^- f\bar{f}$ in the reactor core. The absence of corresponding electron recoil signals of the expected subsequent $e^- f \to e^- f$ scattering process implies the limit, indicated by the gray area in the upper left corner of Fig. 5.1. The observation that the LHC results imply an exclusion region which fills out the gap at around 10^{11} eV was derived in Ref [121].

The absence of invisible orthopositronium decays places a stringent bound on the photon-paraphoton mixing [122] which leads to the yellow excluded area. This limit is also a direct probe for millicharged particles, since it does not depend on further model assumptions (except for the kinetic photon-paraphoton mixing).

The Lamb shift is a high-precision quantum electrodynamics observable from which one can obtain a limit on new small-charged particles. It is not included in Fig. 5.1, but can be found in Fig. 5.3 which also includes the result of this work. Without additional assumptions, millicharged particles would contribute to the Lamb shift at one loop level. The high experimental precision hence allows for obtaining a limit that is stronger than the collider limits at masses up to 10 keV [108, 123].

There are also indirect bounds that are, however, astrophysical and cosmological model dependent. The dominant ones for the low mass region are those derived from stellar evolution (in Fig. 5.1: WD - White Dwarfs, RG - Red Giants, HB - Horizontal Branch). Constraints on the stellar energy loss can be translated in bounds on the millicharge, because pairs of millicharged particles would be produced in plasmon decays $\gamma^* \to f\bar{f}$ and would contribute to the energy loss much more efficiently than photons. The computation of the resulting bound in the charge vs. mass plane was done in previous works [108,115] and updated in Ref. [114]. The energy loss argument

[2]The trident process is the production of electron-positron pairs in strong electromagnetic fields in the form $e^- \to e^- + e^+e^-$. The theoretically correct treatment of such interactions is still of current interest, see for example Ref. [118] for a recent study.

also leads to the bound obtained by the observation of the supernova (SN) 1987A, where the number of observed neutrinos matched with theoretical expectations. If there would have been millicharged particles involved in the cooling of the proton neutron star, one would have observed reduced neutrino fluxes and a shorter neutrino signal [108].

Two other indirect bounds can be deduced from cosmological considerations which are computed and explained in Ref. [114] in great detail. First, the presence of a thermalized dark sector would influence the temperature anisotropies in the cosmic microwave background (CMB). The CMB contains the information of the number of relativistic degrees of freedom at the time of decoupling N_{eff} which would be larger than the one obtained with the CMB data for values of the millicharge and mass inside the light blue area of Fig. 5.1. Second, the knowledge of the helium-4 abundance constrains the amount of extra radiation during the epoch of big bang nucleosynthesis (BBN). In the framework of the dark sector model, the extra radiation increases the expansion of the universe, leading to an earlier freeze-out of electroweak interactions and thus increasing the amount of neutrons during the BBN. This in turn would imply a higher helium-4 abundance and thus leads to the dark blue constraint in Fig. 5.1.

The CMB constraint at masses of around 10^{-12} eV is obtained from an upper limit on the abundance of millicharged particles inferred from the Planck data [124]. The authors of Ref. [114] then translated this limit for the dark sector model into an exclusion area in the charge vs. mass plane.

Finally, the purple DM bound is a rough estimate of Ref. [115] for the sensitivity of dark matter detection experiments on models of millicharged particles with a paraphoton.

5.3. Constraints from neutrino magnetic moments

The non-observation of NMMs places bounds on dark sector models containing millicharged particles, if this sector speaks to the SM particles via the neutrino portal. Let us therefore assume that among the particles of the dark sector there are a millicharged fermion and a scalar with the coupling to the right-handed neutrino given by

$$\mathcal{L}_{\text{portal}} = g_i \overline{\nu_{Ri}} F S + \text{h.c.}, \tag{5.2}$$

where we define the coupling constants g_i, such that it couples to the neutrino mass eigenstates. As we have seen in Sec. 4.2, the presence of such an interaction directly leads to the Dirac NMMs at first order in neutrino mass

$$\mu_{fi} = -\frac{eQ(m_{\nu_f} + m_{\nu_i})}{384\pi^2 M^2} g_f g_i^*, \qquad \epsilon_{fi} = +i\frac{eQ(m_{\nu_f} - m_{\nu_i})}{384\pi^2 M^2} g_f g_i^*. \tag{5.3}$$

Here, Q is the millicharge of S, F is of opposite charge and we assume the masses to be of the same scale, i.e. $m_S = m_F = M = 1$, which leads to the loop function $f_1^s(m_F/m_S = 1) = 1$ (compare to Eq. (4.22)).

For the derivation of constraints on millicharged particles, we use the results of the GEMMA experiment which measured the antineutrino-electron scattering cross-section near a reactor core and thereby obtained the currently best terrestrial limit on NMMs. As discussed in Sec. 3.1, the bound on the NMMs is driven by the sensitivity to low electron recoils. The GEMMA experiment realized an energy threshold of $T = 2.8$ keV [18]. At such electron recoil energies the value for q^2 in the neutrino-electron scattering process is calculated to be $\sqrt{-q^2} = \sqrt{2m_e T} = 53.5$ keV. Also see App. B where we compute the cross-section explicitly. When assuming that the particles running inside the NMM loop are much larger than $\sqrt{-q^2}$, it is reasonable to take the limit $q^2 \to 0$. In that limit the cross-section is given by (see Eq. (B.25))

$$\sum_f \frac{d\sigma}{dT}(\bar{\nu}_e e^- \to \bar{\nu}_f e^-) = \frac{e^2}{4\pi}\left(\frac{1}{T} - \frac{1}{E}\right)(\mu_{\bar{\nu}_e}^{\text{eff}})^2, \tag{5.4}$$

where the effective NMM is approximately given by Eq. (2.30).

For masses of millicharged particles in the regime $M \gg \sqrt{-q^2} = 53.5$ keV, one can therefore directly apply the GEMMA limit of $\mu_{\bar{\nu}_e}^{\text{eff}} < 2.9 \cdot 10^{-11}\mu_B$ [18]. Using Eq. (5.3), we arrive at the inequality

$$\begin{aligned}\mu_{\bar{\nu}_e}^{\text{eff}} &= \sqrt{\sum_j \left|\sum_k U_{ek}^*(\mu_{jk} - i\epsilon_{jk})\right|^2} = \sqrt{\sum_j \left|\sum_k U_{ek}^*\left(\frac{-2eQm_{\nu_k}}{384\pi^2 M^2} g_j g_k^*\right)\right|^2} \\ &= \sqrt{\sum_j |g_j|^2} \cdot \left|\sum_k U_{ek} g_k m_{\nu_k}\right| \cdot \frac{eQ}{192\pi^2 M^2} < 2.9 \cdot 10^{-11}\mu_B.\end{aligned} \tag{5.5}$$

However, we are interested in extending this analysis, allowing for lower masses $M < \sqrt{-q^2}$. In this mass regime, the approximation $q^2 \to 0$ is not valid anymore. Hence, we want to derive a similar inequality for finite q^2. In this case, instead of

Eq. (5.4), the observable cross-section is now given by

$$\sum_f \frac{d\sigma}{dT}(\bar{\nu}_e e^- \to \bar{\nu}_f e^-) = \frac{e^2}{4\pi}\left(\frac{1}{T}-\frac{1}{E}\right)\sum_j \Big|\sum_k U_{ek}^* \frac{\mathcal{F}_2^{jk}(q^2)-\mathcal{G}_2^{jk}(q^2)}{m_{\nu_j}+m_{\nu_k}}\Big|^2, \tag{5.6}$$

according to Eq (2.23). One could think of the term that took the place of $\mu_{\bar{\nu}_e}^{\text{eff}}$ in Eq. (5.4) as a "generalized" effective NMM. This makes sense, because in the limit of zero q^2, the effective NMM is recovered. For the purpose of simplifying the discussion in the rest of this chapter, we therefore define

$$\mu_{\bar{\nu}_e}^{\text{eff}}(q^2) \equiv \sqrt{\sum_j \Big|\sum_k U_{ek}^* \frac{\mathcal{F}_2^{jk}(q^2)-\mathcal{G}_2^{jk}(q^2)}{m_{\nu_j}+m_{\nu_k}}\Big|^2}. \tag{5.7}$$

We repeat the calculation that we have performed in Sec. 4.2 for generic scalar couplings, but now we keep the exact q^2 dependence and expand only in the neutrino mass. We find

$$\frac{\mathcal{F}_2^{jk}(q^2)-\mathcal{G}_2^{jk}(q^2)}{m_{\nu_j}+m_{\nu_k}} = -\frac{eQg_f g_i^* m_{\nu_k}}{16\pi^2}F(M^2,q^2), \tag{5.8}$$

with the definition

$$F(M^2,q^2) = \frac{1}{q^4}\Bigg\{3q^2 + M^2\log^2\left(\frac{\sqrt{q^4-4M^2q^2}+2M^2-q^2}{2M^2}\right) + \sqrt{q^4-4M^2q^2}\log\left(\frac{\sqrt{q^4-4M^2q^2}+2M^2-q^2}{2M^2}\right)\Bigg\}. \tag{5.9}$$

The inequality in analogy to Eq. (5.5) then becomes

$$\mu_{\bar{\nu}_e}^{\text{eff}}(q^2) = \sqrt{\sum_j |g_j|^2}\cdot\Big|\sum_k U_{ek} g_k m_{\nu_k}\Big|\cdot\frac{eQ}{16\pi^2}|F(M^2,q^2)| < 2.9\cdot 10^{-11}\mu_B, \tag{5.10}$$

and is valid for masses $M \gg m_\nu$.

For a numerical estimate, one can use the global fit values of Ref. [47] for the leptonic mixing matrix and neutrino mass differences. We assume the lightest neutrino to have a mass of 0.1 eV and normal neutrino mass ordering. For couplings $g_j \sim 0.6$, one

arrives at

$$\sqrt{\sum_j |g_j|^2} \cdot \left| \sum_k U_{ek} g_k m_{\nu_k} \right| \sim 10^{-1}\,\text{eV}. \tag{5.11}$$

Furthermore, we fix $\sqrt{q^2} = 53.5$ keV which is the value at which GEMMA has the best sensitivity to physics beyond the SM as explained above. In this way, the inequality, Eq. (5.10), implies a constraint on the fractional charge Q and mass M of the millicharged particles.

5.4. Result

Using the results of the previous section and the GEMMA limit we are now able to deduce constraints on millicharged particles. In Fig. 5.2, we show the generalized effective NMM as a function of the millicharged particle's mass M for a fractional charge of $Q_s = 10^{-10}$. Values for $\mu^{\text{eff}}_{\nu_e}(q^2)$ above the experimental limit are excluded, as indicated with the red shaded area. Thus, we can read out of Fig 5.2 that millicharged particles with a coupling to the right-handed neutrino as in Eq. (5.2) with charges up to $Q_s \leq 10^{-2}$ can not be lighter than $\sim 10^5$ eV. Otherwise GEMMA would have already observed a corresponding NMM signal.

Fig. 5.3 summarizes the resulting limits in the plane of mass and millicharge and compares it to already existing constraints. The latter are taken from Refs. [112, 114]. The strongest constraints are driven by astrophysical observations and are thus astrophysics model dependent. In contrast, the new bound is completely astrophysics model independent, since it is given only by laboratory experiments. Note however that it relies on the particle physics model assumption that the new millicharged particles couple to the right-handed neutrino. It also depends on the neutrino mass and mixing parameters, the coupling strength as well as the new particle's masses which we have assumed to be of the same mass scale.

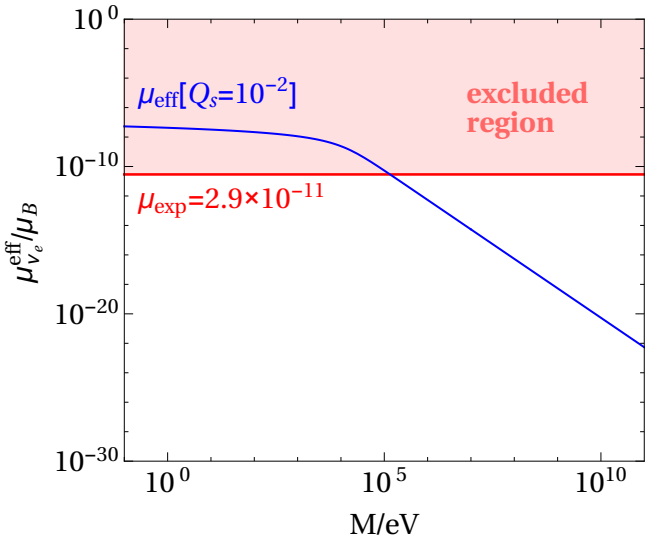

Figure 5.2.: The blue curve shows the generalized (i.e. for finite q^2) effective neutrino magnetic moment as a function of the millicharged particle's mass M. The red shaded area ($\mu \geq 2.9 \times 10^{-11}$) is excluded due to the absence of NMM signals in the GEMMA experiment.

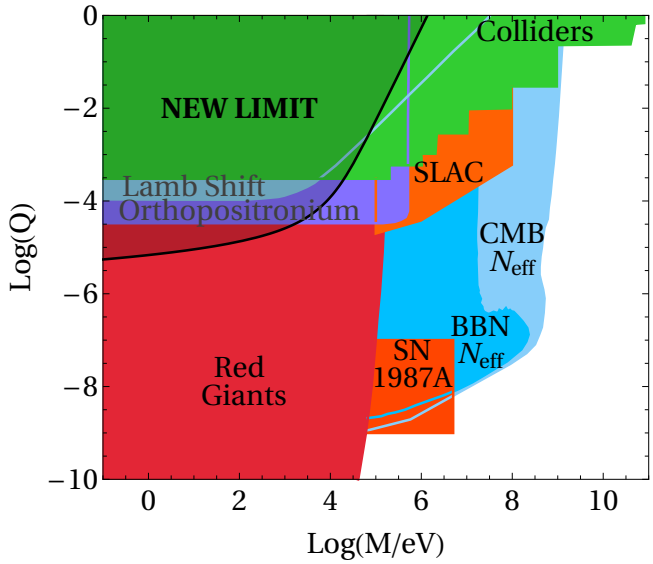

Figure 5.3.: Constraints on millicharged particles in the plane of mass M and fractional charge Q from various observations. The shaded areas corresponds to the excluded regions. The black line is the limit derived from the non-observation of NMMs.

Chapter 6

Naturally large neutrino magnetic moments

In Chap. 4 we have already seen that in the simplest beyond the Standard Model (SM) frameworks that predict a sizable neutrino magnetic moment (NMM) of $\mu_\nu \gg 10^{-19}\mu_B$ simultaneously introduce large neutrino mass corrections $\delta m_\nu \gg m_\nu$. Such contributions have to be canceled by each other or by appropriate counter terms. If we would have the proportionality $\delta m_\nu \propto m_\nu$, the mass could be made naturally small. However, this is typically not the case in models with large NMMs (compare to Sec. 4.2.1). The neutrino mass correction in such models tend to be proportional to masses of heavier particles, which in turn implies a fine-tuning of neutrino masses. The requirement of small and technically natural neutrino masses therefore places a stringent bound on the size of NMMs.

In view of upcoming experiments, which will improve in sensitivity on NMMs, it appears nonetheless important to study those models that can accommodate large NMMs while simultaneously avoiding fine-tuning large neutrino mass corrections. Furthermore, since in the (for neutrino masses minimally extended) SM the NMM prediction is at maximum of the order $\mu_\nu \sim 10^{-19}\mu_B$, a potential measurement of a NMM would hence be a clear indication of physics beyond the SM.

In this chapter we therefore investigate theoretical possibilities how to generate large NMMs with natural small neutrino masses. We start by explaining the fine-tuning problem and the resulting bounds on NMMs in Sec. 6.1. In Sec. 6.2, we consider the NMM in a model with light millicharged particles. In Sec. 6.3, we explicitly demonstrate the generic difficulty of generating large NMMs by means of a insightful radiative neutrino mass model. We then study models with large NMMs that successfully avoid the fine-tuning of m_ν via symmetries in Sec. 6.4.

6.1. Naturalness bounds

6.1.1. New physics above the electroweak scale

Consider a model with new physics scale Λ above the electroweak scale, $\Lambda \gg v_H$, containing particles of electric charge Qe and new couplings G that introduce the NMM at one loop. Fig. 6.1 (a) shows the corresponding Feynman diagram. When removing the photon line, we immediately obtain the neutrino mass contribution depicted in Fig. 6.1 (b). Integrating out particles of scale Λ, leaves us with effective NMM and neutrino mass operators. For Majorana neutrinos the operators of lowest dimension are of dimension seven and five, respectively and given by

$$\mathcal{O}^{(5\text{-dim})} = \frac{1}{\Lambda}\left(\overline{L^c}(-i\sigma_2)\phi\right)\left(\phi^T(-i\sigma_2)L\right), \tag{6.1}$$

$$\mathcal{O}_B^{(7\text{-dim})} = \frac{1}{\Lambda^2}\left(\overline{L^c}(-i\sigma_2)\phi\right)\left(\sigma^{\mu\nu}\phi^T(-i\sigma_2)B_{\mu\nu}L\right), \tag{6.2}$$

$$\mathcal{O}_W^{(7\text{-dim})} = \frac{1}{\Lambda^2}\left(\overline{L^c}(-i\sigma_2)\phi\right)\left(\sigma^{\mu\nu}\phi^T(-i\sigma_2)W_{\mu\nu}L\right), \tag{6.3}$$

where L is the SM lepton doublet, ϕ the SM Higgs doublet, σ_2 the second Pauli matrix acting on the $SU(2)_L$ space and $B_{\mu\nu}$, $W_{\mu\nu}$ are the $U(1)_Y$ and $SU(2)_L$ field strength tensors, respectively. After electroweak spontaneous symmetry breaking, the photon field is identified by $A_\mu = \sin\theta_W B_\mu + \cos\theta_W W_\mu^3$ and the operators $\mathcal{O}_B^{(7\text{-dim})}$, $\mathcal{O}_W^{(7\text{-dim})}$ would thus contribute to the magnetic moment, also compare to Eq. (2.24) and Eq. (2.23). From a dimensional analysis, one can thus make the generic estimate

$$\mu_\nu \sim \frac{QeGv_H^2}{\Lambda^3}, \qquad\qquad \delta m_\nu \sim G\frac{v_H^2}{\Lambda}, \tag{6.4}$$

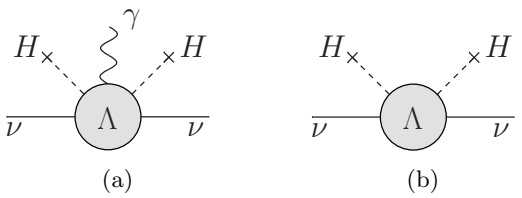

Figure 6.1.: Feynman diagrams generating a Majorana NMM and a radiative neutrino mass induced by new physics above the electroweak scale.

which leads to

$$\frac{\delta m_\nu}{0.1\text{ eV}} \sim \frac{1}{Q}\left(\frac{\mu_\nu}{10^{-19}\mu_B}\right)\left(\frac{\Lambda}{\text{TeV}}\right)^2. \tag{6.5}$$

In the case of Dirac neutrinos, the lowest dimensional effective operators contain only one single Higgs field instead of two. They are given by the operators in Eqs. (6.1)-(6.3) when replacing the expressions $(\overline{L^c}(-i\sigma_2)\phi)$ by $\bar{\nu}_R$. The corresponding effective operators are therefore of dimension six and four, respectively. The estimate thus is

$$\mu_\nu \sim \frac{QeGv_H}{\Lambda^2}, \qquad\qquad \delta m_\nu \sim Gv_H, \tag{6.6}$$

leading to the same relation as for Majorana neutrinos, Eq. (6.5).

For the purpose of avoiding fine-tuning, we require the radiative neutrino mass correction to be at maximum as large as the measured neutrino masses, $\delta m_\nu \lesssim m_\nu$. For a numerical estimate we use $m_\nu \sim 0.1$ eV, $\Lambda \sim$ TeV as well as $Q = 1$ and obtain the naive naturalness bound on NMMs

$$\mu_\nu \lesssim 10^{-19}\mu_B. \tag{6.7}$$

The current best laboratory limit on NMMs is $\mu_\nu \lesssim 2.9 \cdot 10^{-11}\mu_B$ [18]. One can hope for an increase of the sensitivity by future experiments down to about $\mu_\nu \gtrsim 10^{-12}\mu_B$ [24–27]. Hence, the above estimate shows that introducing such large NMMs generically induces neutrino mass corrections that exceeds phenomenological observations by many orders of magnitude. For example, cosmological observations constrain the neutrino masses to be not larger than about $m_\nu \lesssim 0.2$ eV [5]. Therefore a fine-tuning of seven orders of magnitude would be required.

Let us assume for a moment that the Feynman diagram of Fig. 6.1 (b) is forbidden for some reason (while diagram (a) is still allowed). In that case one would expect the naturalness bound to be relaxed. However, even then higher loop diagrams of the type in Fig. 6.2 can not be neglected and can still lead to considerable constraints on

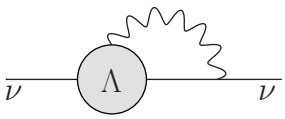

Figure 6.2.: The presence of a NMM induces neutrino mass corrections of this type.

the NMM. For the purpose of deriving those constraints, Bell et al. and Davidson et al. performed detailed effective operator analyses for Dirac neutrinos [125] and Majorana neutrinos [126, 127]. Requiring the naturalness condition $\delta m_\nu \lesssim m_\nu$ for Dirac neutrinos they found the model-independent bound of $\mu_\nu \lesssim 10^{-15}\mu_B$ for a new physics scale of $\Lambda \sim 1$ TeV and neutrino masses of $m_\nu \sim 0.2$ eV [125].

For Majorana neutrinos the NMM operator is flavor antisymmetric while the mass operator is flavor symmetric. That is why one can not obtain a strong model-independent naturalness bound on Majorana NMMs [126, 127]. For $\Lambda = 1$ TeV and $m_\nu \lesssim 0.3$ eV, one can derive the upper limits $\mu_{\nu_\tau\nu_\mu}$, $\mu_{\nu_\tau\nu_e} \lesssim 10^{-9}\mu_B$, $\mu_{\nu_\mu\nu_e} \lesssim 3 \cdot 10^{-7}\mu_B$ [127] which are however worse than current experimental constraints.

6.1.2. New physics below the electroweak scale

It is also interesting to consider models where the new physics scale is below the electroweak scale, $\Lambda \ll v_H$. The corresponding lowest-dimensional effective operators for the NMM and the neutrino mass are then of dimension five and three, respectively, as depicted in Fig. 6.3. We can thus make the naive estimate

$$\mu_\nu \sim \frac{QeG}{\Lambda}, \qquad \delta m_\nu \sim G\Lambda, \tag{6.8}$$

leading to

$$\frac{\delta m_\nu}{0.1\ \text{eV}} \sim \frac{1}{Q}\left(\frac{\mu_\nu}{10^{-13}\mu_B}\right)\left(\frac{\Lambda}{\text{GeV}}\right)^2. \tag{6.9}$$

This relation points out that NMMs can be generated by light particles without fine-tuning neutrino masses. For example, with $Q \sim 0.1$ and $\Lambda \sim 0.1$ GeV our estimate in Eq. (6.9) shows that one can reach $\mu_\nu \sim 10^{-12}\mu_B$ in a technically natural way.

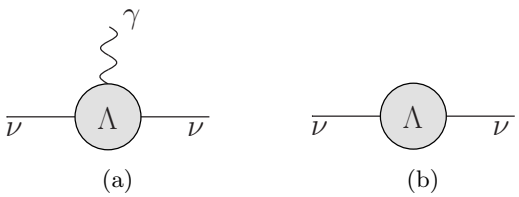

Figure 6.3.: The Feynman diagrams for the NMM and the radiative neutrino mass induced by new physics below the electroweak scale.

Summarizing the discussion so far we are left with two possibilities how to generate naturally large NMMs. Either the new physics is at a high scale and the estimate in Eq. (6.5) applies. In this case one has to find mechanisms to suppress the neutrino mass correction. Or, alternatively, the new particles responsible for the NMM are light with fractional charge $Q < 1$. The latter possibility is examined in the next section. The question of neutrino mass suppression mechanisms will be tackled in Sec. 6.4.

6.2. Naturally large neutrino magnetic moments via millicharged particles?

In Chap. 5, we have already seen that millicharged particles with couplings to neutrinos generate NMMs. There we found that the non-observation of NMMs implies a constraint on the mass and fractional charge of such particles. Motivated by the estimate in the previous section, we are now interested in the possibility of generating large NMMs with the help of millicharged particles. In other words, we want to analyze, whether or not there exist allowed values of millicharge Q and mass M such that the generated NMM is of observable size ($\mu_\nu \sim 10^{-12}\mu_B$) while satisfying the requirement of naturally small neutrino masses. The results in Sec. 5.4 tell us that this is not possible in models where the millicharged particles interact with neutrinos of only one chirality. The values for millicharge and mass that would be needed are excluded by phenomenological observations. Moreover from the theoretical considerations made in Sec. 4.2.1 we have also seen that for generating a sizable NMM one needs both, left- and right-handed couplings. In the following we therefore consider a model with a millicharged complex scalar S and a Dirac fermion F coupling to light Majorana neutrinos via the interaction

$$\mathcal{L} = f_i \overline{F_R} \nu_{Li} S + f'_j \overline{\nu_{Lj}} F_L S^\dagger + \text{h.c.} \tag{6.10}$$

The resulting neutrino electric and magnetic moment matrices have already been computed in Sec. 4.2 and can be read off of Tab. 4.1 with the couplings replaced appropriately. In the limit $M \equiv m_S = m_F$ they are given by

$$\mu_{ji} = \frac{iQe}{32\pi^2 M} \text{Im}[f_i f'_j - f_j f'_i], \qquad \epsilon_{ji} = \frac{iQe}{32\pi^2 M} \text{Re}[f_i f'_j - f_j f'_i]. \tag{6.11}$$

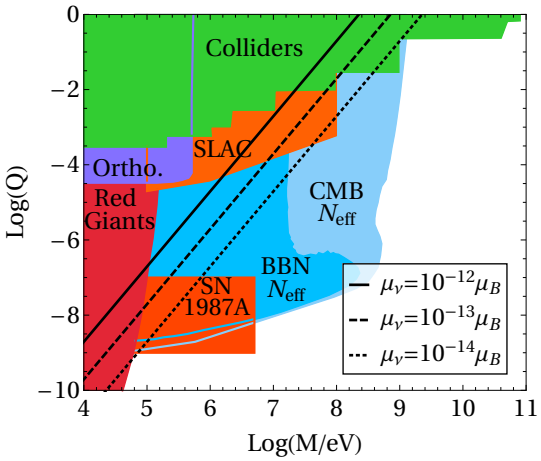

Figure 6.4.: Lines of constant μ_ν for $\delta m_\nu = 0.2$ eV in the plane of mass M and fractional charge Q of the new particles inside the NMM loop. The colored regions corresponds to already existing constraints and are taken from Ref. [114]. See also the working group report and references therein [112].

The neutrino mass correction can be computed from the same diagrams with the photon line removed. The corresponding loop-integrals are simpler than the ones including the photon line, see Eqs. (D.9) and (D.10) in App. D. A straightforward calculation, again in the limit $M \equiv m_S = m_F$, gives

$$\delta m_{ij} = \frac{f_i f'_j + f_j f'_i}{16\pi^2} M \log \frac{M^2}{\mu^2}. \tag{6.12}$$

For a numerical estimate we assume $\log(M/\mu) \sim 1$ and that there is no cancellation in the couplings among the flavors. One arrives at the relation

$$\frac{\mu_\nu}{\delta m_\nu} \simeq \frac{Qe}{4M^2}. \tag{6.13}$$

In this way, one is able to estimate the required values of Q and M that allow for large NMMs while avoiding fine-tuning neutrino masses. We set $\delta m_\nu \sim 0.2$ eV and assume values of the magnetic moment μ_ν close to the current experimental sensitivity. We show the result in Fig. 6.4 in the plane of mass and millicharge of the new particle overlaid over already excluded regions [112, 114]. Note that the existing bounds have been introduced in Sec. 5.2. They are taken from Ref. [114].

As the relevant parameter space is ruled out (predominantly by astrophysical observations) there seems to be no room for large NMMs generated by light millicharged

particles.

6.3. The neutrino magnetic moment in a radiative neutrino mass model

We turn to the discussion of scenarios in which the new particles are heavier than the electroweak scale. The generic problem of such models is the tight connection of the NMM and neutrino mass, see Eq. (6.5). In order to illustrate this in a concrete example, we consider a model inspired by radiative neutrino mass models. In such frameworks the light neutrinos have no tree-level mass term. Instead, the mass is generated in one-loop processes typically involving neutral particles inside the loop, as for example in the well-known model proposed by Ma [128]. In our context, the basic idea is to construct such a model where the new particles responsible for the neutrino mass carries electric charge. In this way, when attaching a photon line to the internal particle, the radiative neutrino mass diagrams also serve as a source of NMMs and we are able to predict the NMMs, given our knowledge of the mass and mixing parameters of the neutrinos.

We start by extending the SM particle content by two scalar $SU(2)_L$ doublets η, ϕ as well as a charged Dirac fermion $\Sigma = \Sigma_L + \Sigma_R$ with the quantum numbers given by

$$\begin{aligned} \eta &= \begin{pmatrix} \eta^0 \\ \eta^- \end{pmatrix} \sim (2, -1/2), & L_i &= \begin{pmatrix} \nu_{Li} \\ l_{Li} \end{pmatrix} \sim (2, -1/2), \\ \phi &= \begin{pmatrix} \phi^- \\ \phi^{--} \end{pmatrix} \sim (2, -3/2), & \Sigma^-_{L/R} &\sim (1, -1). \end{aligned} \tag{6.14}$$

The Yukawa couplings, generating both the neutrino masses as well as the NMMs, are

$$\mathcal{L}_Y = Y_i \overline{\Sigma_R} \tilde{\eta}^\dagger L_i + Y'_j \overline{\Sigma^c_L} \phi^\dagger L_j + \text{h.c.} \tag{6.15}$$

After electroweak symmetry breaking the singly charged components of the scalar doublets mix according to

$$\begin{pmatrix} \eta_1^\pm \\ \eta_2^\pm \end{pmatrix} = \begin{pmatrix} \cos\theta & \sin\theta \\ -\sin\theta & \cos\theta \end{pmatrix} \begin{pmatrix} \eta^\pm \\ \phi^\pm \end{pmatrix}, \tag{6.16}$$

and the Yukawa couplings become

$$\mathcal{L}_Y = Y_i\overline{\Sigma_R}(\cos\theta\eta_1^- - \sin\theta\eta_2^-)\nu_{Li} + Y_j'\overline{\nu_{Lj}^C}(\sin\theta\eta_1^+ + \cos\theta\eta_2^-)\Sigma_L + \text{h.c.} \tag{6.17}$$

The Feynman diagrams for the neutrino mass and NMM matrices are depicted in Fig. 6.5. The computation is very similar to those performed in Chap. 4. We evaluate the loop-integrals with `Mathematica Package-X` [92]. Note that for the neutrino mass, the single η_1 and η_2 diagrams (Fig. 6.5 a) are divergent, but the divergencies are canceled by each other due to the relative minus sign of the two diagrams. The neutrino mass matrix turns out to be

$$\begin{aligned} m_{\nu_i\nu_j} =& \frac{Y_iY_j' + Y_jY_i'}{16\pi^2} m_\Sigma \sin\theta\cos\theta \cdot \\ & \cdot \left[\frac{m_{\eta_1}^2}{m_{\eta_1}^2 - m_\Sigma^2}\log\left(\frac{m_{\eta_1}^2}{m_\Sigma^2}\right) - \frac{m_{\eta_2}^2}{m_{\eta_2}^2 - m_\Sigma^2}\log\left(\frac{m_{\eta_2}^2}{m_\Sigma^2}\right)\right]. \end{aligned} \tag{6.18}$$

We have added only one charged Dirac fermion Σ which implies that one of the three eigenvalues of the mass matrix is zero, i.e. the lightest neutrino remains massless. For the electric and magnetic dipole moment matrices we obtain

$$\mu_{ji} = \frac{-ie\sin\theta\cos\theta}{16\pi^2 m_\Sigma}\text{Im}\left[Y_iY_j' - Y_jY_i'\right] f(\frac{m_{\eta_1}^2}{m_\Sigma^2}, \frac{m_{\eta_2}^2}{m_\Sigma^2}), \tag{6.19}$$

$$\epsilon_{ji} = \frac{-ie\sin\theta\cos\theta}{16\pi^2 m_\Sigma}\text{Re}\left[Y_iY_j' - Y_jY_i'\right] f(\frac{m_{\eta_1}^2}{m_\Sigma^2}, \frac{m_{\eta_2}^2}{m_\Sigma^2}), \tag{6.20}$$

with the loop function

$$\begin{aligned} f(a_1,a_2) =& \frac{a_1(a_2-1)^2\log(a_1) - (a_1-1)}{(a_1-1)^2(a_2-1)^2} \cdot \\ & \cdot \left(-(a_1+1)a_2 + (a_1-1)a_2\log(a_2) + a_1 + a_2^2\right). \end{aligned} \tag{6.21}$$

Let us remark at this point that our model does not allow for fine-tuned cancellations in the neutrino mass, since there is just one single and finite contribution. $m_{\nu_i\nu_j}$ of Eq. (6.18) is therefore given by our knowledge of the two measured neutrino mass square differences Δm_{21}^2, Δm_{31}^2 as well as the PMNS-matrix U according to

$$m_{\nu_j\nu_i} = U\text{diag}(0, \sqrt{\Delta m_{21}^2}, \sqrt{\Delta m_{31}^2})U^\dagger. \tag{6.22}$$

We use the results of the global fit from Ref. [47] and assume all CP-phases of the

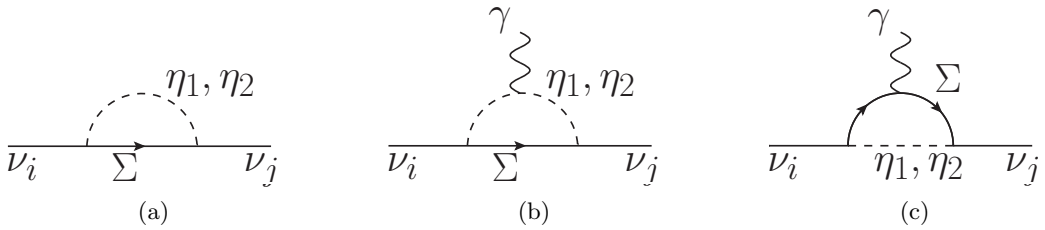

Figure 6.5.: Diagrams for neutrino mass and magnetic moment in the radiative neutrino mass model.

PMNS-matrix U to be zero. For the scalar and fermion masses we set $m_1 = 1.1$ TeV, $m_2 = 0.9$ TeV, $m_\Sigma = 1$ TeV. Solving Eq. (6.22) for the Yukawa couplings one finds

$$\begin{aligned}
\begin{pmatrix} Y_1 \\ Y_2 \\ Y_3 \end{pmatrix} &= \begin{pmatrix} 1 \\ 2.1 \mp 1.6i \\ 0.7 \mp 2.8i \end{pmatrix} \cdot x \cdot 10^{-6}, \\
\begin{pmatrix} Y_1' \\ Y_2' \\ Y_3' \end{pmatrix} &= \begin{pmatrix} 2.9 \\ 6.0 \pm 4.5i \\ 2.0 \pm 8.2i \end{pmatrix} \cdot \frac{1}{x} \cdot 10^{-6}, \quad x \in \mathcal{C}.
\end{aligned} \tag{6.23}$$

Plugging the results into Eq. (6.19) we obtain for the Majorana neutrino electric and dipole moment matrices

$$\epsilon_{ji} = 0, \qquad \mu_{ji} = \pm i \begin{pmatrix} 0 & -2 & -3.5 \\ 2 & 0 & -5.9 \\ 3.5 & 5.9 & 0 \end{pmatrix} \cdot 10^{-21} \mu_B, \tag{6.24}$$

which is many orders of magnitude below current experimental sensitivity.

In summary, we have presented a simple insightful model which illustrates the generic difficulty of generating large NMMs while simultaneously being compatible with the observed upper bound on neutrino masses. Due to the tight connection between neutrino mass and NMM, only very low NMMs are generated. Hence, we conclude that one needs special mechanisms, if one is interested in generating large NMMs in a consistent way. For the same reason, models not providing such a mechanism can not lead to NMMs considerably close to current experimental sensitivity. This also applies for example to well-studied models like the left-right symmetric model [105] (also compare to Sec. 4.4) and the supersymmetric model [129]. On the

other hand, a recent parameter study in the framework of the minimal supersymmetric model found room for large NMM [130], but does not solve the fine-tuning issue of the resulting neutrino mass corrections.

6.4. Naturally large neutrino magnetic moments via symmetries

As argued in Secs. 6.1 and 6.3, for generating sizable NMMs, one is in need of a mechanism suppressing neutrino mass loop contributions. For this purpose, one should rely on some sort of symmetry. One can distinguish two classes of symmetries. First, it seems likely to use one of the quantum numbers of the photon for introducing large NMMs in such a way that the same diagrams with the photon line removed are suppressed. In this spirit, Barr, Freire and Zee (BFZ) proposed a spin suppression mechanism in Ref. [131–133]. We also checked all one loop subdiagram possibilities trying to exploit the other quantum numbers, the parity and charge conjugation, but found no such suppression mechanism. The second ansatz is to exploit the symmetry properties of the effective NMM and mass operators. Such ideas were already proposed in the late 80s, for example the Voloshin-type symmetry [9, 10] (e.g. SU(2) with $\nu \leftrightarrow \nu^C$), SU(2) horizontal symmetry [11, 12] and discrete symmetries [13–17].

In the following we give a brief overview over the BFZ model, the Voloshin-type symmtery as well as the SU(2) horizontal symmetry and discuss which of those are still able to generate large NMMs.

6.4.1. Barr-Freire-Zee model

The spin-suppression mechanism was proposed by BFZ in Ref. [131]. It relies on the observation that the Feynman diagram depicted in Fig. 6.6 (a) is suppressed when removing the photon line like in the diagram of Fig. 6.6 (b). In the latter only the longitudinal degrees of freedom of the W gauge boson contribute, because of spin conservation. The full two-loop neutrino mass diagram in Fig. 6.7 (a) contains the subdiagram with the charged scalar h^+ and the W coupled to the neutrinos and a charged lepton inside the loop. It is proportional to the Yukawa coupling and therefore suppressed by powers of the lepton mass. This suppression do not apply for the NMM contribution and hence allows for NMMs of observable size as we will see in the following. Note that this mechanism also applies for higher order contributions which means that processes like the Feynman diagram in Fig. 6.2 are suppressed in

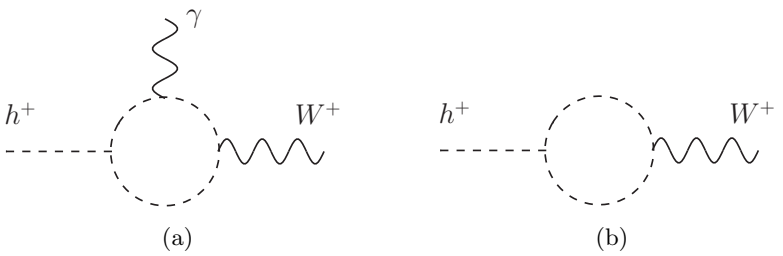

Figure 6.6.: The subdiagrams of the BFZ spin suppression mechanism with and without the photon line. Due to spin conservation only the longitudinal components of the W will contribute in diagram (b).

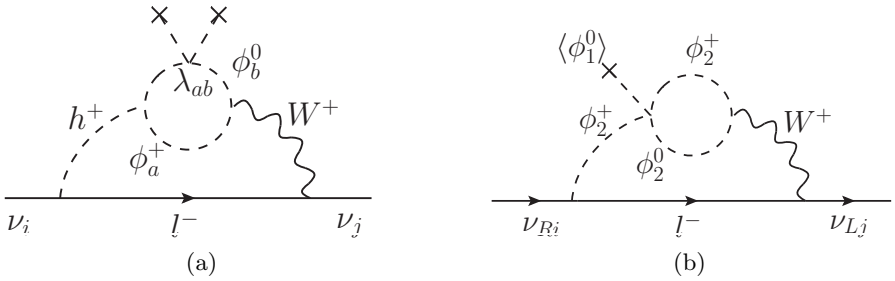

Figure 6.7.: (a) The full two-loop neutrino mass contribution in the BFZ model. The NMM is generated by the same diagram with the photon line attached to any particle inside the loop. (b) A similar diagram for a model variant with Dirac neutrinos.

the same way. The naturalness bounds summarized in Sec. 6.1 can thus be avoided.

The singly charged scalar singlet h^+ is an characteristic ingredient for this mechanism. It is rather difficult to find simple alternatives without such a singlet [132]. Its coupling to the SM lepton doublet is given by

$$\mathcal{L} = f^{ji} h^+ \overline{L_j^c} i\tau_2 L_i. \tag{6.25}$$

Additionally, in the realization of the spin suppression mechanism in [131], there are three scalar doublets ϕ_a with the quantum numbers of the Higgs. One can choose the basis such that the neutral component of only one of them, say ϕ_1 acquires a non-vanishing vacuum expectation value. The scalar doublets couple to the scalar singlet via the antisymmetric interaction

$$\mathcal{L} = \tilde{M}^{ab} h^+ (\phi_a^- \phi_b^0 - \phi_b^- \phi_a^0). \tag{6.26}$$

Together with the quartic term of the scalar potential

$$\mathcal{L} = \lambda_{ab} \langle \phi_1^\dagger \rangle \phi_a \langle \phi_1^\dagger \rangle \phi_b \tag{6.27}$$

one has all ingredients for the NMM diagram in Fig. 6.7(a).

From the relations for the generated radiative neutrino mass correction $\delta m_{\nu_i \nu_j}$ and the NMM μ_{ij} given in Ref. [131] we derive the estimate

$$\begin{aligned} \delta m_{\nu_i \nu_j} = &\left(\frac{m_j^2 - m_i^2}{M_W^2} \right) \cdot \left(\frac{\delta M_2^2 + \delta M_3^2}{2M^2} \right) \cdot \left(\frac{M}{\text{TeV}} \right)^2 \cdot \\ &\cdot \left(\frac{\mu_{ij}}{10^{-12} \mu_B} \right) \cdot 0.5 \cdot 10^6 \,\text{eV}. \end{aligned} \tag{6.28}$$

Here, it is assumed that the masses of the charged and neutral components of ϕ_2 and ϕ_3 are of similar size $M \equiv M_2 \sim M_3$ with small differences δM_2, δM_3. m_i denotes the charged lepton mass and M_W the W boson mass.

In order to check if the model is still viable we use the LHC results of slepton decays in supersymmetry searches [134, 135]. If the new charged scalar particles h^+ or $\phi_{2,3}^+$ would be considerably lighter than 1 TeV, they would already have been detected[1]. The new physics mass scale is therefore assumed to be at TeV scale, $M \sim 1$ TeV.

[1] Because of similar decay channels in the case of massless neutralinos, the bounds are of the same order of magnitude when compared to the sleptons.

Allowing for NMM values of $\mu_{ij} \sim 10^{-12}\mu_B$ will then lead to

$$\delta m_{\nu_e\nu_\mu} = \left(\frac{\delta M_2^2 + \delta M_3^2}{2M^2}\right) \text{eV}, \tag{6.29}$$

$$\delta m_{\nu_\mu\nu_\tau}, \delta m_{\nu_\tau\nu_e} = \left(\frac{\delta M_2^2 + \delta M_3^2}{2M^2}\right) \cdot 2.5 \cdot 10^2 \,\text{eV}. \tag{6.30}$$

We require the cosmological neutrino mass bound to be satisfied, $\delta m_{\nu_i\nu_j} \lesssim m_{\nu_i\nu_j} < 0.2$ eV [5]. In doing so we obtain $\frac{\delta M_2^2+\delta M_3^2}{2M^2} < 0.8\cdot 10^{-3}$, which can be achieved without fine-tuning. Moreover, this implies that one can accommodate naturally large NMMs within the BFZ model although it introduces the NMM at two loop order.

So far we implicitly worked with the assumption of Majorana neutrinos. Is it also possible to generate Dirac NMMs via the spin suppression mechanism? To answer this question, we think about a modified version of this model in order to apply the idea to Dirac neutrinos. For this case, one needs a scalar that connects the right-handed neutrinos and the left-handed charged leptons. In addition to the doublet ϕ_1, which takes the role of the SM Higgs, we could introduce an extra scalar doublet $\phi_2 = (\phi_2^0, \phi_2^-)^T$ with the required interaction $Y\overline{L}\phi_2\nu_R$. The scalar potential would then contain the coupling $\lambda\phi_1^\dagger\phi_2\phi_2^\dagger\phi_2$. In this way, we would get a sizable NMM from the Feynman diagram in Fig. 6.7 (b). However, the potential would also contain the interaction $\lambda'\phi_2^\dagger\phi_1\phi_1^\dagger\phi_1$. When the neutral component of ϕ_1 acquires a non-zero vacuum expectation value, this term would also induce $\langle\phi_2^0\rangle \neq 0$, since it is linear in ϕ_2^0. This in turn would lead to an unsuppressed tree-level neutrino mass. We therefore would again have the issue of fine-tuned neutrino masses. Following this line of thought, we conclude that there seems to be no simple model variant that applies the idea of the spin suppression mechanism to the case of Dirac neutrinos.

6.4.2. Voloshin-type symmetry

Another suppression mechanism proposed in Ref. [9] is based on the observation that under the transformation $\nu_L \to (\nu_R)^C, \nu_R \to -(\nu_L)^C$ the mass and NMM effective operators transform as

$$\overline{\nu_L}\nu_R \to -\overline{\nu_L}\nu_R, \tag{6.31}$$

$$\overline{\nu_L}\sigma_{\mu\nu}\nu_R F^{\mu\nu} \to +\overline{\nu_L}\sigma_{\mu\nu}\nu_R F^{\mu\nu}. \tag{6.32}$$

This property can be exploited when imposing a $SU(2)_\nu$ symmetry with $((\nu_R)^C, \nu_L)^T$ transforming as a doublet. In this way the neutrino mass is suppressed, because it is

not invariant under $SU(2)_\nu$ while the NMM operator respects the symmetry. Note that this mechanism can only suppress Dirac neutrino masses. Also note that for incorporating the idea into an UV-complete theory $(\nu_R)^C$ and ν_L have to be in the same multiplet, implying that the SM $SU(2)_L$ doublet needs to be extended for $(\nu_R)^C$. Hence, the simplest implementation is to use a $SU(3)_L \times U(1)_X$ gauge symmetry as done in Ref. [10]. Obviously the new $SU(2)_\nu$ symmetry can not be exact. The gauge group is thus spontaneously broken and the electroweak gauge symmetry is recovered at low scales. The neutrino mass then becomes proportional to the breaking scale of the new symmetry.

In the model of Barbieri and Mohapatra [10] the Feynman diagrams for the NMM and the neutrino mass correction δm_ν contain two charged components η_1 and η_2 from the scalar $SU(3)_L$ triplet. With the mass difference $\Delta m_\eta^2 = m_{\eta_1}^2 - m_{\eta_2}^2$ they derive the relation [10]

$$\mu_\nu = \delta m_\nu \frac{2e}{\Delta m_\eta^2} \log \frac{m_\eta^2}{m_\tau^2}. \tag{6.33}$$

The size of the NMM is constrained by the naturalness condition on Δm_η^2 arising from radiative corrections after symmetry breaking and depend on the mass of the $SU(2)_\nu$ gauge boson M_V (for more details see Ref. [10]). Barbieri and Mohapatra derive the inequality

$$\Delta m_\eta^2 \gtrsim \frac{\alpha_W}{4\pi} M_V^2, \tag{6.34}$$

where α_W is the electroweak fine-structure constant.

We account for experimental limits on new gauge boson and scalar masses by setting $M_V \sim m_\eta \sim 5\,\text{TeV}$ [136]. Plugging this into Eq. (6.34) we arrive at $\Delta m_\eta^2 \gtrsim 7 \cdot 10^5\,\text{GeV}^2$. Together with the requirement of naturally small neutrino masses $\delta m_\nu \lesssim 0.2\,\text{eV}$ we obtain from Eq. (6.33) potential values for the NMM of $\mu_\nu \lesssim 10^{-16}\mu_B$. There is a lack of four orders of magnitude until the benchmark value of $\mu_\nu \sim 10^{-12}\mu_B$. This shows that within this framework it is not possible to generate NMMs that are observable in next-generation experiments in a theoretically consistent way.

Frère, Heeck and Mollet derived inequalities between the transition moments for Majorana neutrinos [137] and argued that a possible measurement of μ_{ν_τ} at SHiP [138] would hint to the Dirac nature of the neutrino. However, up to now it seems not possible to obtain large Dirac NMMs in a technically natural way. In the case SHiP would indeed measure a non-zero μ_{ν_τ}, one has to find new ideas how to accommodate

large Dirac NMMs while simultaneously avoiding the fine-tuning of neutrino masses.

6.4.3. Horizontal symmetry

In the mechanism proposed by Voloshin, the neutrino mass correction is suppressed with respect to the NMM due to a new $SU(2)$ symmetry under which the right- and left-handed components of the Dirac neutrino field transform as doublets. One can apply the same idea to Majorana neutrinos. We have already seen in Sec. 2.3 that no diagonal Majorana NMMs exist. The question therefore is if it is possible to generate a sizable transition NMM while suppressing the corresponding corrections to the off-diagonal neutrino mass matrix. For this purpose, Babu and Mohapatra proposed in Ref. [11] to introduce the new symmetry as a horizontal flavor symmetry, i.e. where neutrinos of different flavors together form a multiplet under the new $SU(2)_H$.

In their model, the usual tau lepton doublet, here denoted by Ψ_{3L}, as well as the right-handed τ_R are $SU(2)_H$ singlets. The lepton fields of the electron and muon generation form the $SU(2)_H$ doublets

$$\Psi_L = \begin{pmatrix} \nu_e & \nu_\mu \\ e & \mu \end{pmatrix}_L , \qquad \Psi_R = \begin{pmatrix} e & \mu \end{pmatrix}_R . \tag{6.35}$$

In the scalar sector, next to the SM Higgs doublet ϕ_s one introduces the bidoublet ϕ and the $SU(2)_H$ doublet η

$$\phi = \begin{pmatrix} \phi_1^+ & \phi_2^+ \\ \phi_1^0 & \phi_2^0 \end{pmatrix} , \qquad \eta = \begin{pmatrix} \eta_1^+ & \eta_2^+ \end{pmatrix} . \tag{6.36}$$

In addition, in order to break the horizontal symmetry in such a way that tree-level mixing between generation-changing horizontal gauge bosons and the generation-diagonal ones are avoided, Babu and Mohapatra introduce two new $SU(2)_H$ triplet fields, for more details see Ref. [11].

The above set of particles imply a bunch of new Yukawa couplings. The relevant ones for the computation of the NMM and radiative neutrino mass δm_ν are

$$\mathcal{L}_Y \supset f \eta i\tau_2 \overline{\Psi_L^c} i\tau_2 \Psi_{3L} + f' \mathrm{tr}(\overline{\Psi_L \phi}) \tau_R + h.c. \tag{6.37}$$

The scalar potential after electroweak symmetry breaking contains the term $\mu_1 \kappa_s (\eta_1^+ \phi_1^+ + \eta_2^+ \phi_2^+)$ with κ_s being the vacuum expectation value of ϕ_s. It generates mixing between the components of η with the charged components of the bidoublet ϕ. In the

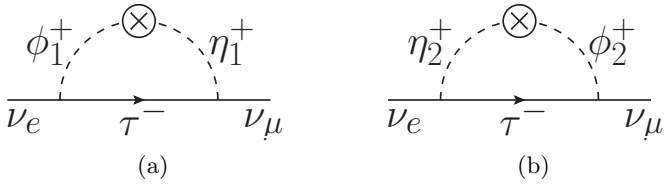

Figure 6.8.: The Feynman diagrams generating the $\nu_e - \nu_\mu$ transition moment, when attaching a photon line to one of the charged particles inside the loop. The circled cross indicates the scalar mixing term.

limit of exact $SU(2)_H$ (but broken $SU(2)_L$), the two resulting diagrams for the radiative neutrino mass $\delta m_{\nu_e\nu_\mu}$, as depicted in Fig. 6.8, cancel each other while the same diagrams with the photon line attached still leads to the non-zero $\nu_e - \nu_\mu$ transition NMM

$$\mu_{\nu_e\nu_\mu} = 2e\frac{ff'}{16\pi^2}m_\tau\frac{\mu_1\kappa_s}{m_\eta^2 - m_\phi^2}\left(\frac{1}{m_\eta^2} - \frac{1}{m_\phi^2}\right), \tag{6.38}$$

where $m_\eta = m_{\eta_1} = m_{\eta_2}$ and $m_\phi = m_{\phi_1} = m_{\phi_2}$. After the spontaneous symmetry breaking of $SU(2)_H$, mass splittings between the scalar charged components $\Delta m_\eta^2 = m_{\eta_2}^2 - m_{\eta_1}^2$ and $\Delta m_\phi^2 = m_{\phi_2}^2 - m_{\phi_1}^2$ are generated. This in turn leads to a non-zero neutrino mass given by

$$\delta m_{\nu_e\nu_\mu} = \frac{ff'}{16\pi^2}m_\tau\mu_1\kappa_s\left(\frac{1}{m_{\phi_1}^2 - m_{\eta_1}^2}\log\frac{m_{\phi_1}^2}{m_{\eta_1}^2} - \frac{1}{m_{\phi_2}^2 - m_{\eta_2}^2}\log\frac{m_{\phi_2}^2}{m_{\eta_2}^2}\right). \tag{6.39}$$

Assuming $\Delta m_\eta^2 \ll m_\eta^2$ and $\Delta m_\phi^2 \ll m_\phi^2$ as well as $\Delta m_\eta^2/m_\eta^2 = \Delta m_\phi^2/m_\phi^2$ one can now derive the estimate

$$\left(\frac{\mu_{\nu_e\nu_\mu}}{10^{-12}\mu_B}\right) = 2\left(\frac{\delta m_{\nu_e\nu_\mu}}{\text{eV}}\right)\left(\frac{\text{GeV}^2}{\Delta m_\eta^2}\right)\left(\frac{m_\eta^2}{m_\phi^2} - 1\right)\log\frac{m_\eta^2}{m_\phi^2}. \tag{6.40}$$

From this relation one can conclude that NMMs of the order $10^{-12}\mu_B$ can be reached without fine-tuning for mass splittings Δm_η^2 at GeV scale. Such small mass splittings do not imply additional fine-tuning. One can choose Δm_η^2 to be small in a technically natural way, since it is generated by a soft cubic interaction with one of the scalar triplets that break the horizontal symmetry.

Let us remark that this model allows for breaking $SU(2)_H$ in such a way that

the charged lepton masses m_e and m_μ are reproduced. It furthermore predicts extra ν_e-ν_τ and ν_μ-ν_τ neutrino mass contributions. We have checked explicitly that the model is compatible with the requirement $\delta m_{\nu_e\nu_\tau}, \delta m_{\nu_\mu\nu_\tau} \lesssim 0.2$ eV as well as with the observed charged lepton masses. We found that choosing the masses of the new particles at TeV scale still allows for a NMM of the order $\mu_{\nu_e\nu_\mu} \sim 10^{-12}\mu_B$.

Only the electron and muon generation is charged under the horizontal symmetry. Hence, in this model of Babu and Mohapatra only the ν_e-ν_μ transition moment can be sizable, while the symmetry protects the corresponding neutrino mass contribution from being too large. It suggests itself to think about applying the same mechanism to the ν_e-ν_τ or ν_μ-ν_τ transition moments. One could either include the τ flavor instead of the e or μ flavor in the horizontal symmetry or one could extend the horizontal symmetry to all three generations, for example by using a horizontal $SU(3)$ symmetry. However, the Higgs decays $h \to \tau\tau$ have been observed by the LHC [139, 140]. It is therefore not possible to introduce the necessary horizontal symmetry breaking in the coupling of the Higgs boson to charged leptons. Hence, the mechanism involving the horizontal symmetry works only for Majorana ν_e-ν_μ transition moments.

Chapter 7

Summary and conclusion

In the pure Standard Model (SM) neutrinos are massless. From the observed phenomenon of neutrino oscillations, we know that neutrinos carry a small, but non-zero mass. We briefly discussed how to introduce Dirac and Majorana neutrino masses in minimally extended SM frameworks in Chap. 2 and explained the concept of neutrino oscillations. The presence of neutrino masses inevitably implies the existence of non-vanishing neutrino magnetic and electric moments. Since the neutrino is neutral, the underlying quantum field theoretical processes occur at loop-level only and are in general model dependent. We introduced the effective neutrino electromagnetic vertex function and derived the physical observable of neutrino experiments, a combination of the electric and magnetic moment, which is typically referred to as neutrino magnetic moment (NMM).

We continued in Chap. 3 by summarizing the experimental status on NMMs. Although astrophysical observations provide for Majorana (Dirac) neutrinos up to one (three) order(s) of magnitude stronger constraints than direct laboratory experiments, they depend on the underlying astrophysical assumptions. The constraints obtained in terrestrial experiments are mainly driven by reactor neutrino experiments yielding a model-independent upper limit of $2.9 \cdot 10^{-11} \mu_B$.

In contrast to the relatively low experimental sensitivity on NMMs, the SM, minimally extended for allowing neutrino masses, predicts substantially lower values. We explicitly derived the corresponding Dirac and Majorana predictions in Chap. 4, thereby explaining the methods of the NMM computation. We reproduced the results of previous works and found Dirac electric and magnetic dipole moments of the order $10^{-20} \mu_B$. For Majorana neutrinos, only the off-diagonal transition moments exist. For those as well as for the Dirac transition moments the NMMs are additionally suppressed due to the GIM-mechanism. This small SM prediction raises the question,

what kind of new particle physics scenarios could generate NMMs that are observable in future experiments which will further increase the sensitivity. We showed that reaching NMMs close to the benchmark point of $10^{-12}\mu_B$ is a challenge for model building due to the tight connection of the neutrino mass and the NMM. The first problem is that the chirality flip of the NMM operator leads to the requirement of a mass insertion inside the NMM loop diagram. That is why in the minimally extended SM, the NMM is proportional to the neutrino mass and consequently very small. In order to avoid the suppression by the neutrino mass, one can introduce new particles with left- as well as right-handed couplings to the neutrino. We systematically analyzed this possibility, classified and calculated the electric and magnetic moments for generic scalar and vector couplings in the case of Majorana and Dirac neutrinos. We found that the NMM can then indeed be large. We have shown this explicitly in the two simplest models, a model with a charged scalar singlet and the left-right-symmteric model and thereby cross-checked the results from our generic calculations. However, we have seen that a second problem arises. In such models, radiative neutrino mass corrections are introduced being proportional to the mass of the particle inside the NMM loop-diagram. This, in turn, leads to a fine-tuning problem for the neutrino masses.

In Chap. 5, we used the result of our generic NMM calculation and studied models in which millicharged particles couple to right-handed neutrinos. We briefly introduced the concept of millicharge and summarized existing bounds. From the GEMMA upper limit on NMMs, one can infer new limits on the charge and mass of such particles which however turned out to be less stringent than limits from astrophysical observations.

The problem of fine-tuned neutrino masses in models generating NMMs of observable size was explained and dealt with in Chap. 6. We found that large NMMs generated by millicharged particles below the electroweak scale can in principle be achieved while simultaneously avoiding a fine-tuning of neutrino masses, but it would be in strong tension with astrophysical and cosmological observations. We showed by means of a very insightful model that theories with new physics above the electroweak scale predicting sizable NMMs generically lead to large neutrino mass corrections, thus requiring fine-tuning of several orders of magnitude. We finally reviewed mechanisms proposed in the literature that suppress such problematic neutrino mass corrections by a symmetry. For Majorana neutrinos, one can build models using a $SU(2)_H$ horizontal symmetry and obtain large ν_e-ν_μ transition moments. A second possibility is the Barr-Freire-Zee model in which all three ν_e-ν_μ, ν_e-ν_τ and ν_μ-ν_τ transition mo-

ments can be large due to a spin-suppression mechanism. For Dirac neutrinos, on the other hand, it does not seem to be possible anymore to build models predicting NMMs of observable size in a technically natural way.

Appendices

Appendix A

Feynman rules

There already exists various helpful lists of Feynman rules in literature, see for example Refs. [30, 35], but they are dependent on some formal conventions. For example in this work we use the metric tensor $g_{\mu\nu} = \mathrm{diag}(1, -1, -1, -1)$ opposed to the convention in Ref. [35]. In order not to confuse the reader, in this chapter, we shortly comment on some of our conventions and summarize a small set of Feynman rules that we use for our computations of quantum amplitudes.

A.1. Propagators

The propagators for scalars, fermions and vector bosons respectively are given by

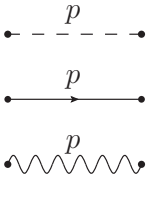

$$= \frac{i}{p^2 - m^2 + i\epsilon},$$

$$= \frac{i(\not{p} + m)}{p^2 - m^2 + i\epsilon},$$

$$= \frac{-i}{p^2 - m^2 + i\epsilon}\left(g^{\mu\nu} - (1-\xi)\frac{p^\mu p^\nu}{p^2}\right),$$

where the vector boson propagator is given in the R_ξ gauge. Choosing for example $\xi = 1$ corresponds to Feynman gauge and taking $\xi \to \infty$ results in the unitarity gauge. The latter has the advantage that the unphysical scalar degrees of freedom are removed from the Lagrangian. However, in most cases, using the unitarity gauge is not convenient for computing Feynman diagrams beyond tree-level, since it can lead to artificial divergencies in the calculation of loop-integrals[1]. In this gauge the

[1] Such gauge dependent divergencies are unphysical and will thus cancel in the sum of all contributing diagrams.

propagator becomes

$$\frac{-i}{p^2 - m^2}\left(g^{\mu\nu} - \frac{p^\mu p^\nu}{m^2}\right). \tag{A.1}$$

A.2. Electroweak interactions

We do not give the complete set of electroweak Feynman rules. Instead, we list only those that are needed for the computations performed in this work.

We begin with the interactions between photons with charged fermion fields. They can be derived from the kinetic Lagrangian replacing the derivative with the gauge-covariant derivative $\partial \to D$. We use the convention $D_\mu = \partial_\mu + ieQA_\mu$ where $e > 0$ is the electric charge of a positron and Q the charge of the respective particle in units of e. The gauge kinetic terms of such minimally coupled charged fermion particles reads

$$\mathcal{L}_{\text{fermion}} = i\overline{\psi}\not{D}\psi \supset -eQ_\psi A_\mu \overline{\psi}\gamma^\mu\psi, \tag{A.2}$$

resulting in the Feynman rule

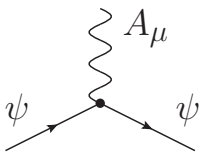

$$= -ieQ_\psi\gamma^\mu.$$

For the purpose of calculating the NMM in the SM, we are interested in the WWA, WHA and HHA triple boson interactions. Those can be derived from the gauge kinetic terms of the W and the Higgs

$$\mathcal{L}_W = -\frac{1}{2}\text{tr}\left[W^{\mu\nu}W_{\mu\nu}\right], \tag{A.3}$$

$$\mathcal{L}_\phi = \left(D_\mu\phi\right)^\dagger D^\mu\phi. \tag{A.4}$$

Here, ϕ is the Higgs doublet, W_μ is the gauge boson associated with the $SU(2)_L$ symmetry, B_μ the gauge boson associated with the weak hypercharge and $D_\mu\phi = (\partial_\mu + ig_1/2B_\mu + ig_2W_\mu)\phi$. The field tensor is given by

$$W_{\mu\nu} = \partial_\mu W_\nu - \partial_\nu W_\mu + ig_2\left[W^\mu, W^\nu\right], \tag{A.5}$$

where $W_\mu = \sum_a W_\mu^a\sigma_a/2$ with the Pauli matrices σ_i. Using the relations of the boson

fields

$$W_\mu^\pm = \frac{1}{\sqrt{2}}(W_\mu^1 \mp iW_\mu^2), \tag{A.6}$$

$$A_\mu = \sin\theta_W W_\mu^3 + \cos\theta_W B_\mu \tag{A.7}$$

with the Weinberg angle $\sin\theta_W = e/g_2$, $\cos\theta_W = e/g_1$ as well as the Higgs doublet $\phi = (H^+, h + v/\sqrt{2} + iH^0/\sqrt{2})^T$ expanded around the vacuum expectation value v we have all the ingredients for deriving the triple boson Feynman rules

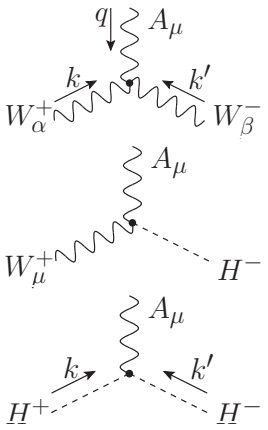

$$= -ie\left[g^{\alpha\beta}(-k^\mu + k'^\mu) + g^{\beta\mu}(q^\alpha - k'^\alpha) + g^{\mu\alpha}(k^\beta - q^\beta)\right],$$

$$= ieM_W g^{\mu\nu},$$

$$= ie(k'^\mu - k^\mu).$$

The SM neutrino charged current interaction is derived from the interaction Lagrangian

$$\mathcal{L}_{\text{cc}} = -\frac{g_2}{\sqrt{2}}\bar{l}_L\gamma^\mu U_{li}\nu_{Li}W_\mu^- + h.c. \tag{A.8}$$

U is the PMNS-matrix and the sum over lepton flavors $l = e, \mu, \tau$ as well as neutrino mass eigenstates $i = 1, 2, 3$ is implicitly assumed. The corresponding Feynman rule is

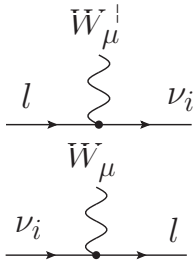

$$= -i\tfrac{g_2}{\sqrt{2}}U_{li}^*\gamma^\mu P_L,$$

$$= -i\tfrac{g_2}{\sqrt{2}}U_{li}\gamma^\mu P_L.$$

The coupling of neutrinos to the charged leptons and Goldstone boson H^+ is obtained from the Yukawa interaction. For a minimal extension one usually adds right-handed sterile neutrinos introducing the Yukawa couplings Y_ν. The relevant

Lagrangian after electroweak symmetry breaking then becomes

$$\mathcal{L}_{Yukawa} = -Y_l \overline{L}_L \phi l_R - Y_\nu \overline{L}_L (i\sigma_2 \phi^*) \nu_R + h.c. \tag{A.9}$$

$$\supset -\frac{g_2 m_l}{\sqrt{2} M_W} U_{li}^* \overline{\nu}_{Li} H^- l_R + \frac{g_2 m_{\nu_i}}{\sqrt{2} M_W} U_{li} \bar{l}_{Li} H^+ \nu_R + h.c. \tag{A.10}$$

where we have used that the non-zero vacuum expectation value of the neutral Higgs component v leads to masses $M_W = g_2 v/2$, $m_l = Y_l v/\sqrt{2}$ and $m_\nu = Y_\nu v/\sqrt{2}$. The Feynman rule is thus given by

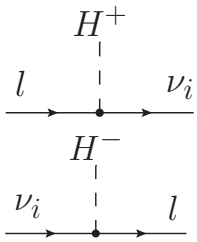

$$= -i \tfrac{g_2}{\sqrt{2} M_W} U_{li}^* (m_l P_R - m_{\nu_i} P_L),$$

$$= -i \tfrac{g_2}{\sqrt{2} M_W} U_{li} (m_l P_L - m_{\nu_i} P_R).$$

A.3. Majorana fermions

Standard textbooks usually give very detailed information about the Feynman rules for Dirac fermions. Since Majorana fermion fields are not present in the original SM, there currently does not exist a wide-spread common way, how to obtain the Feynman rules for Majorana particles in an easy way. Deriving the matrix element each time from basic principles using Wick contractions, while carefully tracking all minus signs correctly, seems to be very extensive. However, one can find several simpler approaches in the literature that help to obtain simplified Majorana Feynman rules similar to the Dirac case [141–146]. Very helpful pedagogical reviews on Majorana particles in general can be found in Refs. [29, 147]. In this work we use the Feynman rules as proposed in Ref. [146] which are briefly summarized in this section.

Dirac fields ψ contain the annihilation operator of the particle and the creation operator of the anti-particle, while Majorana fields χ contain the creation as well as the annihilation operator of the particle. The field expansions are given by

$$\psi(x) = \int \frac{d^3p}{(2\pi)^3 2E_p} \left(b_s(p) u_s(p) e^{-ipx} + d_s^\dagger(p) v_s(p) e^{ipx} \right), \tag{A.11}$$

$$\chi(x) = \int \frac{d^3p}{(2\pi)^3 2E_p} \left(a_s(p) u_s(p) e^{-ipx} + a_s^\dagger(p) v_s(p) e^{ipx} \right). \tag{A.12}$$

As a consequence Majorana the field contractions $\overbracket{\chi \chi^T}$ as well as $\overbracket{\chi^T \chi}$ are non-zero

(unlike for Dirac fermions) and lead to additional propagators. In this way, there exists a larger number of Feynman diagrams for processes involving Majorana fermions. Moreover, due to the existence of new Wick contractions, one has to make sure to keep track of the minus signs arising when commuting two fermion fields.

In order to incorporate these differences, we define the Majorana Feynman rules in the following way [146]:

1) Majorana fermions do not carry a fermion number flow. Majorana fermion lines are therefore drawn without arrows. Instead for each fermion chain, an arbitrary orientation ("fermion flow") is chosen.

2) When Drawing all possible Feynman diagrams for the given process, one has to account for additional diagrams, since Majorana fermion lines do not carry arrows.

3) The correct order of the Dirac matrices is the opposite direction as the chosen fermion flow.

4) The expressions for a fermion propagator has to be modified with respect to the usual one, if the particle is Dirac and the direction of fermion flow and fermion number flow are opposite. In that case one has to replace the propagator $S(p)$ with $S(-p)$.

5) The expression for a vertex has to be modified with respect to the usual one, if there are Dirac fermion lines attached to that vertex and if the direction of the fermion flow and the Dirac fermion number flow are opposite. In that case one has to replace the vertex Γ with the reversed vertex $\Gamma' = C\Gamma^T C^{-1}$.

6) The spinors corresponding to the external states depend only on the chosen fermion flow and are given by

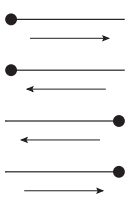

$= \bar{u}_s(p),$

$= v_s(p),$

$= \bar{v}_s(p),$

$= u_s(p).$

Appendix B

Electromagnetic neutrino-electron scattering

The most sensitive laboratory experiments measuring the NMM are designed to detect low electron recoil energies of the neutrino-electron scattering process. Next to the SM contribution, a non-zero NMM would also contribute to the scattering in form of the Feynman diagram in Fig. B.1. Early computations of the cross-section can be found in Refs. [62, 148], see also Ref. [149] for a more recent work. Since this process is crucial for the phenomenological analyses in this thesis, we give a short explicit derivation of the NMM mediated neutrino-electron cross-section in the following.

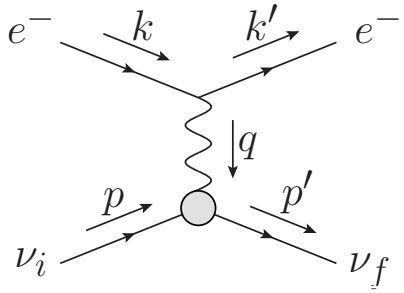

Figure B.1.: The neutrino-electron scattering process mediated by a NMM. The gray blob vertex depicts the effective NMM interaction.

It is convenient to calculate the cross-section in terms of the effective NMM operator. The electric and magnetic moments contribute to similar amount. The relevant part of the neutrino-photon vertex therefore is

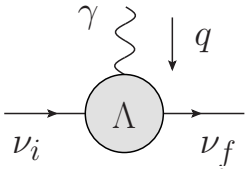

$$= i\sigma^{\mu\nu} q_\nu \frac{\mathcal{F}_2^{fi}(q^2)+\mathcal{G}_2^{fi}(q^2)\gamma_5}{m_{\nu_i}+m_{\nu_f}},$$

with the form factors $\mathcal{F}_2^{fi}$ and $\mathcal{G}_2^{fi}$ introduced in Chap. 2. We label the momenta as shown in Fig. B.1. In the massless limit, the incoming left-chiral neutrino is at good approximation in a negative helicity state. We thus obtain the following matrix element for this process

$$i\mathcal{M} = \bar{u}_{s'}(k')ie\gamma_\mu u_s(k)\frac{-i}{q^2}\bar{u}_r(p')i\sigma^{\mu\nu}q_\nu\frac{\mathcal{F}_2^{fi}(q^2)+\mathcal{G}_2^{fi}(q^2)\gamma_5}{m_{\nu_i}+m_{\nu_f}}u_-(p), \tag{B.1}$$

where $u_s(k)$ denotes a spinor of momentum k and spin s. We assume the ingoing electrons to be unpolarized. Averaging over the initial electron spin and summing over the spins of the final spinors, we obtain

$$\begin{aligned}\overline{|M|^2} = \frac{1}{2}\sum_{s,r,s'} MM^* = \frac{e^2}{2q^4}\sum_{s,r,s'}\Big[\bar{u}_{s'}(k')\gamma_\mu u_s(k)\bar{u}_s(k)\gamma^0\gamma_\nu^\dagger\gamma^0 u_{s'}(k')\Big]\cdot \\ \cdot\Bigg[\bar{u}_r(p')\sigma^{\mu\alpha}q_\alpha\frac{\mathcal{F}_2^{fi}(q^2)+\mathcal{G}_2^{fi}(q^2)\gamma_5}{m_{\nu_i}+m_{\nu_f}}u_-(p)\cdot \\ \cdot\bar{u}_-(p)\gamma^0\left(\sigma^{\nu\beta}q_\beta\frac{\mathcal{F}_2^{fi}(q^2)+\mathcal{G}_2^{fi}(q^2)\gamma_5}{m_{\nu_i}+m_{\nu_f}}\right)^\dagger\gamma^0 u_r(p')\Bigg].\end{aligned} \tag{B.2}$$

Using the Dirac properties $\gamma^0\gamma_\mu^\dagger\gamma^0 = \gamma_\mu$, $\gamma^0\sigma_{\mu\nu}^\dagger\gamma^0 = \sigma_{\mu\nu}$ as well as $\gamma^0\gamma_5^\dagger\sigma_{\mu\nu}^\dagger\gamma^0 = -\sigma_{\mu\nu}\gamma_5$, one arrives at

$$\begin{aligned}\overline{|M|^2} = \frac{e^2}{2q^4}\sum_{s,r,s'}\mathrm{tr}\left[u_{s'}(k')\bar{u}_{s'}(k')\gamma_\mu u_s(k)\bar{u}_s(k)\gamma_\nu\right]\mathrm{tr}\Bigg[u_r(p')\bar{u}_r(p')\sigma^{\mu\alpha}q_\alpha\cdot \\ \cdot\frac{\mathcal{F}_2^{fi}(q^2)+\mathcal{G}_2^{fi}(q^2)\gamma_5}{m_{\nu_i}+m_{\nu_f}}u_-(p)\bar{u}_-(p)\sigma^{\nu\beta}q_\beta\frac{\mathcal{F}_2^{fi*}(q^2)-\mathcal{G}_2^{fi*}(q^2)\gamma_5}{m_{\nu_i}+m_{\nu_f}}\Bigg].\end{aligned} \tag{B.3}$$

The polarized spinor relations in the ultra-relativistic limit are [35]

$$u_s(p)\bar{u}_s(p) = \frac{1+s\gamma_5}{2}\not{p}, \tag{B.4}$$

$$v_s(p)\bar{v}_s(p) = \frac{1-s\gamma_5}{2}\not{p}, \tag{B.5}$$

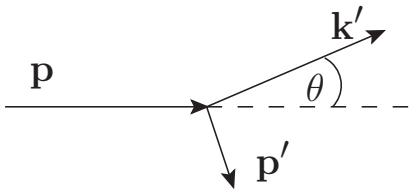

Figure B.2.: Momenta and scattering angle in the lab frame, where the initial electron is at rest, i.e. $\mathbf{k} = 0$.

and for the unpolarized electron spinors we use

$$\sum_s u_s(p)\bar{u}_s(p) = \not{p} + m, \tag{B.6}$$

$$\sum_s v_s(p)\bar{v}_s(p) = \not{p} - m, \tag{B.7}$$

and obtain for the averaged squared matrix element

$$\overline{|M|^2} = \frac{e^2}{2q^4}\mathrm{tr}\left[(\not{k}' + m_e)\gamma_\mu(\not{k} + m_e)\gamma_\nu\right]\mathrm{tr}\Bigg[\not{p}'\sigma^{\mu\alpha}q_\alpha \cdot \cdot \frac{\mathcal{F}_2^{fi}(q^2) + \mathcal{G}_2^{fi}(q^2)\gamma_5}{m_{\nu_i} + m_{\nu_f}}\frac{1-\gamma_5}{2}\not{p}\sigma^{\nu\beta}q_\beta\frac{\mathcal{F}_2^{fi*}(q^2) - \mathcal{G}_2^{fi*}(q^2)\gamma_5}{m_{\nu_i} + m_{\nu_f}}\Bigg]. \tag{B.8}$$

For the evaluation of the Dirac traces we use mathematica package X [92]. In terms of the Mandelstam variables

$$s = (k' + p)^2 = (k + p)^2, \tag{B.9}$$

$$t = (k - k')^2 = (p' - p)^2 = q^2, \tag{B.10}$$

$$u = (k - p')^2 = (k' - p)^2, \tag{B.11}$$

$$s + t + u = 2m_e^2, \tag{B.12}$$

we obtain

$$\overline{|M|^2} = 4e^2\left|\frac{\mathcal{F}_2^{fi}(q^2) - \mathcal{G}_2^{fi}(q^2)}{m_{\nu_i} + m_{\nu_f}}\right|^2\frac{(m_e^2 - s)(m_e^2 - u)}{t}. \tag{B.13}$$

The differential cross-section can be computed from the phase space and the matrix

element according to [35]

$$d\sigma = \frac{\overline{|M|^2}}{4(k\cdot p)} \frac{d\mathbf{k}' d\mathbf{p}'}{(2\pi)^2 4E_e' E_\nu'} \delta^4(p + k - p' - k'). \tag{B.14}$$

For the evaluation of the phase space we parametrize the momenta in the lab frame as depicted in Fig. B.2 with the 4-momenta explicitly given by

$$k^\mu = \begin{pmatrix} m_e & 0 & 0 & 0 \end{pmatrix}, \tag{B.15}$$

$$p^\mu = \begin{pmatrix} E_\nu & 0 & 0 & E_\nu \end{pmatrix}, \tag{B.16}$$

$$k'^\mu = \begin{pmatrix} T + m_e & 0 & |\mathbf{k}'|\sin\theta & |\mathbf{k}'|\cos\theta \end{pmatrix}, \tag{B.17}$$

$$p'^\mu = \begin{pmatrix} E_\nu - T & 0 & -|\mathbf{k}'|\sin\theta & E_\nu - |\mathbf{k}'|\cos\theta \end{pmatrix}, \tag{B.18}$$

where one finds $|\mathbf{k}'| = \sqrt{T^2 + 2m_e T}$. Here, T denotes the electron recoil energy. The integration over the phase space can now be performed in four steps.

1) Integrate over $d\mathbf{p}'\delta^3(\mathbf{k}' + \mathbf{p}' - \mathbf{k} - \mathbf{p})$ and thereby eliminate $\mathbf{p}'$.

2) Use $d\mathbf{k}' = 2\pi|\mathbf{k}|^2 d(\cos\theta) d|\mathbf{k}|$.

3) The remaining integral is of the form

$$\mathcal{I} = \int \mathcal{A}\left(|\mathbf{k}'|, E_e'(|\mathbf{k}'|), E_\nu'(|\mathbf{k}'|)\right) \delta\left(E_e + E_\nu - E_e'(|\mathbf{k}'|) - E_\nu'(|\mathbf{k}'|)\right) d|\mathbf{k}|, \tag{B.19}$$

and can be simplified by defining $x \equiv E_e + E_\nu - E_e' - E_\nu'$. The correct integration over the δ function then gives

$$\mathcal{I} = \int \mathcal{A}(x)\delta(x)dx \left(\frac{dx}{d|\mathbf{k}|}\right)^{-1} = \mathcal{A}(x) \left(\frac{dx}{d|\mathbf{k}|}\right)^{-1}\Bigg|_{x=0}, \tag{B.20}$$

where we find

$$\left(\frac{dx}{d|\mathbf{k}|}\right)^{-1} = \left(\frac{dE_e'}{d|\mathbf{k}|} + \frac{dE_\nu'}{d|\mathbf{k}|}\right)^{-1} = \left(\frac{|\mathbf{k}'|}{E_e'} + \frac{|\mathbf{k}'| - E_\nu\cos\theta}{E_\nu'}\right)^{-1}. \tag{B.21}$$

4) For expressing the final result in terms of dT we use

$$-2m_e T = (k' - k)^2 = t = (p' - p)^2 = -2\left(E_\nu(E_\nu - T) - E_\nu(E_\nu - |\mathbf{k}'|\cos\theta)\right) \tag{B.22}$$

and find

$$\cos\theta = \frac{m_e + E_\nu}{E_\nu}\sqrt{\frac{T}{T+2m_e}}, \tag{B.23}$$

$$\frac{d(\cos\theta)}{dT} = \frac{m_e(E_\nu + m_e)}{E_\nu}\frac{1}{\sqrt{T}}\frac{1}{(2m_e+T)^{3/2}}. \tag{B.24}$$

Putting everything together we finally arrive at the differential cross-section

$$\begin{aligned}\frac{d\sigma}{dT} &= \frac{e^2}{4\pi}\left|\frac{\mathcal{F}_2^{fi}(q^2) - \mathcal{G}_2^{fi}(q^2)}{m_{\nu_i} + m_{\nu_f}}\right|^2\left(\frac{1}{T} - \frac{1}{E_\nu}\right) \\ &= \frac{e^2}{4\pi}\left|\mu^{fi} - i\epsilon^{fi}\right|^2\left(\frac{1}{T} - \frac{1}{E_\nu}\right).\end{aligned} \tag{B.25}$$

In the second equality we used Eq. (2.23) as well as the limit $q^2 \to 0$. Note that the computation is performed for neutrino fields with distinct masses, i.e. the indices f and i refer to neutrino mass eigenstates. Since at the point of detection, neutrino fields are typically in a (coherent) superposition of neutrino mass eigenstates, the quantity $|\mu^{fi} - i\epsilon^{fi}|^2$ has to be replaced by the effective NMM $(\mu^{\text{eff}})^2$, which takes into account oscillation effects, see Sec. 2.4.

Appendix C

Projectors for neutrino electromagnetic form factors

A standard technique for calculations of quantities like the electric and magnetic dipole moments is to project out the relevant Lorentz structure before evaluating the full loop-integral. Such a technique is essential, especially when dealing with one, two or higher loop orders. In the following, we derive the projection operators for the electromagnetic form factors. We used this derivation at an earlier stage of the package X [92] development in order to cross-check the projectors for the case of transition moments. For a derivation of the diagonal form factors, see for example [150].

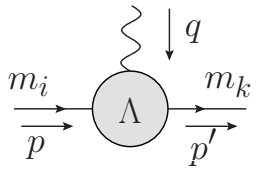

Figure C.1.: Effective NMM operator.

We start by the most general matrix element of the electromagnetic vertex with two different external masses as depicted in Fig. C.1. Note that unlike in Eq. (2.21) we absorb the mass dimension into the form factors $\mathcal{F}_2$ and $\mathcal{G}_2$ for simplicity. There are six linearly independent Dirac operators. We therefore define

$$\Lambda_\mu^{ki} = \mathcal{F}_1^{ki}\gamma_\mu + \mathcal{F}_2^{ki} i\sigma_{\mu\nu}q^\nu + \mathcal{F}_3^{ki} q_\mu + \left(\mathcal{G}_1^{ki}\gamma_\mu + \mathcal{G}_2^{ki} i\sigma_{\mu\nu}q^\nu + \mathcal{G}_3^{ki} q_\mu\right)\gamma_5. \tag{C.1}$$

In the following we skip the indices for better readability. We choose as ansatz for

the projectors

$$\mathcal{P}^{\mu}_{\mathcal{F}_i} = (\not{p} + m_i)\left[a_i\gamma^{\mu} + b_i P_{\mu} + c_i q_{\mu}\right](\not{p}' + m_k), \tag{C.2}$$

$$\mathcal{P}_{\mathcal{G}_i} = (\not{p} + m_i)\left[d_i\gamma^{\mu} + e_i P_{\mu} + f_i q_{\mu}\right]\gamma_5(\not{p}' + m_k), \tag{C.3}$$

where we have defined $P_{\mu} = (p_{\mu} + p'_{\mu})/2$. Now, our task is to find the correct coefficients a_i-f_i and verify that the projectors fulfill

$$\mathrm{tr}[\mathcal{P}^{\mu}_{\mathcal{F}_i}\Lambda_{\mu}] = \mathcal{F}_i, \qquad \mathrm{tr}[\mathcal{P}^{\mu}_{\mathcal{G}_i}\Lambda_{\mu}] = \mathcal{G}_i. \tag{C.4}$$

Applying the Dirac trace with the help of mathematica package Feyn Arts [151] we find

$$\begin{aligned}
\mathrm{tr}[\mathcal{P}^{\mu}_{\mathcal{F}_i}\Lambda_{\mu}] = {}& \mathcal{F}_1\Big[a_i\left(2(d-2)q^2 - 8(d-1)\Delta^2 + 8M^2\right) + b_i\left(2M(4M^2 - q^2)\right) \\
& + c_i(q^2 - 4M^2)4\Delta\Big] \\
& + \mathcal{F}_2\Big[a_i(d-1)4M + b_i(4M^2 - q^2)\Big](q^2 - 4\Delta^2) \\
& + \mathcal{F}_3\Big[4\Delta a_i + 4\Delta M b_i - 2q^2 c_i\Big](q^2 - 4M^2), \qquad \text{(C.5)} \\
\mathrm{tr}[\mathcal{P}^{\mu}_{\mathcal{G}_i}\Lambda_{\mu}] = {}& \mathcal{G}_1\Big[d_i\left(2(d-2)q^2 - 8(d-1)M^2 + 8\Delta^2\right) + e_i\left(2\Delta(4\Delta^2 - q^2)\right) \\
& + f_i(q^2 - 4\Delta^2)4M\Big] \\
& + \mathcal{G}_2\Big[d_i(d-1)4\Delta + e_i(4\Delta^2 - q^2)\Big](4M^2 - q^2) \\
& + \mathcal{G}_3\Big[4M d_i + 4M\Delta e_i - 2q^2 f_i\Big](4\Delta^2 - q^2), \qquad \text{(C.6)}
\end{aligned}$$

where we have defined $M = (m_i + m_k)/2$ and $\Delta = (m_i - m_k)/2$. In order to be able to use dimensional regularization in the evaluation process of the loop-integrals, we have used that the trace of the unit matrix equals to d. Furthermore for displaying the result in a nicer form we have used the kinematical relations

$$p \cdot p' = \frac{1}{2}(m_i^2 + m_k^2 - q^2), \tag{C.7}$$

$$p \cdot q = \frac{1}{2}(-m_i^2 + m_k^2 - q^2), \tag{C.8}$$

$$p' \cdot q = \frac{1}{2}(m_i^2 - m_k^2 - q^2), \tag{C.9}$$

$$P \cdot q = \frac{1}{2}(-m_i^2 + m_k^2). \tag{C.10}$$

In one last step Eqs. (C.5) and (C.5) can be solved in order to reproduce Eq. (C.4).

In doing so, we finally obtain the projector coefficients

$$\begin{aligned}
a_1 =& \frac{q^2(q^2-4M^2)}{2A}, & b_1 =& \frac{2(d-1)Mq^2}{A}, & c_1 =& \frac{\Delta\left(4(d-2)M^2+q^2\right)}{A},\\
a_2 =& \frac{M(4M^2-q^2)}{A}, & b_2 =& -\frac{(d-2)q^2+4M^2}{A}, & c_2 =& -\frac{2(d-1)\Delta M}{A},\\
a_3 =& -\frac{\Delta(4M^2-q^2)}{A}, & b_3 =& \frac{4(d-1)\Delta M}{A}, & c_3 =& \frac{4(d-1)\Delta^2+(d-2)(4M^2-q^2)}{2A},
\end{aligned} \tag{C.11}$$

$$\begin{aligned}
d_1 =& \frac{q^2(q^2-4\Delta^2)}{2B}, & e_1 =& \frac{2(d-1)\Delta q^2}{B}, & f_1 =& \frac{M\left(4(d-2)\Delta^2+q^2\right)}{B},\\
d_2 =& \frac{\Delta(q^2-4\Delta^2)}{B}, & e_2 =& \frac{(d-2)q^2+4\Delta^2}{B}, & f_2 =& \frac{2(d-1)\Delta M}{B},\\
d_3 =& -\frac{M(q^2-4\Delta^2)}{B}, & e_3 =& -\frac{4(d-1)\Delta M}{B}, & f_3 =& -\frac{4(d-1)M^2-(d-2)(q^2-4\Delta^2)}{2B},
\end{aligned} \tag{C.12}$$

with

$$A = (d-2)(q^2-4M^2)^2(q^2-4\Delta^2), \tag{C.13}$$

$$B = (d-2)(q^2-4M^2)(q^2-4\Delta^2)^2. \tag{C.14}$$

In the limit $\Delta = 0$ and $M = m$ the projectors for the diagonal form factors are reproduced correctly and agree with the projectors of package X [92].

Appendix D

List of loop-integrals

In the following we explicitly list some of the loop-integrals that appear in our calculations of NMM loop diagrams.

The loop-integrals for the Dirac neutrinos in the SM calculation (Sec. 4.1.1) are

$$D_a = U_{lf}^* U_{li} \frac{e g_2^2}{2} \int \frac{d^4k}{(2\pi)^4} \frac{\gamma^\alpha P_L (\not{k} + m_l) \gamma^\beta P_L}{\left(k^2 - m_l^2\right)\left((p-k)^2 - M_W^2\right)\left((p'-k)^2 - M_W^2\right)} \cdot \\ \cdot \left(g_{\alpha\beta}(2k - p - p')_\mu + g_{\alpha\mu}(2p' - p - k)_\beta + g_{\mu\beta}(2p - p' - k)_\alpha\right), \tag{D.1}$$

$$D_b = U_{lf}^* U_{li} \frac{e g_2^2}{2} \int \frac{d^4k}{(2\pi)^4} \frac{(m_l P_R - m_{\nu_f} P_L)(\not{k} + m_l) \gamma_\mu P_L}{\left(k^2 - m_l^2\right)\left((p-k)^2 - M_W^2\right)\left((p'-k)^2 - M_W^2\right)}, \tag{D.2}$$

$$D_c = U_{lf}^* U_{li} \frac{e g_2^2}{2} \int \frac{d^4k}{(2\pi)^4} \frac{\gamma_\mu P_L (\not{k} + m_l)(m_l P_L - m_{\nu_i} P_R)}{\left(k^2 - m_l^2\right)\left((p-k)^2 - M_W^2\right)\left((p'-k)^2 - M_W^2\right)}, \tag{D.3}$$

$$D_d = -U_{lf}^* U_{li} \frac{e g_2^2}{2M_W^2} \int \frac{d^4k}{(2\pi)^4} \frac{(m_l P_R - m_{\nu_f} P_L)(\not{k} + m_l)(m_l P_L - m_{\nu_i} P_R)}{\left(k^2 - m_l^2\right)\left((p-k)^2 - M_W^2\right)\left((p'-k)^2 - M_W^2\right)} \cdot \\ \cdot (2k - p - p')_\mu, \tag{D.4}$$

$$D_e = U_{lf}^* U_{li} \frac{e g_2^2}{2} \int \frac{d^4k}{(2\pi)^4} \frac{\gamma^\alpha P_L (\not{p}' - \not{k} + m_l) \gamma_\mu (\not{p} - \not{k} + m_l) \gamma_\alpha P_L}{\left(k^2 - M_W^2\right)\left((p-k)^2 - m_l^2\right)\left((p'-k)^2 - m_l^2\right)}, \tag{D.5}$$

$$D_f = -U_{lf}^* U_{li} \frac{e g_2^2}{2M_W^2} \int \frac{d^4k}{(2\pi)^4} \frac{(m_l P_R - m_{\nu_f} P_L)(\not{p}' - \not{k} + m_l) \gamma_\mu (\not{p} - \not{k} + m_l)}{\left(k^2 - M_W^2\right)\left((p-k)^2 - m_l^2\right)\left((p'-k)^2 - m_l^2\right)} \cdot \\ \cdot (m_l P_L - m_{\nu_i} P_R). \tag{D.6}$$

The labeling is referring to the corresponding Feynman diagram in Fig. 4.1.

For the Majorana case, calculated in unitarity gauge, there are the following diagrams in addition to Eqs. (D.1) and (D.5) with the W boson propagator replaced by

the one for unitarity gauge

$$D_a^M = U_{li}^* U_{lf} \frac{e g_2^2}{2} \int \frac{d^4k}{(2\pi)^4} \frac{\gamma_\alpha P_R(-\not{k} + m_l)\gamma_\beta P_R}{\left(k^2 - m_l^2\right)\left((p-k)^2 - M_W^2\right)\left((p'-k)^2 - M_W^2\right)} \cdot$$
$$\cdot \left(g^{\alpha\alpha'} - \frac{(p'-k)^\alpha (p'-k)^{\alpha'}}{M_W^2}\right)\left(g^{\beta\beta'} - \frac{(p-k)^\beta (p-k)^{\beta'}}{M_W^2}\right) \cdot$$
$$\cdot \left(g_{\alpha'\beta'}(2k-p-p')_\mu + g_{\alpha'\mu}(2p'-p-k)_{\beta'} + g_{\mu\beta'}(2p-p'-k)_{\alpha'}\right), \tag{D.7}$$

$$D_b^M = -U_{li}^* U_{lf} \frac{e g_2^2}{2} \int \frac{d^4k}{(2\pi)^4} \frac{\gamma_\alpha P_R(-\not{p}' + \not{k} + m_l)\gamma_\mu(-\not{p} + \not{k} + m_l)\gamma_\beta P_R}{\left(k^2 - M_W^2\right)\left((p-k)^2 - m_l^2\right)\left((p'-k)^2 - m_l^2\right)} \cdot$$
$$\cdot \left(g^{\alpha\beta} - \frac{k^\alpha k^\beta}{M_W^2}\right). \tag{D.8}$$

In the context of the classification of NMM couplings in Sec. 4.2 we calculated the loop-integrals for the generic scalar case, which are

$$D_a = eQ_S \int \frac{d^4k}{(2\pi)^4} \frac{(g_{fl}P_L + h_{fl}P_R)(\not{k} + m_{F_l})(g_{il}^* P_R + h_{il}^* P_L)}{(k^2 - m_{F_l}^2)\left((p-k)^2 - m_S^2\right)\left((p'-k)^2 - m_S^2\right)} \cdot$$
$$\cdot \left(p_\mu + p'_\nu - 2k_\mu\right), \tag{D.9}$$

$$D_b = eQ_F \int \frac{d^4k}{(2\pi)^4} \frac{(g_{fl}P_L + h_{fl}P_R)(\not{p}' - \not{k} + m_{F_l})\gamma_\mu(\not{p} - \not{k} + m_{F_l})}{(k^2 - m_S^2)\left((p-k)^2 - m_{F_l}^2\right)\left((p'-k)^2 - m_{F_l}^2\right)} \cdot$$
$$\cdot (g_{il}^* P_R + h_{il}^* P_L), \tag{D.10}$$

and for the generic vector couplings

$$D_a = eQ_V \int \frac{d^4k}{(2\pi)^4} \frac{\gamma^\rho(g_{fl}P_L + h_{fl}P_R)(\not{k} + m_{F_l})\gamma^\nu(g_{il}^* P_L + h_{il}^* P_R)}{\left(k^2 - m_{F_l}^2\right)\left((p-k)^2 - m_V^2\right)\left((p'-k)^2 - m_V^2\right)} \cdot$$
$$\cdot \left(g_{\alpha\beta}(2k-p-p')_\mu + g_{\alpha\mu}(2p-p'-k)_\beta + g_{\mu\beta}(2p'-p-k)_\alpha\right) \cdot$$
$$\cdot \left(g_\nu^\alpha - \frac{(p-k)_\nu (p-k)^\alpha}{m_V^2}\right)\left(g_\rho^\beta - \frac{(p'-k)_\rho (p'-k)^\beta}{m_V^2}\right), \tag{D.11}$$

$$D_b = -eQ_F \int \frac{d^4k}{(2\pi)^4} \frac{\gamma^\beta(g_{fl}P_L + h_{fl}P_R)(\not{p}' - \not{k} + m_{F_l})\gamma_\mu(\not{p} - \not{k} + m_{F_l})}{\left(k^2 - m_V^2\right)\left((p-k)^2 - m_{F_l}^2\right)\left((p'-k)^2 - m_{F_l}^2\right)} \cdot$$
$$\cdot \gamma^\alpha(g_{il}^* P_L + h_{il}^* P_R)\left(g_{\alpha\beta} - \frac{k_\alpha k_\beta}{m_V^2}\right). \tag{D.12}$$

For Majorana neutrinos we additionally have the contributions for the scalar case

$$D_a^M = -eQ_S \int \frac{d^4k}{(2\pi)^4} \frac{(g_{fl}^* P_R + h_{fl}^* P_L)(-\not{k} + m_{F_l})(g_{il} P_L + h_{il} P_R)}{(k^2 - m_{F_l}^2)\left((p-k)^2 - m_S^2\right)\left((p'-k)^2 - m_S^2\right)} \cdot$$
$$\cdot \left(p_\mu + p'_\nu - 2k_\mu\right), \tag{D.13}$$

$$D_b^M = eQ_F \int \frac{d^4k}{(2\pi)^4} \frac{(g_{fl}^* P_R + h_{fl}^* P_L)(-\not{p}' + \not{k} + m_{F_l})\gamma_\mu(-\not{p} + \not{k} + m_{F_l})}{(k^2 - m_S^2)\left((p-k)^2 - m_{F_l}^2\right)\left((p'-k)^2 - m_{F_l}^2\right)} \cdot$$
$$\cdot (g_{il} P_L + h_{il} P_R), \tag{D.14}$$

and for the vector case

$$D_a^M = -eQ_V \int \frac{d^4k}{(2\pi)^4} \frac{\gamma^\rho (g_{fl}^* P_R + h_{fl}^* P_L)(-\not{k} + m_{F_l})\gamma^\delta (g_{il} P_R + h_{il} P_L)}{\left(k^2 - m_{F_l}^2\right)\left((p-k)^2 - m_V^2\right)\left((p'-k)^2 - m_V^2\right)} \cdot$$
$$\cdot \left(g_{\alpha\beta}(2k - p - p')_\mu + g_{\alpha\mu}(2p - p' - k)_\beta + g_{\mu\beta}(2p' - p - k)_\alpha\right) \cdot$$
$$\cdot \left(g_\delta^\alpha - \frac{(p-k)_\delta (p-k)^\alpha}{m_V^2}\right)\left(g_\rho^\beta - \frac{(p'-k)_\rho (p'-k)^\beta}{m_V^2}\right), \tag{D.15}$$

$$D_b^M = -eQ_F \int \frac{d^4k}{(2\pi)^4} \frac{\gamma^\beta (g_{fl}^* P_R + h_{fl}^* P_L)(-\not{p}' + \not{k} + m_{F_l})\gamma_\mu(-\not{p} + \not{k} + m_{F_l})}{\left(k^2 - m_V^2\right)\left((p-k)^2 - m_{F_l}^2\right)\left((p'-k)^2 - m_{F_l}^2\right)} \cdot$$
$$\cdot \gamma^\alpha (g_{il} P_R + h_{il} P_L)\left(g_{\alpha\beta} - \frac{k_\alpha k_\beta}{m_V^2}\right). \tag{D.16}$$

In the left-right symmetric model we have found in Sec. 4.4 the loop-integrals

$$D_a = \frac{eg^2}{2}\int \frac{d^4k}{(2\pi)^4}\frac{\gamma^\alpha(P_L + \frac{\kappa_1\kappa_2}{v_R^2}P_R)(\not{k}+m_e)\gamma^\beta(P_L+\frac{\kappa_1\kappa_2}{v_R^2}P_R)}{(k^2-m_e^2)\left((p-k)^2-M_{W_l}^2\right)\left((p'-k)^2-M_{W_l}^2\right)}\cdot$$
$$\cdot\left(g_{\alpha\beta}(2k-p-p')_\mu + g_{\alpha\mu}(2p'-p-k)_\beta + g_{\mu\beta}(2p-p'-k)_\alpha\right), \tag{D.17}$$

$$D_b = -\frac{eg^2}{2}\left(1-\frac{\kappa_1^2\kappa_2^2}{\kappa_1^2+\kappa_2^2}\frac{1}{v_R^2}\right)\cdot$$
$$\cdot\int\frac{d^4k}{(2\pi)^4}\frac{(G_LP_L+G_RP_R)(\not{k}+m_e)\gamma_\mu(P_L+\frac{\kappa_1\kappa_2}{v_R^2}P_R)}{(k^2-m_e^2)\left((p-k)^2-M_{W_l}^2\right)\left((p'-k)^2-M_{W_l}^2\right)}, \tag{D.18}$$

$$D_c = -\frac{eg^2}{2}\left(1-\frac{\kappa_1^2\kappa_2^2}{\kappa_1^2+\kappa_2^2}\frac{1}{v_R^2}\right)\cdot$$
$$\cdot\int\frac{d^4k}{(2\pi)^4}\frac{\gamma_\mu(P_L+\frac{\kappa_1\kappa_2}{v_R^2}P_R)(\not{k}+m_e)(G_RP_L+G_LP_R)}{(k^2-m_e^2)\left((p-k)^2-M_{W_l}^2\right)\left((p'-k)^2-M_{W_l}^2\right)}, \tag{D.19}$$

$$D_d = -\frac{2e}{\kappa_1^2+\kappa_2^2}\int\frac{d^4k}{(2\pi)^4}\frac{(G_LP_L+G_RP_R)(\not{k}+m_e)(G_RP_L+G_LP_R)}{(k^2-m_e^2)\left((p-k)^2-M_{W_l}^2\right)\left((p'-k)^2-M_{W_l}^2\right)}\cdot$$
$$\cdot(2k-p-p')_\mu, \tag{D.20}$$

$$D_e = \frac{eg^2}{2}\int\frac{d^4k}{(2\pi)^4}\frac{\gamma^\alpha(P_L+\frac{\kappa_1\kappa_2}{v_R^2}P_R)(\not{p}'-\not{k}+m_e)\gamma_\mu(\not{p}-\not{k}+m_e)\gamma_\alpha}{\left(k^2-M_{W_l}^2\right)((p-k)^2-m_e^2)\,((p'-k)^2-m_e^2)}\cdot$$
$$\cdot(P_L+\frac{\kappa_1\kappa_2}{v_R^2}P_R), \tag{D.21}$$

$$D_f = -\frac{2e}{\kappa_1^2+\kappa_2^2}\int\frac{d^4k}{(2\pi)^4}\frac{(G_LP_L+G_RP_R)(\not{p}'-\not{k}+m_e)\gamma_\mu(\not{p}-\not{k}+m_e)}{\left(k^2-M_{W_l}^2\right)((p-k)^2-m_e^2)\,((p'-k)^2-m_e^2)}\cdot$$
$$\cdot(G_RP_L+G_LP_R), \tag{D.22}$$

where we have defined for better readability

$$G_L = m_\nu + \frac{\kappa_1\kappa_2}{(\kappa_1^2+\kappa_2^2)v_R^2}\left(m_\nu\kappa_1\kappa_2 - m_e(\kappa_1^2+\kappa_2^2)\right) + \mathcal{O}(v_R^{-3}), \tag{D.23}$$

$$G_R = -m_e + \frac{\kappa_1\kappa_2}{(\kappa_1^2+\kappa_2^2)v_R^2}\left(-m_e\kappa_1\kappa_2 + m_\nu(\kappa_1^2+\kappa_2^2)\right) + \mathcal{O}(v_R^{-3}). \tag{D.24}$$

$$\tag{D.25}$$

Bibliography

[1] J. Kopp and J. Welter, "*The Not-So-Sterile 4th Neutrino: Constraints on New Gauge Interactions from Neutrino Oscillation Experiments*," JHEP **12** (2014) 104, arXiv:1408.0289 [hep-ph].

[2] M. Lindner, B. Radovčić, and J. Welter, "*Revisiting Large Neutrino Magnetic Moments*," JHEP **07** (2017) 139, arXiv:1706.02555 [hep-ph].

[3] **ATLAS**, G. Aad *et al.*, "*Observation of a new particle in the search for the Standard Model Higgs boson with the ATLAS detector at the LHC*," Phys. Lett. **B716** (2012) 1–29, arXiv:1207.7214 [hep-ex].

[4] **CMS**, S. Chatrchyan *et al.*, "*Observation of a new boson at a mass of 125 GeV with the CMS experiment at the LHC*," Phys. Lett. **B716** (2012) 30–61, arXiv:1207.7235 [hep-ex].

[5] **Particle Data Group**, C. Patrignani *et al.*, "*Review of Particle Physics*," Chin. Phys. **C40** (2016) no. 10, 100001.

[6] B. Pontecorvo, "*Inverse beta processes and nonconservation of lepton charge*," Sov. Phys. JETP **7** (1958) 172–173. [Zh. Eksp. Teor. Fiz.34,247(1957)].

[7] **Super-Kamiokande**, Y. Fukuda *et al.*, "*Evidence for oscillation of atmospheric neutrinos*," Phys. Rev. Lett. **81** (1998) 1562–1567, arXiv:hep-ex/9807003 [hep-ex].

[8] **SNO**, Q. R. Ahmad *et al.*, "*Direct evidence for neutrino flavor transformation from neutral current interactions in the Sudbury Neutrino Observatory*," Phys. Rev. Lett. **89** (2002) 011301, arXiv:nucl-ex/0204008 [nucl-ex].

[9] M. B. Voloshin, "*On Compatibility of Small Mass with Large Magnetic Moment of Neutrino*," Sov. J. Nucl. Phys. **48** (1988) 512. [Yad. Fiz.48,804(1988)].

[10] R. Barbieri and R. N. Mohapatra, "*A Neutrino With a Large Magnetic Moment and a Naturally Small Mass*," Phys. Lett. **B218** (1989) 225–229.

[11] K. S. Babu and R. N. Mohapatra, "*Model for Large Transition Magnetic Moment of the ν_e*," Phys. Rev. Lett. **63** (1989) 228.

[12] M. Leurer and N. Marcus, "*A Model for a Large Neutrino Magnetic Transition Moment and Naturally Small Mass*," Phys. Lett. **B237** (1990) 81–87.

[13] D. Chang, W.-Y. Keung, S. Lipovaca, and G. Senjanovic, "*Neutrino magnetic moment and the dicyclic group*," Phys. Rev. Lett. **67** (1991) 953–956.

[14] G. Ecker, W. Grimus, and H. Neufeld, "*A Light Zeldovich-konopinski-mahmoud Neutrino With a Large Magnetic Moment*," Phys. Lett. **B232** (1989) 217–221.

[15] K. S. Babu and R. N. Mohapatra, "*Supersymmetry and Large Transition Magnetic Moment of the Neutrino*," Phys. Rev. Lett. **64** (1990) 1705.

[16] D. Chang, W.-Y. Keung, and G. Senjanovic, "*Neutrino transitional magnetic moment and nonAbelian discrete symmetry*," Phys. Rev. **D42** (1990) 1599–1603.

[17] H. Georgi and L. Randall, "*Charge Conjugation and Neutrino Magnetic Moments*," Phys. Lett. **B244** (1990) 196–202.

[18] A. G. Beda, V. B. Brudanin, V. G. Egorov, D. V. Medvedev, V. S. Pogosov, M. V. Shirchenko, and A. S. Starostin, "*The results of search for the neutrino magnetic moment in GEMMA experiment*," Adv. High Energy Phys. **2012** (2012) 350150.

[19] K. Fujikawa and R. Shrock, "*The Magnetic Moment of a Massive Neutrino and Neutrino Spin Rotation*," Phys. Rev. Lett. **45** (1980) 963.

[20] P. B. Pal and L. Wolfenstein, "*Radiative Decays of Massive Neutrinos*," Phys. Rev. **D25** (1982) 766.

[21] R. E. Shrock, "*Electromagnetic Properties and Decays of Dirac and Majorana Neutrinos in a General Class of Gauge Theories*," Nucl. Phys. **B206** (1982) 359–379.

[22] M. Dvornikov and A. Studenikin, "*Electric charge and magnetic moment of massive neutrino*," Phys. Rev. **D69** (2004) 073001, `arXiv:hep-ph/0305206 [hep-ph]`.

[23] M. S. Dvornikov and A. I. Studenikin, "*Electromagnetic form-factors of a massive neutrino*," J. Exp. Theor. Phys. **99** (2004) 254–269, `arXiv:hep-ph/0411085 [hep-ph]`.

[24] C. Giunti, K. A. Kouzakov, Y.-F. Li, A. V. Lokhov, A. I. Studenikin, and S. Zhou, "*Electromagnetic neutrinos in laboratory experiments and*

astrophysics," Annalen Phys. **528** (2016) 198–215, arXiv:1506.05387 [hep-ph].

[25] T. S. Kosmas, O. G. Miranda, D. K. Papoulias, M. Tortola, and J. W. F. Valle, "*Probing neutrino magnetic moments at the Spallation Neutron Source facility*," Phys. Rev. **D92** (2015) no. 1, 013011, arXiv:1505.03202 [hep-ph].

[26] T. S. Kosmas, O. G. Miranda, D. K. Papoulias, M. Tortola, and J. W. F. Valle, "*Sensitivities to neutrino electromagnetic properties at the TEXONO experiment*," Phys. Lett. **B750** (2015) 459–465, arXiv:1506.08377 [hep-ph].

[27] C. Buck, J. Hakenmüller, G. Heusser, M. Lindner, W. Maneschg, T. Rink, H. Strecker, T. Schierhuber, V. Wagner, K. Fülber, and R. Wink, "*CONUS: The COhernt NeUtrino Scattering experiment.*". in preparation.

[28] C. Giunti and A. Studenikin, "*Neutrino electromagnetic interactions: a window to new physics*," Rev. Mod. Phys. **87** (2015) 531, arXiv:1403.6344 [hep-ph].

[29] E. Akhmedov, "*Majorana neutrinos and other Majorana particles:Theory and experiment*," 2014. arXiv:1412.3320 [hep-ph]. http://inspirehep.net/record/1333680/files/arXiv:1412.3320.pdf.

[30] M. Srednicki, *Quantum field theory*. Cambridge University Press, 2007.

[31] C. Giunti and C. W. Kim, *Fundamentals of Neutrino Physics and Astrophysics*. 2007.

[32] M. Fukugita and T. Yanagida, *Physics of neutrinos and applications to astrophysics*. 2003.

[33] E. K. Akhmedov, "*Neutrino physics*," in *Proceedings, Summer School in Particle Physics: Trieste, Italy, June 21-July 9, 1999*, pp. 103–164. 1999. arXiv:hep-ph/0001264 [hep-ph].

[34] R. N. Mohapatra and P. B. Pal, "*Massive neutrinos in physics and astrophysics. Second edition*," World Sci. Lect. Notes Phys. **60** (1998) 1–397. [World Sci. Lect. Notes Phys.72,1(2004)].

[35] M. E. Peskin and D. V. Schroeder, *An Introduction to quantum field theory*. 1995. http://www.slac.stanford.edu/spires/find/books/www?cl=QC174.45%3AP4.

[36] Z. Maki, M. Nakagawa, and S. Sakata, "*Remarks on the unified model of elementary particles*," Prog. Theor. Phys. **28** (1962) 870–880.

[37] **Super-Kamiokande**, Y. Fukuda *et al.*, "*The Super-Kamiokande detector*," Nucl. Instrum. Meth. **A501** (2003) 418–462.

[38] P. Minkowski, "$\mu \to e\gamma$ *at a Rate of One Out of* 10^9 *Muon Decays?*," Phys. Lett. **67B** (1977) 421–428.

[39] M. Gell-Mann, P. Ramond, and R. Slansky, "*Complex Spinors and Unified Theories*," Conf. Proc. **C790927** (1979) 315–321, arXiv:1306.4669 [hep-th].

[40] P. Ramond, "*The Family Group in Grand Unified Theories*," in *International Symposium on Fundamentals of Quantum Theory and Quantum Field Theory Palm Coast, Florida, February 25-March 2, 1979*, pp. 265–280. 1979. arXiv:hep-ph/9809459 [hep-ph].

[41] T. Yanagida, "*HORIZONTAL SYMMETRY AND MASSES OF NEUTRINOS*," Conf. Proc. **C7902131** (1979) 95–99.

[42] R. N. Mohapatra and G. Senjanovic, "*Neutrino Mass and Spontaneous Parity Violation*," Phys. Rev. Lett. **44** (1980) 912.

[43] **SNO**, J. Boger *et al.*, "*The Sudbury neutrino observatory*," Nucl. Instrum. Meth. **A449** (2000) 172–207, arXiv:nucl-ex/9910016 [nucl-ex].

[44] N. Foundation, "*The Nobel Prize in Physics 2015*," 2015. http://www.nobelprize.org/nobel_prizes/physics/laureates/2015/.

[45] L. Wolfenstein, "*Neutrino Oscillations in Matter*," Phys. Rev. **D17** (1978) 2369–2374.

[46] S. P. Mikheyev and A. Yu. Smirnov, "*Resonant neutrino oscillations in matter*," Prog. Part. Nucl. Phys. **23** (1989) 41–136.

[47] I. Esteban, M. C. Gonzalez-Garcia, M. Maltoni, I. Martinez-Soler, and T. Schwetz, "*Updated fit to three neutrino mixing: exploring the accelerator-reactor complementarity*," JHEP **01** (2017) 087, arXiv:1611.01514 [hep-ph].

[48] F. Jegerlehner, "*The Anomalous Magnetic Moment of the Muon*," Springer Tracts Mod. Phys. **274** (2017) pp.1–693.

[49] W. J. Marciano and A. I. Sanda, "*Exotic Decays of the Muon and Heavy Leptons in Gauge Theories*," Phys. Lett. **67B** (1977) 303–305.

[50] B. W. Lee and R. E. Shrock, "*Natural Suppression of Symmetry Violation in Gauge Theories: Muon - Lepton and Electron Lepton Number Nonconservation*," Phys. Rev. **D16** (1977) 1444.

[51] S. T. Petcov, "*The Processes mu –¿ e Gamma, mu –¿ e e anti-e, Neutrino' –¿ Neutrino gamma in the Weinberg-Salam Model with Neutrino Mixing*," Sov. J. Nucl. Phys. **25** (1977) 340. [Erratum: Yad. Fiz.25,1336(1977)].

[52] J. F. Nieves, "*Electromagnetic Properties of Majorana Neutrinos*," Phys. Rev. **D26** (1982) 3152.

[53] B. Kayser, "*Majorana Neutrinos and their Electromagnetic Properties*," Phys. Rev. **D26** (1982) 1662.

[54] B. Kayser, "*CPT, CP, and c Phases and their Effects in Majorana Particle Processes*," Phys. Rev. **D30** (1984) 1023.

[55] W. Grimus and P. Stockinger, "*Effects of neutrino oscillations and neutrino magnetic moments on elastic neutrino - electron scattering*," Phys. Rev. **D57** (1998) 1762–1768, arXiv:hep-ph/9708279 [hep-ph].

[56] J. F. Beacom and P. Vogel, "*Neutrino magnetic moments, flavor mixing, and the Super-Kamiokande solar data*," Phys. Rev. Lett. **83** (1999) 5222–5225, arXiv:hep-ph/9907383 [hep-ph].

[57] H. T. Wong and H.-B. Li, "*Neutrino magnetic moments*," Mod. Phys. Lett. **A20** (2005) 1103–1117.

[58] A. G. Beda, V. B. Brudanin, E. V. Demidova, V. G. Egorov, M. G. Gavrilov, M. V. Shirchenko, A. S. Starostin, and T. Vylov, "*First Result for Neutrino Magnetic Moment from Measurements with the GEMMA Spectrometer*," Phys. Atom. Nucl. **70** (2007) 1873–1884, arXiv:0705.4576 [hep-ex].

[59] C. Broggini, C. Giunti, and A. Studenikin, "*Electromagnetic Properties of Neutrinos*," Adv. High Energy Phys. **2012** (2012) 459526, arXiv:1207.3980 [hep-ph].

[60] R. Barbieri and G. Fiorentini, "*The Solar Neutrino Puzzle and the Neutrino (L) → Neutrino (R) Conversion Hypothesis*," Nucl. Phys. **B304** (1988) 909–920.

[61] P. Stockinger and W. Grimus, "*Effects of scalar exchange and neutrino magnetic and electric dipole moments in electron-neutrino e- scattering*," Phys. Lett. **B327** (1994) 327–334.

[62] P. Vogel and J. Engel, "*Neutrino Electromagnetic Form-Factors*," Phys. Rev. **D39** (1989) 3378.

[63] K. A. Kouzakov and A. I. Studenikin, "*Neutrino-atom collisions*," J. Phys. Conf. Ser. **718** (2016) no. 6, 062031, arXiv:1603.02462 [hep-ph].

[64] C. L. Cowan, F. Reines, and F. B. Harrison, "*Upper limit on the neutrino magnetic moment*," Phys. Rev. **96** (1954) 1294.

[65] C. L. Cowan and F. Reines, "*Neutrino magnetic moment upper limit*," Phys. Rev. **107** (1957) 528–530.

[66] F. Reines, H. S. Gurr, and H. W. Sobel, "*Detection of anti-electron-neutrino e Scattering*," Phys. Rev. Lett. **37** (1976) 315–318.

[67] G. S. Vidyakin, V. N. Vyrodov, I. I. Gurevich, Yu. V. Kozlov, V. P. Martemyanov, S. V. Sukhotin, V. G. Tarasenkov, E. V. Turbin, and S. K. Khakhimov, "*Limitations on the magnetic moment and charge radius of the electron-anti-neutrino*," JETP Lett. **55** (1992) 206–210. [Pisma Zh. Eksp. Teor. Fiz.55,212(1992)].

[68] A. I. Derbin, A. V. Chernyi, L. A. Popeko, V. N. Muratova, G. A. Shishkina, and S. I. Bakhlanov, "*Experiment on anti-neutrino scattering by electrons at a reactor of the Rovno nuclear power plant*," JETP Lett. **57** (1993) 768–772. [Pisma Zh. Eksp. Teor. Fiz.57,755(1993)].

[69] **TEXONO**, H. T. Wong *et al.*, "*A Search of Neutrino Magnetic Moments with a High-Purity Germanium Detector at the Kuo-Sheng Nuclear Power Station*," Phys. Rev. **D75** (2007) 012001, arXiv:hep-ex/0605006 [hep-ex].

[70] L. A. Ahrens *et al.*, "*Determination of electroweak parameters from the elastic scattering of muon-neutrinos and anti-neutrinos on electrons*," Phys. Rev. **D41** (1990) 3297–3316.

[71] **LSND**, L. B. Auerbach *et al.*, "*Measurement of electron - neutrino - electron elastic scattering*," Phys. Rev. **D63** (2001) 112001, arXiv:hep-ex/0101039 [hep-ex].

[72] **DONUT**, R. Schwienhorst *et al.*, "*A New upper limit for the tau - neutrino magnetic moment*," Phys. Lett. **B513** (2001) 23–29, arXiv:hep-ex/0102026 [hep-ex].

[73] R. C. Allen *et al.*, "*Study of electron-neutrino electron elastic scattering at LAMPF*," Phys. Rev. **D47** (1993) 11–28.

[74] **Super-Kamiokande**, D. W. Liu *et al.*, "*Limits on the neutrino magnetic moment using 1496 days of Super-Kamiokande-I solar neutrino data*," Phys. Rev. Lett. **93** (2004) 021802, arXiv:hep-ex/0402015 [hep-ex].

[75] **Borexino**, "*Limiting neutrino magnetic moments with Borexino Phase-II solar neutrino data*," arXiv:1707.09355 [hep-ex].

[76] A. Ayala, J. C. D'Olivo, and M. Torres, "*Bound on the neutrino magnetic moment from chirality flip in supernovae*," Phys. Rev. **D59** (1999) 111901, arXiv:hep-ph/9804230 [hep-ph].

[77] A. Ayala, J. C. D'Olivo, and M. Torres, "*Right-handed neutrino production in dense and hot plasmas*," Nucl. Phys. **B564** (2000) 204–222, arXiv:hep-ph/9907398 [hep-ph].

[78] R. Barbieri and R. N. Mohapatra, "*Limit on the Magnetic Moment of the Neutrino from Supernova SN 1987a Observations*," Phys. Rev. Lett. **61** (1988) 27.

[79] G. G. Raffelt, *Stars as laboratories for fundamental physics*. 1996. http://wwwth.mpp.mpg.de/members/raffelt/mypapers/199613.pdf.

[80] G. G. Raffelt, "*Limits on neutrino electromagnetic properties: An update*," Phys. Rept. **320** (1999) 319–327.

[81] G. G. Raffelt, "*Particle physics from stars*," Ann. Rev. Nucl. Part. Sci. **49** (1999) 163–216, arXiv:hep-ph/9903472 [hep-ph].

[82] J. Bernstein, M. Ruderman, and G. Feinberg, "*Electromagnetic Properties of the neutrino*," Phys. Rev. **132** (1963) 1227–1233.

[83] G. G. Raffelt, "*Core Mass at the Helium Flash From Observations and a New Bound on Neutrino Electromagnetic Properties*," Astrophys. J. **365** (1990) 559.

[84] G. G. Raffelt, "*New bound on neutrino dipole moments from globular cluster stars*," Phys. Rev. Lett. **64** (1990) 2856–2858.

[85] N. Viaux, M. Catelan, P. B. Stetson, G. Raffelt, J. Redondo, A. A. R. Valcarce, and A. Weiss, "*Particle-physics constraints from the globular cluster M5: Neutrino Dipole Moments*," Astron. Astrophys. **558** (2013) A12, arXiv:1308.4627 [astro-ph.SR].

[86] A. Heger, A. Friedland, M. Giannotti, and V. Cirigliano, "*The Impact of Neutrino Magnetic Moments on the Evolution of Massive Stars*," Astrophys. J. **696** (2009) 608–619, arXiv:0809.4703 [astro-ph].

[87] M. Radomski, "*Neutrino Magnetic Moment, Plasmon Cherenkov Radiation, and the Solar Neutrino Problem*," Phys. Rev. **D12** (1975) 2208–2211.

[88] S. Mohanty and M. K. Samal, "*Cherenkov radiation by neutrinos in a supernova core*," Phys. Rev. Lett. **77** (1996) 806–809, arXiv:hep-ph/9506385 [hep-ph].

[89] A. Cisneros, "*Effect of neutrino magnetic moment on solar neutrino observations*," Astrophys. Space Sci. **10** (1971) 87–92.

[90] M. B. Voloshin and M. I. Vysotsky, "*Neutrino Magnetic Moment and Time Variation of Solar Neutrino Flux*," Sov. J. Nucl. Phys. **44** (1986) 544. [Yad. Fiz.44,845(1986)].

[91] L. B. Okun, M. B. Voloshin, and M. I. Vysotsky, "*Neutrino Electrodynamics and Possible Effects for Solar Neutrinos*," Sov. Phys. JETP **64** (1986) 446–452. [Zh. Eksp. Teor. Fiz.91,754(1986)].

[92] H. H. Patel, "*Package-X: A Mathematica package for the analytic calculation of one-loop integrals*," Comput. Phys. Commun. **197** (2015) 276–290, arXiv:1503.01469 [hep-ph].

[93] T. Nakano and K. Nishijima, "*Charge Independence for V-particles*," Prog. Theor. Phys. **10** (1953) 581–582.

[94] M. Fukugita and T. Yanagida, "*A Particle Physics Model for Voloshin-Vysotskii-Okun Solution to the Solar Neutrino Problem*," Phys. Rev. Lett. **58** (1987) 1807.

[95] J. Gluza and M. Zralek, "*Neutrino production in e+ e- collisions in a left-right symmetric model*," Phys. Rev. **D48** (1993) 5093–5105.

[96] N. G. Deshpande, J. F. Gunion, B. Kayser, and F. I. Olness, "*Left-right symmetric electroweak models with triplet Higgs*," Phys. Rev. **D44** (1991) 837–858.

[97] M. Czakon, J. Gluza, and M. Zralek, "*Neutrino magnetic moments in left-right symmetric models*," Phys. Rev. **D59** (1999) 013010.

[98] T. Appelquist and J. Carazzone, "*Infrared Singularities and Massive Fields*," Phys. Rev. **D11** (1975) 2856.

[99] J. C. Pati and A. Salam, "*Lepton Number as the Fourth Color*," Phys. Rev. **D10** (1974) 275–289. [Erratum: Phys. Rev.D11,703(1975)].

[100] R. N. Mohapatra and J. C. Pati, "*A Natural Left-Right Symmetry*," Phys. Rev. **D11** (1975) 2558.

[101] R. N. Mohapatra and J. C. Pati, "*Left-Right Gauge Symmetry and an Isoconjugate Model of CP Violation*," Phys. Rev. **D11** (1975) 566–571.

[102] G. Senjanovic and R. N. Mohapatra, "*Exact Left-Right Symmetry and Spontaneous Violation of Parity*," Phys. Rev. **D12** (1975) 1502.

[103] M. Dine, "*TASI lectures on the strong CP problem*," in *Flavor physics for the millennium. Proceedings, Theoretical Advanced Study Institute in elementary particle physics, TASI 2000, Boulder, USA, June 4-30, 2000*, pp. 349–369. 2000. arXiv:hep-ph/0011376 [hep-ph].

[104] R. N. Mohapatra, *UNIFICATION AND SUPERSYMMETRY. THE FRONTIERS OF QUARK - LEPTON PHYSICS*. Springer, Berlin, 1986.

[105] M. Nemevsek, G. Senjanovic, and V. Tello, "*Connecting Dirac and Majorana Neutrino Mass Matrices in the Minimal Left-Right Symmetric Model*," Phys. Rev. Lett. **110** (2013) no. 15, 151802, arXiv:1211.2837 [hep-ph].

[106] R. Foot, G. C. Joshi, H. Lew, and R. R. Volkas, "*Charge quantization in the standard model and some of its extensions*," Mod. Phys. Lett. **A5** (1990) 2721–2732.

[107] R. Foot, H. Lew, and R. R. Volkas, "*Electric charge quantization*," J. Phys. **G19** (1993) 361–372, arXiv:hep-ph/9209259 [hep-ph]. [Erratum: J. Phys.G19,1067(1993)].

[108] S. Davidson, S. Hannestad, and G. Raffelt, "*Updated bounds on millicharged particles*," JHEP **05** (2000) 003, arXiv:hep-ph/0001179 [hep-ph].

[109] L. B. Okun, M. B. Voloshin, and V. I. Zakharov, "*ELECTRICAL NEUTRALITY OF ATOMS AND GRAND UNIFICATION MODELS*," Phys. Lett. **138B** (1984) 115–120.

[110] A. I. Studenikin and I. Tokarev, "*Millicharged neutrino with anomalous magnetic moment in rotating magnetized matter*," Nucl. Phys. **B884** (2014) 396–407, arXiv:1209.3245 [hep-ph].

[111] B. Holdom, "*Two U(1)'s and Epsilon Charge Shifts*," Phys. Lett. **166B** (1986) 196–198.

[112] R. Essig *et al.*, "*Working Group Report: New Light Weakly Coupled Particles*," in *Proceedings, 2013 Community Summer Study on the Future of U.S. Particle Physics: Snowmass on the Mississippi (CSS2013): Minneapolis, MN, USA, July 29-August 6, 2013*. 2013. arXiv:1311.0029 [hep-ph]. http://inspirehep.net/record/1263039/files/arXiv:1311.0029.pdf.

[113] R. Foot and S. Vagnozzi, "*Dissipative hidden sector dark matter*," Phys. Rev. **D91** (2015) 023512, arXiv:1409.7174 [hep-ph].

[114] H. Vogel and J. Redondo, "*Dark Radiation constraints on minicharged particles in models with a hidden photon*," JCAP **1402** (2014) 029, arXiv:1311.2600 [hep-ph].

[115] S. Davidson, B. Campbell, and D. C. Bailey, "*Limits on particles of small electric charge*," Phys. Rev. **D43** (1991) 2314–2321.

[116] E. Golowich and R. W. Robinett, "*Limits on Millicharged Matter From Beam Dump Experiments*," Phys. Rev. **D35** (1987) 391.

[117] R. C. Ball *et al.*, "*Supersymmetry Mass and Lifetime Limits From a Proton Beam Dump Experiment*," Phys. Rev. Lett. **53** (1984) 1314.

[118] H. Hu, C. Muller, and C. H. Keitel, "*Complete QED theory of multiphoton trident pair production in strong laser fields*," Phys. Rev. Lett. **105** (2010) 080401, arXiv:1002.2596 [physics.atom-ph].

[119] A. A. Prinz *et al.*, "*Search for millicharged particles at SLAC*," Phys. Rev. Lett. **81** (1998) 1175–1178, arXiv:hep-ex/9804008 [hep-ex].

[120] S. N. Gninenko, N. V. Krasnikov, and A. Rubbia, "*Search for millicharged particles in reactor neutrino experiments: A Probe of the PVLAS anomaly*," Phys. Rev. **D75** (2007) 075014, arXiv:hep-ph/0612203 [hep-ph].

[121] J. Jaeckel, M. Jankowiak, and M. Spannowsky, "*LHC probes the hidden sector*," Phys. Dark Univ. **2** (2013) 111–117, arXiv:1212.3620 [hep-ph].

[122] T. Mitsui, R. Fujimoto, Y. Ishisaki, Y. Ueda, Y. Yamazaki, S. Asai, and S. Orito, "*Search for invisible decay of orthopositronium*," Phys. Rev. Lett. **70** (1993) 2265–2268.

[123] E. W. Hagley and F. M. Pipkin, "*Separated oscillatory field measurement of hydrogen S-21/2- P-23/2 fine structure interval*," Phys. Rev. Lett. **72** (1994) 1172–1175.

[124] A. D. Dolgov, S. L. Dubovsky, G. I. Rubtsov, and I. I. Tkachev, "*Constraints on millicharged particles from Planck data*," Phys. Rev. **D88** (2013) no. 11, 117701, arXiv:1310.2376 [hep-ph].

[125] N. F. Bell, V. Cirigliano, M. J. Ramsey-Musolf, P. Vogel, and M. B. Wise, "*How magnetic is the Dirac neutrino?*," Phys. Rev. Lett. **95** (2005) 151802, arXiv:hep-ph/0504134 [hep-ph].

[126] S. Davidson, M. Gorbahn, and A. Santamaria, "*From transition magnetic moments to majorana neutrino masses*," Phys. Lett. **B626** (2005) 151–160, arXiv:hep-ph/0506085 [hep-ph].

[127] N. F. Bell, M. Gorchtein, M. J. Ramsey-Musolf, P. Vogel, and P. Wang, "*Model independent bounds on magnetic moments of Majorana neutrinos*," Phys. Lett. **B642** (2006) 377–383, arXiv:hep-ph/0606248 [hep-ph].

[128] E. Ma, "*Verifiable radiative seesaw mechanism of neutrino mass and dark matter*," Phys. Rev. **D73** (2006) 077301, arXiv:hep-ph/0601225 [hep-ph].

[129] M. Gozdz, W. A. Kaminski, F. Simkovic, and A. Faessler, "*Transition magnetic moments of Majorana neutrinos in supersymmetry without R-parity in light of neutrino oscillations*," Phys. Rev. **D74** (2006) 055007, arXiv:hep-ph/0606077 [hep-ph].

[130] A. Aboubrahim, T. Ibrahim, A. Itani, and P. Nath, "*Large Neutrino Magnetic Dipole Moments in MSSM Extensions*," Phys. Rev. **D89** (2014) no. 5, 055009, arXiv:1312.2505 [hep-ph].

[131] S. M. Barr, E. M. Freire, and A. Zee, "*A Mechanism for large neutrino magnetic moments*," Phys. Rev. Lett. **65** (1990) 2626–2629.

[132] S. M. Barr and E. M. Freire, "*Large neutrino magnetic moments and the existence of singly charged scalar fields*," Phys. Rev. **D43** (1991) 2989–2998.

[133] K. S. Babu, D. Chang, W.-Y. Keung, and I. Phillips, "*Comment on 'Mechanism for large neutrino magnetic moments'*," Phys. Rev. **D46** (1992) 2268–2269.

[134] **CMS**, V. Khachatryan *et al.*, "*Searches for electroweak production of charginos, neutralinos, and sleptons decaying to leptons and W, Z, and Higgs bosons in pp collisions at 8 TeV*," Eur. Phys. J. **C74** (2014) no. 9, 3036, arXiv:1405.7570 [hep-ex].

[135] **ATLAS**, G. Aad *et al.*, "*Search for direct production of charginos, neutralinos and sleptons in final states with two leptons and missing transverse momentum in pp collisions at $\sqrt{s} = 8$ TeV with the ATLAS detector*," JHEP **05** (2014) 071, arXiv:1403.5294 [hep-ex].

[136] C. Salazar, R. H. Benavides, W. A. Ponce, and E. Rojas, "*LHC Constraints on 3-3-1 Models*," JHEP **07** (2015) 096, arXiv:1503.03519 [hep-ph].

[137] J.-M. Frère, J. Heeck, and S. Mollet, "*Triangle Inequalities for Majorana-Neutrino Magnetic Moments*," Phys. Rev. **D92** (2015) no. 5, 053002, arXiv:1506.02964 [hep-ph].

[138] **SHiP**, M. Anelli *et al.*, "*A facility to Search for Hidden Particles (SHiP) at the CERN SPS*," arXiv:1504.04956 [physics.ins-det].

[139] **ATLAS**, G. Aad *et al.*, "*Evidence for the Higgs-boson Yukawa coupling to tau leptons with the ATLAS detector*," JHEP **04** (2015) 117, arXiv:1501.04943 [hep-ex].

[140] **CMS**, S. Chatrchyan *et al.*, "*Evidence for the 125 GeV Higgs boson decaying to a pair of τ leptons*," JHEP **05** (2014) 104, arXiv:1401.5041 [hep-ex].

[141] S. K. Jones and C. H. Llewellyn Smith, "*Leptoproduction of Supersymmetric Particles*," Nucl. Phys. **B217** (1983) 145–171.

[142] H. E. Haber and G. L. Kane, "*The Search for Supersymmetry: Probing Physics Beyond the Standard Model*," Phys. Rept. **117** (1985) 75–263.

[143] E. I. Gates and K. L. Kowalski, "*MAJORANA FEYNMAN RULES*," Phys. Rev. **D37** (1988) 938.

[144] J. Gluza and M. Zralek, "*Feynman rules for Majorana neutrino interactions*," Phys. Rev. **D45** (1992) 1693–1700.

[145] M. A. Luty, "*Baryogenesis via leptogenesis*," Phys. Rev. **D45** (1992) 455–465.

[146] A. Denner, H. Eck, O. Hahn, and J. Kublbeck, "*Feynman rules for fermion number violating interactions*," Nucl. Phys. **B387** (1992) 467–481.

[147] P. B. Pal, "*Dirac, Majorana and Weyl fermions*," Am. J. Phys. **79** (2011) 485–498, arXiv:1006.1718 [hep-ph].

[148] A. V. Kyuldjiev, "*Searching for Effects of Neutrino Magnetic Moments at Reactors and Accelerators*," Nucl. Phys. **B243** (1984) 387–397.

[149] W. Grimus and T. Schwetz, "*Elastic neutrino electron scattering of solar neutrinos and potential effects of magnetic and electric dipole moments*," Nucl. Phys. **B587** (2000) 45–66, arXiv:hep-ph/0006028 [hep-ph].

[150] A. Czarnecki and B. Krause, "*On the dipole moments of fermions at two loops*," Acta Phys. Polon. **B28** (1997) 829–834, arXiv:hep-ph/9611299 [hep-ph].

[151] J. Kublbeck, M. Bohm, and A. Denner, "*Feyn Arts: Computer Algebraic Generation of Feynman Graphs and Amplitudes*," Comput. Phys. Commun. **60** (1990) 165–180.